Structural analysis of the cancer promoting Matrix Metalloproteinase–9 in complexes with novel pharmacological inhibitors

Molecular structure of the hemopexin domain of MT1-MMP, including novel dimerization models

Anna Maria Tochowicz

Max-Planck-Institute für Biochemie

Abteilung Strukturforschung

D-82152 Martinsried, München

Max-Planck-Institute für Biochemie

Abteilung Strukturforschung

Structural analysis of the cancer promoting Matrix Metalloproteinase–9 in complexes with novel pharmacological inhibitors

Molecular structure of the hemopexin domain of MT1-MMP, including novel dimerization models

Anna Maria Tochowicz

Acknowledgments

Acknowledgements

Chapter 1   Summary

Cancer is a life-threatening disorder and one of the major prevailing health problems. The Matrix Metalloproteinase-9, also called gelatinase B, is a critical component of the angiogenic switch driving metastasis in various cancers. Additionally it promotes osteoarthritis, atherosclerosis or heart failure. Under healthy conditions, the MMP-9 proteolytic activity is strictly regulated by the endogenous tissue inhibitors of matrix metalloproteinases (TIMPs), while disruption of this balance leads to a detrimental excess of active MMP-9. Specific inhibition of MMP-9 may prevent tumor growth therefore, it is essential to design potent inhibitors in order to compensate for the loss at physiological regulation. Even though many inhibitors have been studied, none was sufficiently specific and efficient for any individual MMP. In an attempt to clarify important determinants for the specific inhibition of MMP-9, the inactive E402Q mutant of the truncated catalytic domain of human MMP-9 was prepared, and the X-ray crystal structures of this recombinant miniMMP-9 were determined with a number of catalytic zinc-directed synthetic inhibitors of different binding type. The complex structures of MMP-9 with relatively selective, tight binding inhibitors, namely a pyrimidine-2,4,6-trione (RO206-0222), a phosphinic acid (AM409), a carboxylate (An1), a trifluoromethyl hydroxamic acid inhibitor (MS560), and a difluoro carboxylate inhibitor (MJ24) were solved. The crystal structures revealed that these five inhibitors bind in a similar manner, compromising between optimal coordination of the catalytic zinc, favorable hydrogen bond formation in the active-site cleft, and accommodation of their large P1' groups in the overall rigid S1' cavity. Furthermore, three MMP inhibitors were designed which are capable of differentiating the gelatinases MMP-2 and -9 from the other members of the MMPs family, by applying the concept of bivalent inhibitors: Al134 (Peg$_4$), Al134 (Peg$_6$), and Al134 (Peg$_8$). The latter one proved that the bivalent inhibition concept for MMP-9 is working in principle, but requires additional fine tuning of the compound.

Dimerization is an important mechanism to regulate activity of MMPs, in particular for the cancer related MMP-2. MT1-MMP Hpex fixes, through a bound TIMP-2, a proMMP-2 molecule presenting a scissile peptide bond toward a second non-inhibited MT1-MMP molecule, which facilitates proMMP-2 activation. For a structural analysis of

the MT1-MMP dimerization the recombinant MT1-MMP hemopexin domain was crystallized. The crystals contain a monomer with two different, symmetrical and asymmetrical binding sites. The symmetrical MT1-MMP-Hpex dimer interface is mixed polar and hydrophobic, and served as a model for MT1-MMP dimerization. In contrast to the corresponding asymmetrical MT1-MMP dimer, the symmetrical complex is in accordance with the known dimerization of the transmembrane segments including the cytoplasmic tail. Furthermore, the complex formation of Hpex MT1-MMP and one TIMP-2 molecule via its C-terminal part is also possible.

Zusammenfassung

Lebensbedrohliche Krebserkrankungen sind eines der größten medizinischen Probleme unserer Zeit. Matrixmetalloproteinase 9 (MMP-9), oder Gelatinase B, ist eine der entscheidenden Komponenten bei der Gefäßneubildung, welche die Metastasierung diverser Krebsarten vorantreibt, sowie Osteoarthritis, Atherosklerose und Herzversagen fördert. Im gesunden Zustand wird die proteolytische Aktivität von MMP-9 durch die endogenen Gewebsinhibitoren der Matrixmetalloproteinasen (TIMP) streng reguliert, während die Störung dieses Gleichgewichts zu einem schädlichen Überschuss aktiver MMP-9 führt. Da die gezielte Inhibition von MMP-9 das Tumorwachstum verhindern könnte, ist es erforderlich, wirksame Inhibitoren herzustellen, die den Verlust der physiologischen Regulation kompensieren. Obwohl eine Vielzahl von Inhibitoren untersucht wurde, besaß bisher keiner genügend spezifische Wirksamkeit für die einzelnen MMP. Zur Bestimmung der molekularen Grundlagen der MMP-9-Inhibition wurden die inaktive E402Q-Mutante der verkürzten katalytischen Domäne von humaner MMP-9 gereinigt und die Röntgenkristallstrukturen dieser rekombinanten Mini-MMP-9 mit synthetischen Inhibitoren bestimmt, die das katalytische Zink in unterschiedlicher Weise binden. Die MMP-9-Komplexe mit folgenden selektiven, stark bindenden Inhibitoren wurden strukturell aufgeklärt: ein Pyrimidin-2,4,6-trion (RO206-222), eine Phosphinsäure (AM409), ein Carboxylat (An1), eine Trifluoromethylhydroxamsäure (MS560) und ein Difluorocarboxylat (MJ24). Die Kristallstrukturen zeigten, dass die fünf Inhibitoren ähnlich binden, wobei ein Ausgleich zwischen optimaler Koordination des katalytischen Zink, günstigen Wasserstoffbrücken in der Spalte des aktiven Zentrums und der Aufnahme großer P1´-Reste in der insgesamt rigiden S1´-Tasche gefunden wird. Des Weiteren wurden drei MMP-Inhibitoren synthetisiert, die aufgrund bivalenter Funktionalität die Gelatinasen MMP-2 und -9 von den anderen MMPs unterscheiden sollten: Al134(Peg$_4$), Al134(Peg$_6$) und Al134(Peg$_8$). Letzterer bestätigte prinzipiell die Anwendbarkeit des Konzepts der bivalenten Inhibition für MMP-9, wenngleich eine weitere Optimierung der Verbindung notwendig ist.

Die Dimerisierung ist ein wichtiger Mechanismus bei der Steuerung der MMP-Aktivität, insbesondere für die an Krebs beteiligte MMP-2. Die MT1-MMP (MMP-14) bindet im Komplex mit dem Inhibitor TIMP-2 ein Pro-MMP-2-Molekül, das einem zweiten, nicht-

6

inhibierten MT1-MMP eine Spaltstelle für die Pro-MMP-2-Aktivierung präsentiert. Zur strukturellen Untersuchung der MT1-Dimerisierung wurde die rekombinante MT1-MMP- Hämopexindomäne (Hpex) kristallisiert. Die Kristalle enthielten Monomere mit jeweils einer relevanten symmetrischen und asymmetrischen Bindungsstelle. Die symmetrische MT1-MMP-Hpex-Dimerenkontaktfläche besitzt gemischt polaren und hydrophoben Charakter und diente als Modell für die MT1-Dimerisierung. Im Gegensatz zum entsprechenden asymmetrischen MT1-MMP-Dimerenmodell ist der symmetrische Komplex mit der bekannten Dimerisierung der Transmembransegmente und der cytoplasmatischen Domänen vereinbar. Außerdem wird die Komplexbildung der MT1-MMP mit einem TIMP-2-Molekül durch dessen C-Terminus ermöglicht.

Chapter 2   Introduction

2.1 Proteases

Proteolytic enzymes (that comprise proteases or proteinases and peptidases) perform essential functions in all living organisms. Proteolytic processing events are fundamental in ovulation, fertilization, embryonic development, bone formation, control of homeostatic tissue remodeling, neuronal outgrowth, antigen presentation, cell-cycle regulation, immune and inflammatory cell migration and activation, wound healing, angiogenesis and apoptosis. Accordingly, alterations in the structure and expression patterns of proteases determine many human pathological processes including cancer, arthritis, osteoporosis, neurodegenerative disorders and cardiovascular diseases (Rawlings & Barrett, 1998; Hooper, 2002).

Proteinases/Proteases are able to cleave other proteins, by cutting the peptide bond between the amino acid residues. They are classified by the International Union of Biochemistry and Molecular Biology (IUBMB) as enzymes of class 3, the hydrolases, and subclass 3.4, the peptide hydrolases or peptidases. They constitute a large family (E.C.3.4) divided as endopeptidases or proteinases (E.C.3.4.21-99) and exopeptidases (E.C.3.4.11-19) according to the point at which they break the peptide chain.

Schematically:

- Endopeptidases or proteinases (E.C. 3.4. 21-99.-) that cleave internal peptide bonds in proteins and peptides.

- Exopeptidases (E.C.3.4.11-19.-) that cleave near the N- and C- termini of peptides and proteins, removing amino acids sequentially from those ends.

Peptidases (or proteases)
(E.C.3.4.-.-)

Endopeptidases (or proteinases)
(E.C.3.4.21-99.-)

Exopeptidases
(E.C.3.4.11-19.-)
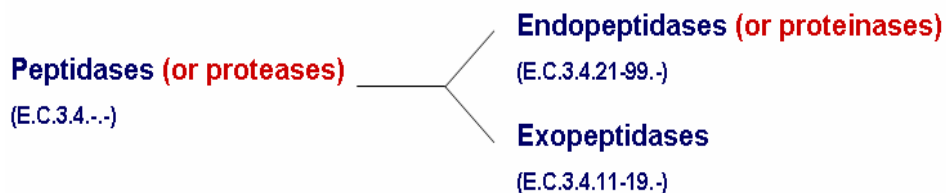
2.1.1   Types of Proteases

On the basis of the mechanism of catalysis, proteases are subdivided into six distinct classes: aspartic, metallo, cysteine, serine, threonine and glutamic proteases so far (Barrett & Rawlings, 1991; Rawlings & Barrett, 1993). Proteases in two classes (aspartic and metalloproteinases) use an activated water molecule as a nucleophile to attack the peptide bond of the substrate, whereas in the remaining classes the nucleophile is a catalytic amino acid residue (Cys, Ser or Thr, respectively) that is located in the active site from which the class names derive. The different classes can be further divided into families on the basis of amino acid comparison, and these families can be assembled into clans on the basis of similarities in their three-dimensional folding.

The most recent release of the MEROPS database (6.2; 24.03.2003) annotates 553 entries for human proteases and homologues in the different catalytic classes. Metalloproteases and serine proteases are the most populated groups, with 186 and 176 members, respectively, followed by 143 cysteine proteases. Threonine and aspartic proteases are highly specialized and are therefore less numerous with 27 and 21 members, respectively.

Serine proteinases are the most intensively studied group of proteins in biology, which is due to their well-characterized, widespread and diverse role in a host of physiological and pathological processes (Walker & Lynas, 2001).

This class comprises three distinct families. The chymotrypsin family which includes the mammalian enzymes such as chymotrypsin, trypsin, elastase, the coagulation cascade proteinases or kallikrein, the subtilisin family which includes bacterial enzymes such as subtilisin and α/β hydrolases family with important human enzymes as dipeptidyl peptidase IV (DP IV) or propyl oligopeptidase (POP).

The general 3D structure is different in the three families but they have the same active site geometry and the catalysis proceeds via the same mechanism. Serine proteinases exhibit different substrate specificities, which depend on the amino acid composition in the various enzyme subsites interacting with the substrate residues.

Three residues which form the catalytic triad are essential in the catalytic process, i.e., His 57, Asp 102 and Ser 195 (chymotrypsinogen numbering).

Cysteine proteinases contain a cysteine residue at the active center. The activity of all these enzymes depends on a catalytic dyad of cysteine and histidine. Cysteine peptidases are widely distributed among living organisms. They have been found in viruses, bacteria, protozoa, plants and mammals. According to the most recent classification (Barrett, 1998b) they can be subdivided into more than 40 different families, which are grouped into 6 clans (CA, CB, CC, CD, CE and CX).

The best known and the best described family of cysteine peptidases is that of *papain* (Drenth et al., 1971). It is the archetypal enzyme of a family of proteinases that includes plant (papain, bromelain) and mammalian enzymes (calpains–calcium activated, cathepsins), as well as proteases from parasites, such as *Trypanasoma* and *Schistosoma*. A second family, with a different fold is represented by caspases (cysteine dependent aspartyl proteinases), such as ICE (interleukin-1β converting enzyme).

Threonine proteinases constitute the newest class of endopeptidases, for which only one family has been identified so far, the multicatalytic endopeptidase complex family of proteinases. The best known example is the yeast 20S proteasome (Groll et al., 1997).

Aspartic proteinases are a group of proteolytic enzymes which (generally) operate at acidic pH. Most of aspartic proteinases belong to the *pepsin* family. The pepsin family includes digestive enzymes (pepsin and chymosin) as well as lysosomal (cathepsins D and E), processing enzymes (rennin) and certain fungal proteases (penicillopepsin, rhizopuspepsin, endothiapepsin). A second family comprises viral proteinases such as the protease from the HIV virus (AIDS) also called *retropepsin*.

2.1.1.1   Metalloproteinases

The Metalloproteinases are probably the oldest class of proteinases. They have been identified in all kingdoms of living organisms, from bacteria, fungi, in green algae and plants, in invertebrates such as *Caenorhabditis elegans,* see urchin, hydra, *Drosophila*, in

10

vertebrates such as frogs, as well as in mammals (Woessner et al*.,* 2000; Sternlicht et al*.,* 2001).

Metalloproteinases differ widely in their sequences and their structures but the great majority of enzymes contain a zinc atom which is catalytically active. In some cases, zinc may be replaced by another metal such as cobalt or nickel without loss of the activity. The catalytic zinc can be bound by various side chains. For example, bacterial thermolysin crystal structure has zinc coordinated by two histidines and one glutamic acid. Many enzymes contain the sequence HEXXH (being X any residue), which provides two histidine ligands for the zinc, whereas the third ligand is either a glutamic acid (thermolysin, neprilysin, alanyl aminopeptidase) or a histidine (astacin). Other families exhibit a distinct mode of binding of the Zn atom.
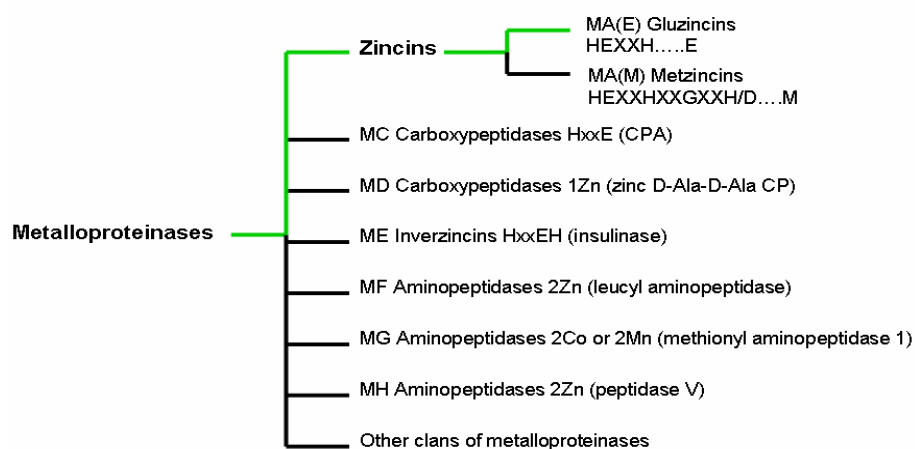
Figure 1. Scheme of metalloproteinases classification. Conserved ion binding motives or metal ions involved in catalysis are indicated beside the family name.

The catalytic mechanism leads to the formation of a non-covalent tetrahedral intermediate after the attack of a zinc-bound water molecule on the carbonyl group of the scissile bond. This resulting intermediate is further decomposed by transfer of the glutamic acid proton to the leaving group (see Figure 2).
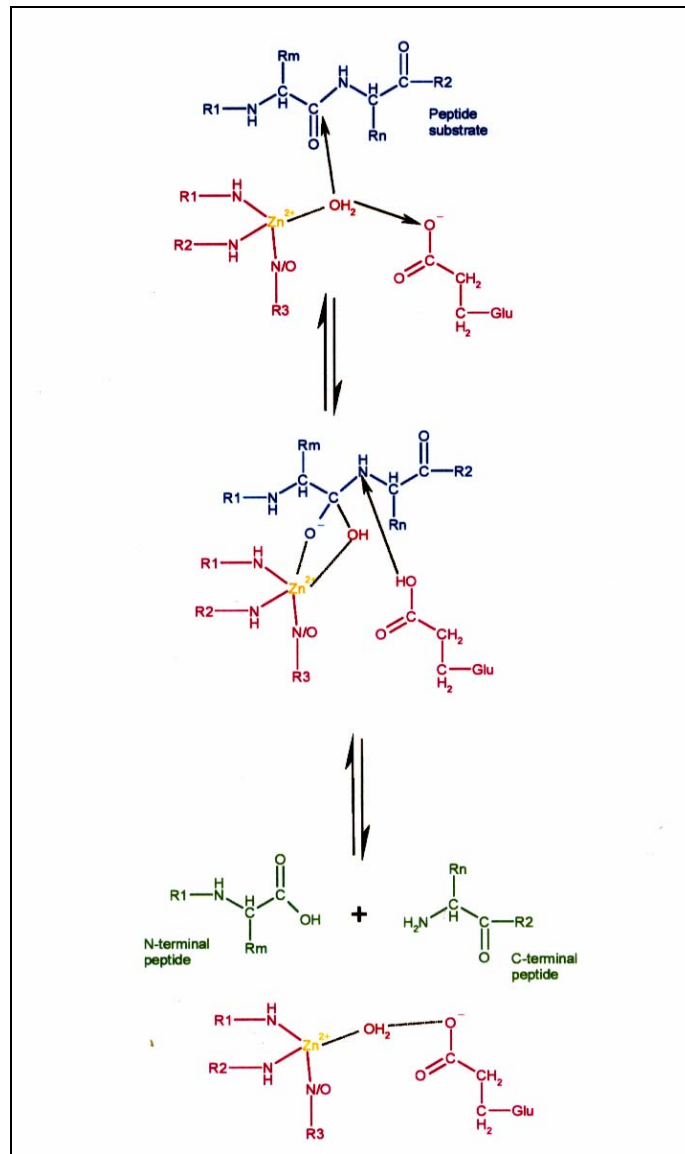
Figure 2. Representation of the activity cascade of metalloproteinases.

The matrix metalloproteinase collectively called matrixins (MMPs), belong to the family of Metalloproteinases. The first matrix metalloproteinases discovered was collagenase, detected in 1962 as a metamorphogenic 'activity' in involuting tadpole tails (Gross J. & Lapiere C. M. 1962).

In mammals, matrix metalloproteinases are either stored in the specific granules of polymorphonuclear leukocytes (MMP-8 and MMP-9), or transported as active enzymes

to the cellular membrane, or secreted as latent pro-enzymes. Some of them are activated during secretion by furin-like serine proteinases (MMP-11, MMP-27 and the MT1-MMP), while the other MMPs are activated in the extracellular space by plasmin and other trypsin-like serine proteinases, or by already activated MMPs. Some of them, are membrane anchored called matrix-type metalloproteinases (MT-MMPs).

The matrix metalloproteinases are ubiquitous and widely involved in metabolism regulation through their ability either to extensively degrade proteins or to selectively hydrolyze specific peptide bonds. They are collectively able to degrade all kinds of extracellular matrix protein (ECM) components such as interstitial and basement membrane collagens, proteoglycans, fibronectin, elastin, aggrecan and laminin, and are thus implicated in the connective tissue remodeling processes associated with embryonic development, angiogenesis, tissue growth, wound healing and so on. Many of these MMPs, however, are also involved in the shedding and release of latent growth factors, growth factor binding proteins, cytokines, and cell surface receptors; in the activation of proMMPs and other pro-proteinases, and in the inactivation of proteinase and angiogenesis inhibitors, thus participating in diverse physiological processes (Murphy & Gavrilovic, 1999; Nagase & Woessner, 1999). Only a few MMPs are expressed at detectable levels in normal, healthy resting tissues, while most MMPs are only expressed in growing cultures, diseased or inflamed tissues, and activated cells.

2.1.1.1.1   Structural features of Matrix metalloproteinases (MMPs)

Structural features of MMPs have been several times well described and characterized (Bode et al., 2004; van den Steen et al., 2002; Overall et al., 2002; Gururajan et al., 1998; Pei et al., 2000). There are twenty-four human MMP genes (three genes for MMP-23) which encode 23 different active MMPs, and they are classified by sequential numbers, which run from MMP-1 to MMP-28, omitting numbers 4 to 6.

MMPs can be divided into eight subgroups, based on their domain structure. All of them contain an N-terminal prodomain (PRO; about 80 amino acid residues) that is required for the correct secretion of the enzymes. The prodomain forms the essential contact through the "cysteine switch" PRCGXPD consensus sequence, blocks the catalytic zinc

ion and thus maintains the latency. The prodomain is followed by a catalytic domain (CAT), which contains the characteristic features of zinc-dependent metalloenzymes. The catalytic center of MMPs contains a zinc-binding **HE**B**XH**X**BGBXH**S motif, where H is histidine, E is glutamic acid, B is a bulky hydrophobic amino acid and S is serine. Only in gelatinases CAT domains contain additional inserts, domains of the fibronectin type II (FN; about 175 amino acid residues). Except MMP-23 (with a different C-terminal domain), MMP-7 and MMP-26, all other human MMPs exhibit an ~195 residue C-terminal hemopexina-like domain (Hpex).
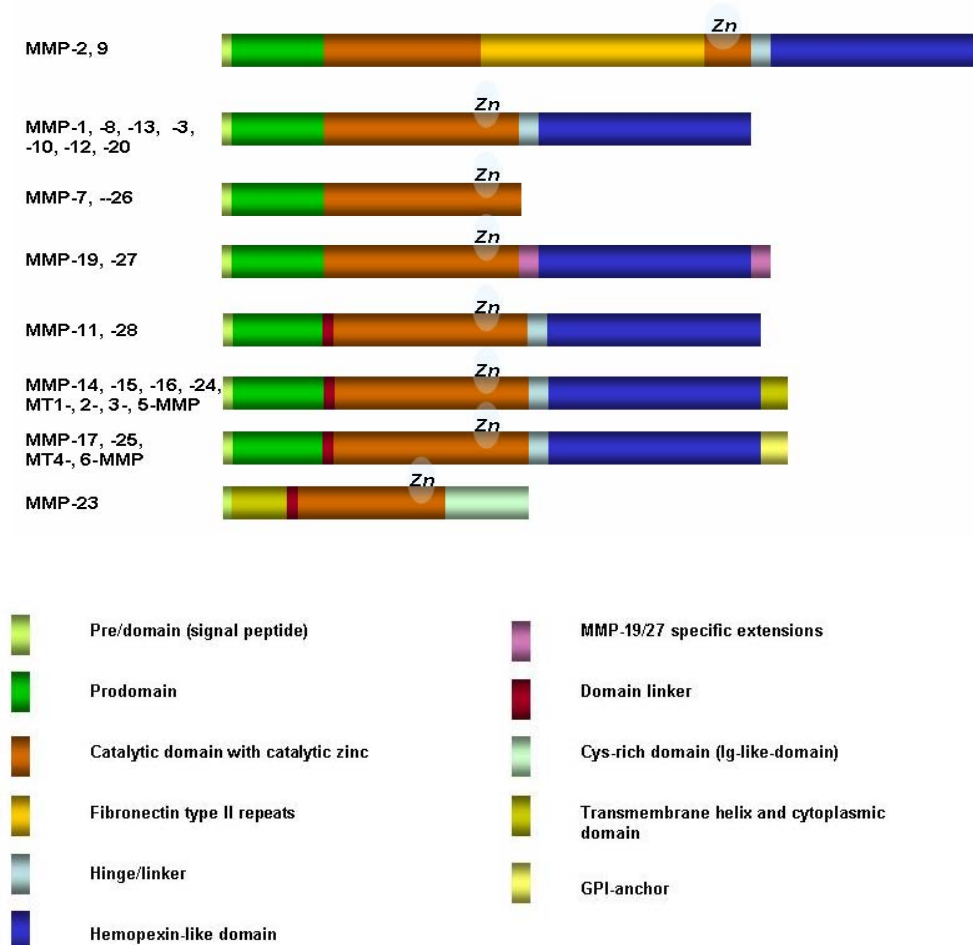
Figure 3. Schematic representation of the domain structure of the human MMPs, grouped according to different domains.

Currently, the only proMMP structures known are those of the C-terminally truncated MMP-3 (Becker et al., 1995), the full-length proMMP-2 (Morgunova et al., 1999) (Figure 4) and proMMP-1 (Jozic et al., 2005).

14
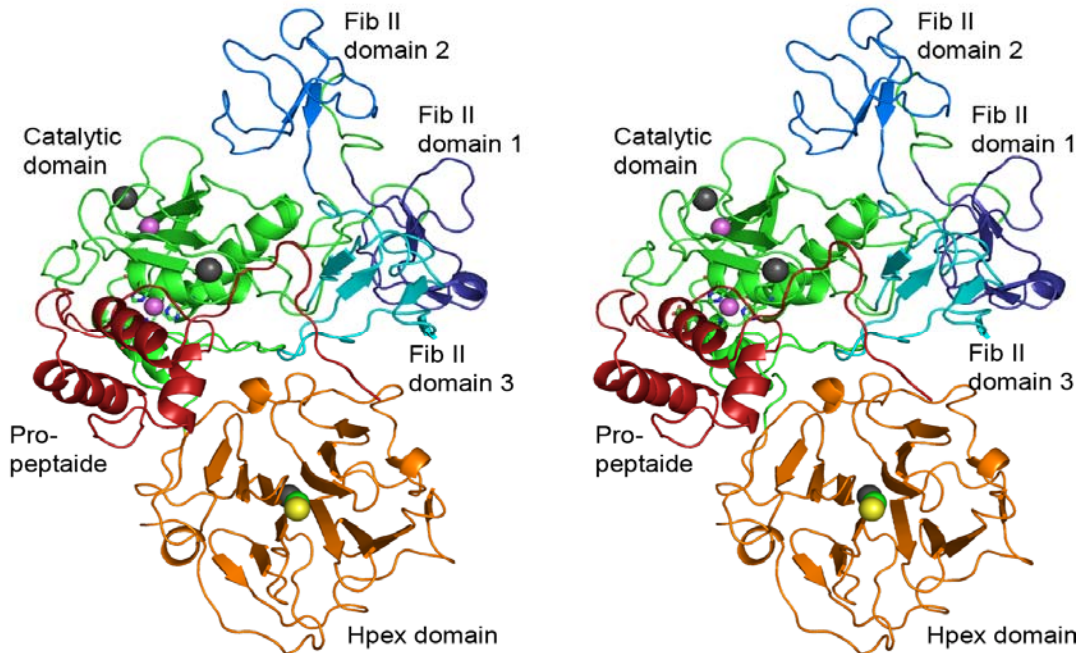
Figure 4. Stereo view of proMMP-2. The prodomain, catalytic domain, fibronectin domains, and hemopexin domain are shown in red, green, blue, and orange, respectively. Zn^{2+} ions are indicated in magenta, Ca^{2+} ions are gray, Na^+ is yellow and Cl^- is green. (Morgunova et al., 1999).

2.2   Gelatinase B (MMP-9)

The Matrix Metalloproteinases (MMPs) form zinc endopeptidase family of which gelatinases A and B (MMP-2, MMP-9) represent the largest and the most complex members. They are called gelatinases, because they preferentially degrade denatured collagen, i.e., gelatine.

2.2.1   Physiological and pathological implications of gelatinases

Gelatinases play a role in a wide variety of physiological and pathological conditions, among which the involvement in cancer has been most extensively studied. The gelatinases are required in invasive processes during reproduction, growth and development, leucocyte mobilization, inflammation and wound healing (Van den Steen et al., 2002). Increased gelatinase activity has been observed in a variety of pathological

conditions including cancer, inflammation, infective diseases, degenerative diseases of the brain and vascular diseases (Van den Steen et al., 2002).

Both gelatinases are implicated in cardiovascular diseases and MMP-9 is involved in the pathogenesis of atherosclerosis (Luttun et al., 2004). However both participate in wound repair (Legrand et al., 1999; and Mohan et al., 2002) and are typically expressed from the beginning to the end of the healing process (Salo et al., 1994). Gelatinases and other MMPs are also able to participate in the regulation of apoptosis and MMP-9 has been observed to decrease cancer-cell apoptosis (Bergers et al., 2000).

2.2.2   Gelatinase B in cancer

Cancer cells grow and divide without normal regulation. They can be local or metastasize. A complex process is involved in the development of metastases: invasion of primary tumor cells, circulation, extravasation, seeding, and proliferation at distant sites (Liotta et al., 1990; Chambers et al., 1997). An essential step involves angiogenesis, recruitment of new blood vessels, for the new lesions. Therapy is aimed to target metastasis and angiogenesis. Until recently, the only treatment of metastatic tumors was cytotoxic chemotherapy.

Gelatinase B is involved in tumor cell invasion and metastasis due to its ability to degrade basement membrane collagenes (Himelsten et al., 1994). There are many different examples of tumors in which specifically gelatinase B expression has been shown to be elevated. For example, increased expression of gelatinase B has been described in brain tumors and cerebrospinal fluid of patients with brain tumors (Rao et al., 1993; Freidberg et al., 1998), in bladder cancer (Davies et al., 1993), basal cells and squamous cell cancers of the skin (Karelina et al., 1993), malignant pigment lesions of the skin (van den Oord et al., 1997), squamous cell carcinomas of the lung (Canete-Soler et al., 1994), colon and breast carcinomas (Zucker et al., 1993), endometrial carcinoma (Takemura et al., 1992), ovarian cancer (Takemura et al., 1994), prostatic carcinoma (Hamdy et al., 1994), pancreatic cancer (Gress et al., 1995), and gastric cancer (Nomura et al., 1996).
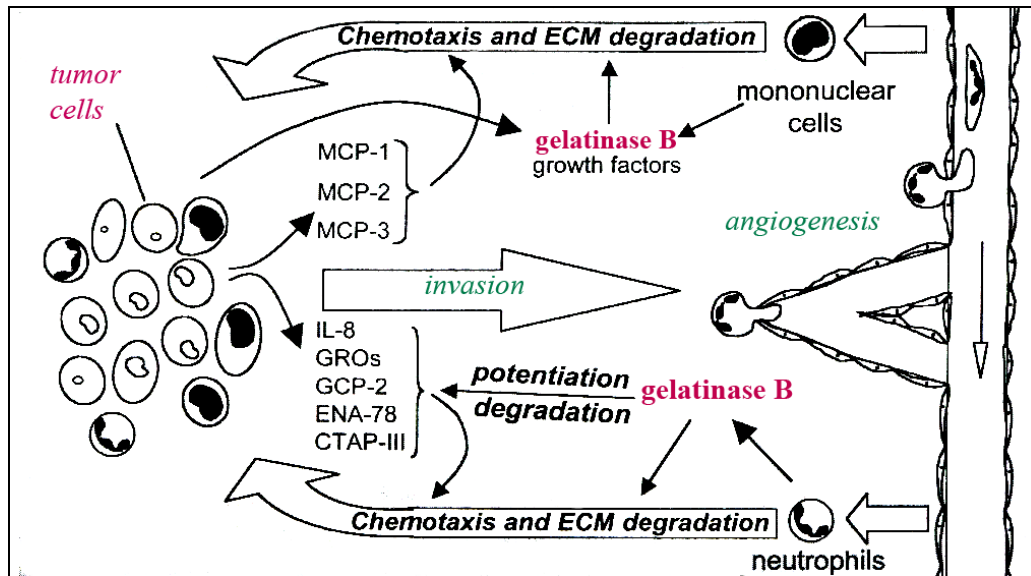
Figure 5. Gelatinase B involved in tumor cell invasion and metastasis (Van den Steen et al., 2002).

Leucocyte gelatinase B assists in the migration of cancer cells. Cancer cells secrete chemokines or instruct stromal cells to produce chemokines. This results in the attraction and activation of leucocytes such as neutrophiles and monocytes. By secreting gelatinase B, the leukocytes degrade the extracellular matrix and create a channel towards the cancer cells. The cancer cells use this path in the opposite direction, resulting in the directional migration towards blood vessels (invasion and metastasis) (Van Coillie et al., 2001). In addition, gelatinase B processes different CXC-chemokines (an unique family of cytokines important in the regulation of angiogenesis), resulting in positive or negative feedback loops, depending on the chemokine, and both gelatinase B and ELR-containing CXC-chemokineses also promote angiogenesis. Gelatinase B may also be produced at the invasion front by the cancer cells or by stromal cells (Figure 5).

2.2.3   Principal features of the human MMP-9

MMP-9 belongs to the family of matrix metalloproteinases. Similar to the other MMPs, the enzyme possesses the common domains including a pre/prodomain, a catalytic domain, a hemopexin domain of 195 amino acids residues (Hpex) and as described above (paragraph 2.1.1.1) a gelatine binding fibronectin domain, composed of three fibronectin-

repeats, inserted between the active-site domain and the Zn^{2+}-binding domain. MMP-9 possesses additionally a unique Ser/Thr/Pro-rich collagen V-like 70 aa residues insertion (hinge region), between the catalytic domain and the C-terminal, hemopexin-like domain.
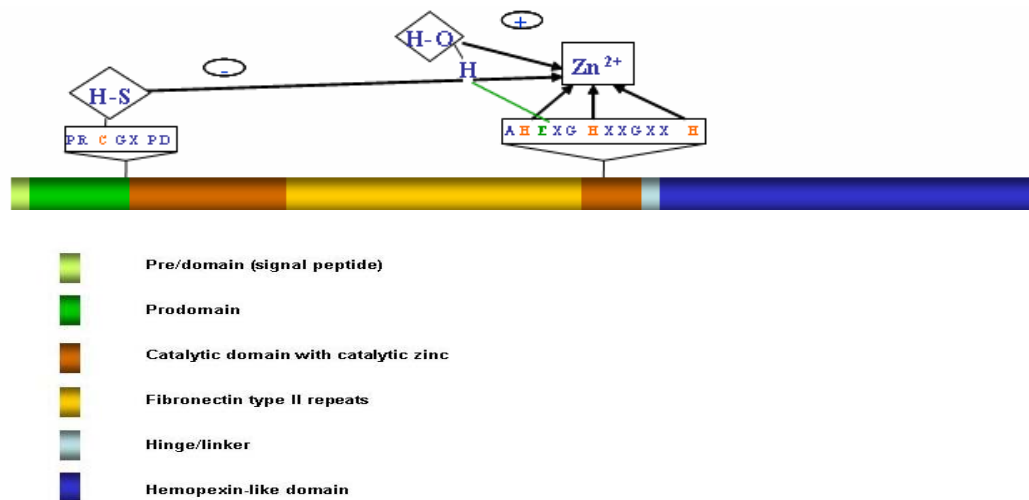
Figure 6. Schematic primary structure of full length MMP-9.

Figures 7a and 7b shows a schematic structural representation of two different constructs revealed in this work. Longer, pro-catalytic MMP-9 (ProMMP9ΔcollVΔpex) and short, "mini" fragment of MMP-9 catalytic domain (Mini-MMP-9). The active wild type as well as an inactive mutant (E402Q) in both cases was studded.

a)

b)
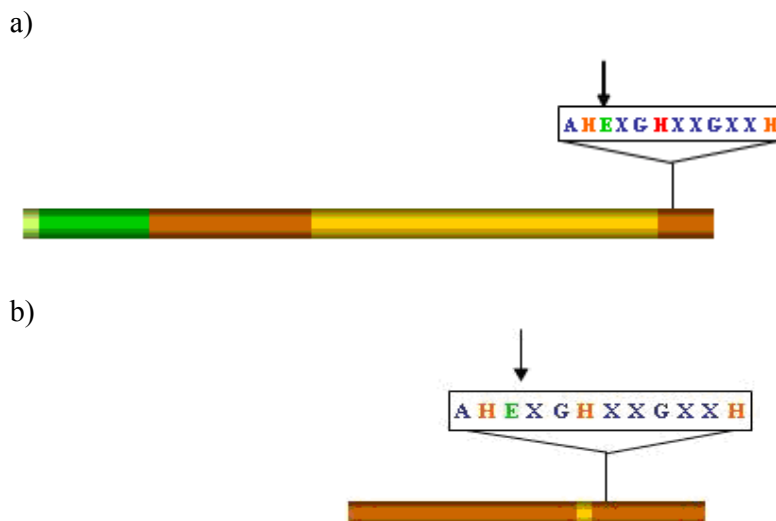
Figure 7. Schematic representation: a) of the ProMMP-9 (ProMMP9ΔcollVΔpex) construct; b) of the Mini-MMP-9 construct.

2.2.4   Substrate specificity of gelatinase

The specificity of proteases is the result of the geometry and the chemical character of various regions which the enzyme interacts with the substrate residues. For this case, a nomenclature was suggested (Schechter & Berger, 1967), which defines the binding site for polypeptide substrates in a protease as a series of subsites, each interacting with different residue of the substrate. The substrate amino acid residues are called P and P' (for peptide) and the subsites in the protease that interact with the substrate are named S and S' (for subsite).
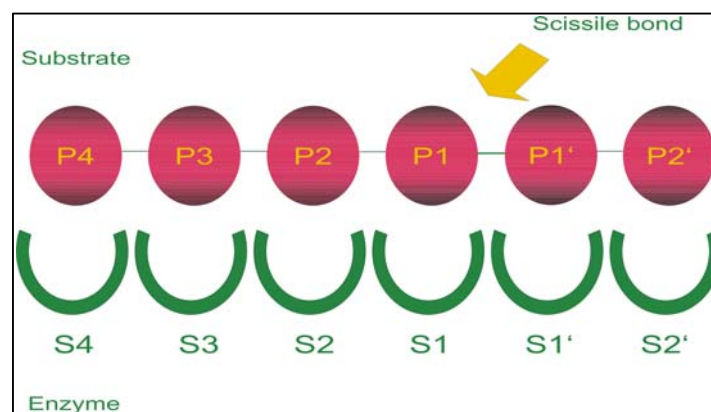
Figure 8. Schematic representation of a protease/substrate interaction, according to the nomenclature of Schechter and Berger (1967). The amino acid residues on the N-terminal side of the scissile bond are numbered P1, P2, P3, P4 ….counting towards the N-terminus and the residues on the C- terminal side of the scissile bond are numbered P1', P2'. Accordingly, the corresponding subsites on the protease are termed S4, S3, S2, S1, S1', S2'.

Gelatinase substrates include a wide variety of proteins including extracellular matrix (ECM) proteins, proteinases, proteinase inhibitors, blood clotting factors, chemotactic molecules, latent growth factors and growth factor binding proteins, cell surface receptors, adhesion molecules and even intracellular substrates. However, the relevance of the rule in vivo is unclear at present. The substrate specificities of MMP-2 and MMP-9 are similar but not identical. The most notable difference is the ability of MMP-1 to degrade human type I collagen. The major difference in the substrate specificity of gelatinases has been attributed to the S2 subsite in the catalytic site, where MMP-9 contains an aspartic acid, and MMP-2 a glutamic acid (Chen et al., 2003).

The specificity depends on the primary sequence of the substrate, because in general, endoproteases possess a clear preference for peptide sequences that can bind in the groove of the catalytic site. However, the three-dimensional conformation and accessibility of the cleavage site in a substrate is important too. Finally, exosites on the enzyme may bind to distant sites on the substrate and also promote hydrolysis.

The strongest amino acid preference was found at the S1 and S1' sites. Only small amino acids (Gly, Ala, Pro) are well tolerated at the P1 site. A possible explanation for this comes from the crystal structure of MMP-8 (Bode et al., 1994), where the S1 site is rather undefined and unable to bind larger amino acids. At the P1' site, a clear preference is noticed for hydrophobic residues (Ile, Leu, Tyr, Met), which is in accordance with the general observation that the S1' site of MMPs consists of a hydrophobic pocket of various depth (Imper and Van Wart, 1998; Rowsell et al., 2002).

The best studied substrates for gelatinase B are denatured collagens (gelatins). The cleavage site of gelatinase B in type II gelatin, a major substrate of neutrophil gelatinase B in rheumatoid arthritis, has been analyzed in detail only recently (Van den Steen et al., 2002). This study confirmed the characteristic specificity of gelatinase B by findings with synthetic peptide substrates, but also provided new important clues. The comparison of the cleavage sites in type II gelatin shows that gelatinase B cleaves collagen type II always after a Gly-residue (P1 position). Recently, the aminoterminal prodomain of procollagen type II was shown to be cleaved by gelatinase B (Fukui et al., 2002). Collagen type V can also be cleaved by gelatinase B (Hibbs et al., 1987); however, it is unclear whether gelatinase B can cleave native full length type IV collagen (Wilhelm et al., 1989; Mackay et al., 1990; Okada et al., 1992). Other extracellular matrix substrates include aggrecan (Fosang et al., 1992), link protein (Nguyen et al., 1993) and elastin (Senior et al., 1991). Human gelatinase B was also shown to degrade myelin basic protein, resulting in the release of encephalitogenic peptides (Proost et al., 1993a).

In addition to these structural components, other gelatinase B substrates are functional proteins. These include the serine protease inhibitors α1-proteinase inhibitor, α1-antitrypsin, and α1-antichymotrypsin (Desrochers et al., 1992; Sires et al., 1994), substance P (Backstrom and Tökés, 1995), galactoside binding proteins CBP30 and CBP35 (Mehul et al., 1994; Ochieng et al., 1994), interleukin(IL)-2 receptor-α (Sheu et

al., 2001), transforming growth factor-β (TGF-β) (Yu and Stamenkovic, 2000), and tissue factor pathway inhibitor (TFPI) (Belaaouaj et al., 2000). It was also found that gelatinase B can degrade amyloid-β peptide (1-40) (Aβ1-40), with possible implications for the pathogenesis of Alzheimer's disease (Backstrom et al., 1996). The proinflammatory cytokine IL-1β is activated (Schönbeck et al., 1998), and angiostatin is cleaved from plasminogen by gelatinase B (Cornelius et al., 1998; Patterson and Sang, 1997). Also, protumor necrosis factor-α (proTNF-α) can be processed by gelatinase B, although with lower efficiency than by other MMPs (Gearing et al., 1994). Recently it was shown that gelatinase B is able to process CXC-chemokines. In particular, gelatinase B cleaves the six aminoterminal amino acid residues from IL-8(1-77), generating the more active IL-8(7-77) and thereby providing a positive feedback loop, because IL-8 is able to induce the release of gelatinase B from neutrophils (Van den Steen et al., 2000). Other CXC chemokines, such as connective tissue activating peptide-III (CTAP-III), growth-related oncogene-α (GRO-α), platelet factor-4 (PF-4) (Van den Steen et al., 2000), and stromal-cell derived factor-1 (SDF-1) (McQuibban et al., 2001) are inactivated. A positive feedback loop was also demonstrated between neutrophil gelatinase B and endothelin-1 (ET-1), because ET-1 (1-32) induces the release of gelatinase B from neutrophils and gelatinase B cleaves big ET-1 into ET-1(1-32) (Fernandez-Patron et al., 2001).

2.2.5   Regulation of gelatinase B activity

2.2.6   Activation of MMP-9 *in vitro* by Trypsin, APMA and Stromelysin

Gelatinase B is a Zn^{2+} and Ca^{2+} dependent endopeptidase that is secreted from cells as an inactive proenzyme. The enzyme can be activated *in vitro* by the proteolytic enzymes trypsin (cleavage at Arg_{87} – Phe_{88}) (Masure et al., 1990; Duncan et al., 1998), chymotrypsin and stromelysin (MMP-3) (Bu et al., 1996). The enzyme can also be converted from a latent to an active form by autocatalytic cleavage of the NH_2– terminal domain, either by a conformational change induced by limited proteolysis of one or more sites within the pro-domain, or by reaction with the organomercurial compounds (4-aminophenylmercuric acetate, APMA) (Birkedal-Hansen 1993). Studies using *pro-MMP-1* (Stetler-Stevenson et al., 1989), MMP-2 (Nagase et al., 1990), and MMP-3 (Springman et al., 1990) reported that fully activated enzymes obtained by APMA treatment all lack the NH_2– terminal pro-peptide including a highly conserved

PRCGVPD sequence. This mechanism described as the "cysteine switch" was suggested to explain the *in vitro* activation of MMPs (Springman et al., 1990; Van Wart et al*.,* 1990). Activation is believed to be initiated by disruption of the interaction of the conserved cysteine in the PRCGVPD sequence with the catalytic zinc, followed by autoproteolytic processing of the NH_2– terminal pro-domain generating an active enzyme species. It was also shown (Chen et al., 1993) that the disruption of the cysteine-zinc linkage is not sufficient to activate proMMP-3 but data emerging from several laboratories suggest a distinct mechanism of activation for gelatinase B (Wilhelm et al., 1989; Triebel et al., 1984; Okada et al., 1992; Mordomi et al., 1992; O'Connell et al., 1994). Based on the NH_2 terminal sequence analyses, it has been demonstrated that the APMA-activated gelatinase B retains the conserved [78]PRCGVPD sequence in the molecule (Wilhelm et al., 1989; Triebel et al., 1984; Okada et al., 1992). Tribel and co-workers (Triebel et al., 1992) have reported that autoprocessing of gelatinase B in the presence of $HgCl_2$ occurs with a four-step truncation if the NH_2 –terminal pro-peptide to Met-75 and a three–step loss of the COOH-terminal fragment to Ala-398, generating a 63-kDa species. Murphy and co-workers (O'Connell et al., 1994) have demonstrated that exposure of gelatinase B to APMA causes rapid self-processing of both the NH_2-terminal pro-peptide and the COOH-terminal domain. However, they concluded that this does not involve the COOH-terminal domain in activation. Together, these data suggest that disruption of the cysteine-zinc interaction is not sufficient to activate pro-gelatinase B and that other factors may play a role in gelatinase B activation.

Pourmotabbed and co-workers (Bu et al., 1996) have studied the mechanism of Ca^{2+} depended activity of human MMP-9. They concluded that activation of the progelatinase B either by 4-aminophenylmercuric acetate (APMA) or chymotrypsin, absolutely required Ca^{2+}, regardless of the pH of the reaction mixture. The trypsin- and stromelysin-activated gelatinases, on the other hand, did not require Ca^{2+} for activity at pH 7.5, but activity of the trypsin-activated enzyme became Ca^{2+} dependent as the pH increased. N-terminal sequencing confirmed that trypsin- and stromelysin-activated enzymes had the same NH_2 termini (Phe^{88}), but APMA and chymotrypsin-activated enzymes had Met^{75} and Gln^{89} or Glu^{92} as the NH_2– terminal amino acid, respectively (Bu et al., 1996).

Proteolytic cleavage of the propeptide of gelatinase B occurs in two steps, with a first cleavage at Gln_{40}-Met_{41} and a second cleavage at Arg_{87}-Phe_{88}, as was shown for the

activation by interstitial collagenase (MMP-1), gelatinase A, stromelysin-1, and collagenase-3 (Sang et al., 1995). The activation of gelatinase B by stromelysin-1 results in a further slow degradation of gelatinase B by cleavage at Pro_{428}-Glu_{429} (Shapiro et al., 1995).

Gelatinase B (and gelatinase A) was also shown to bind to insoluble elastin. When progelatinase B is bound to elastin, it remains completely unaffected by any enzymatic activator. In contrast, gelatinase A, bound to elastin, seems to undergo a fast autoactivation (Emonard and Hornebeck, 1997).

The activation of gelatinase B can also be performed by chemicals, for example organomercurials (APMA, described above), urea and detergents, which probably induce the disruption of the interaction of the Cys in the prodomain with the catalytic Zn^{2+} (Sopata and Maslinski, 1991).

Interestingly, it was also found that gelatinase B can be activated by reactive oxygen species, such as hypochlorous acid. Reactive oxygen may be produced by activated neutrophils, constituting a possible physiological pathway for the activation of neutrophil gelatinase B (Peppin and Weiss, 1986).

Finally, binding of progelatinase B to gelatin or type IV collagen can already confer some activity to the enzyme without proteolytic release of the propeptide (Bannikov et al., 2002).

Different proteases are known to activate gelatinase B, for example, the serine proteases tissue kallikrein (Desrivières et al., 1993), cathepsin G (Sakata et al., 1989), mast cell chymase (Fang et al., 1996), and neutrophil elastase, which is present in azurophilic granules of neutrophils (Ferry et al., 1997). However, different MMPs can also activate each other, resulting in the creation of an activation cascade, or rather an activation network. Figure 9 illustrates known activation ways, so far documented by experimental evidence.

Two major protease families merge into the MMP activation network: the plasminogen activator/plasmin system and the MT-MMPs. Plasminogen can be converted by tissue-

type plasminogen activator (t-PA) or by urokinase (u-PA) into plasmin, which is an activator for different MMPs. These MMPs can activate other MMPs, leading finally to the activation of gelatinase B, which is a terminal member of the activation network as displayed in Figure 10 (Cuzner and Opdenakker, 1999). MT-MMPs contain a furin-sensitive motif in their propeptide, and might therefore be activated intracellularly. The MT-MMPs can activate some secreted MMPs through a complex with TIMP-2, for example, gelatinase A or collagenase-3 (MMP-13), both of which in turn can activate gelatinase B.
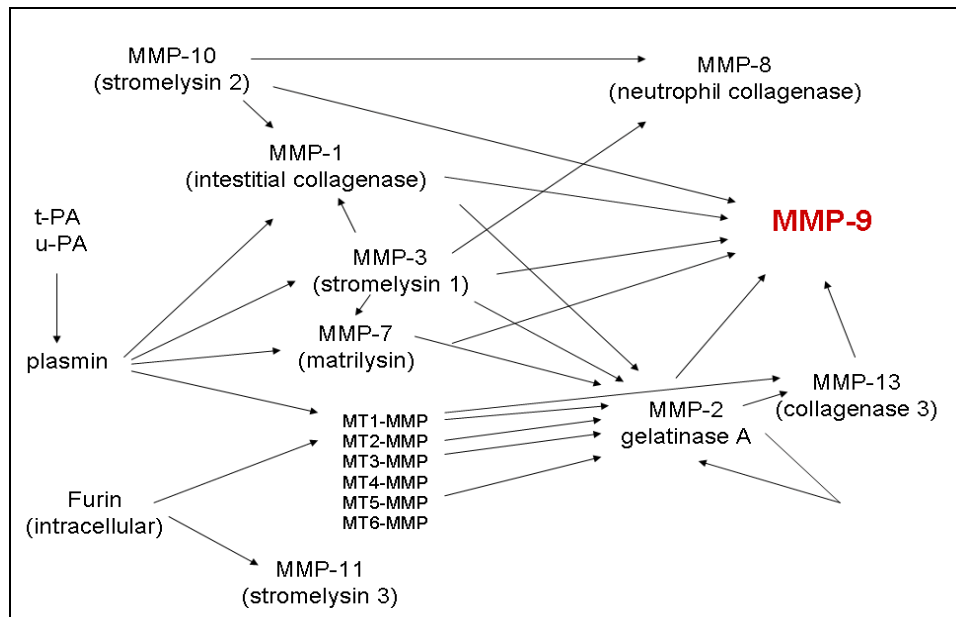
Figure 9. The activation network of gelatinase B by MMPs. Most soluble MMPs are secreted as latent proenzymes that need to be processed for activation. Possible pathways for the activation of gelatinase B by other MMPs are shown. Arrows from one enzyme to another indicate that the active form of the first enzyme converts the proform of the second enzyme to its active form (Van den Steen et al., 2002).

2.2.7   Inhibition of MMP-9

2.2.7.1   Tissue Inhibitors of Metalloproteinases, TIMPs

Physiologically, the proteolytic activity of the MMPs is regulated by their endogenous inhibitors of metalloproteinases, the TIMPs. Disruption of this regulation results in diseases such as arthritis, atherosclerosis, tumour growth and metastasis (Elkins et al., 2002). TIMPs are stable proteins with a molecular weight of 20 to 30 kDa and they

contain six conserved disulfide bridges (Murphy & Willenbrock, 1995). These disulfide bridges belong to six protein loops, of which the first three form an aminoterminal (N-terminal) domain and the others comprise a carboxyterminal (C-terminal) domain. These domains fold independently from each other, and the N-terminal domain is capable of inhibiting MMPs without the C-terminal domain (Zalipsky et al., 1995). The N-terminal domain of 120 amino acids mainly folds as a closed five-stranded ß-barrel, and the C-terminal part of 60 amino acids forms ß-turn (see Figure 10).

The TIMP family currently comprises four members of 184 (TIMP-1) and 194 (TIMP-2, 3, 4) amino acid residues, which are glycosylated (TIMP 1 at two sites) or not (TIMP-2 and TIMP-3), and exhibit 44 to 52 % sequence identity, TIMPs bind MMPs in a 1:1 stoichiometry. Under pathological conditions associated with unbalanced MMP activities, changes of TIMP levels are considered to be important because they directly affect the level of MMP activity.

The first structure of the N-terminal domain of TIMP-2 was solved by NMR (Yamaoka et al., 1994). The first complete structure of TIMP, deglycosylated human TIMP-1, in complex with the catalytic domain of human MMP-3 and of the inhibition mechanism was determined by X-ray crystallographic studies of the TIMP-1–MMP-3 by Gomis-Rüth and co-workers (Figure 11) in 1997 and one year after that of the TIMP-2–MT1-MMP complex was determined by Fernandez-Catalan and co-workers (Fernandez-Catalan et al., 1998).
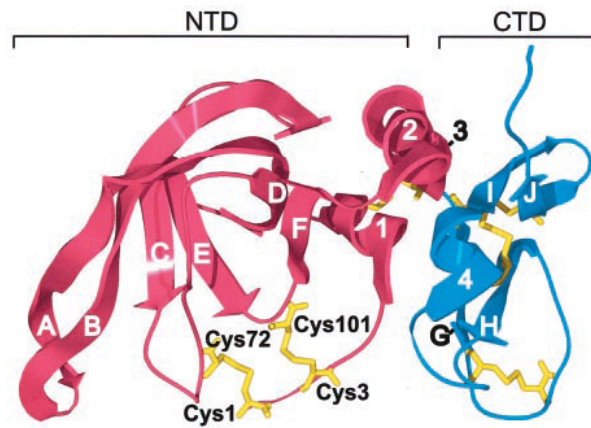
Figure 10. The diagram of TIMP-2 shown as a ribbon model. The disulfide bonds stabilizing the protein are shown. The ß-strands are labelled A through J; the α-helices are numbered 1 through 4 (Fernandez-Catalan et al., 1998).
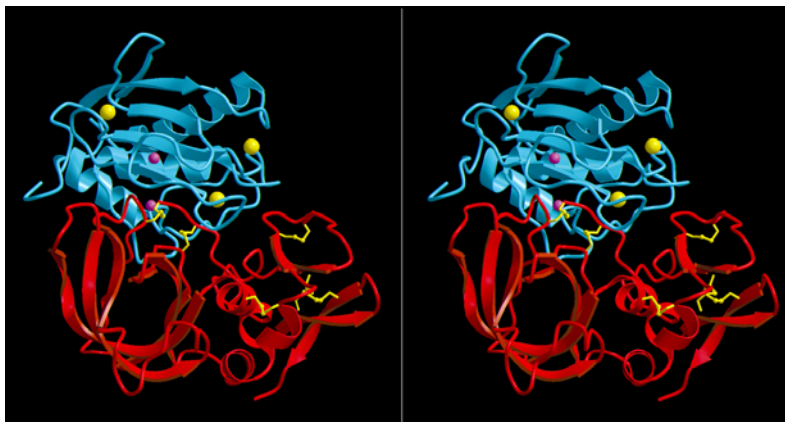
Figure 11. Stereo ribbon diagram of the complex formed between TIMP-1 (red) and the MMP-3 catalytic domain (blue). Yellow bonds indicate disulphide bridges, and the spheres represent the MMP-3 bound 2 zinc (pink) and 3 calcium (yellow) ions (Gomis-Rüth et al., 1997).

Four different TIMP genes and proteins have been described in man, of which TIMP-1 binds with high affinity to gelatinase B, and TIMP-2 and –3 with lower affinity. TIMP-2, –3, and –4 bind with high affinity to gelatinase A. TIMP-1 is an inducible protein, in contrast to TIMP-2, which is constitutively expressed (reviewed in Gomis-Rüth et al., 1997). The inhibition by TIMPs follows the slow tight binding kinetics and is highly complex as different binding sites for TIMPs are present on both gelatinases. Not only the activated gelatinase B can bind to different TIMPs, but the proenzyme is also able to bind TIMP-1 and TIMP-3 (Olson et al., 1997).

Once gelatinase B is secreted and activated, its activity can still be regulated by degradation or inhibition. Gelatinase B is inhibited by α2-macroglobulin, the universal protease-inhibitor present in human serum (Birkedal-Hansen et al., 1993). However, the more specific TIMPs are shown to be more important in regulating their activity (Murphy & Docherty, 1992).

The interaction between pro-gelatinase B and TIMP-1 seems to occur mainly through the C-terminal domains of both molecules, because a C-terminal deletion mutant of TIMP-1 does not bind to progelatinase B (Murphy et al., 1991) and as C-terminal mutants of gelatinase B also do not bind TIMP-1 (Goldberg et al., 1992). Complexes of progelatinase B and TIMP-1 are able to inhibit other MMPs by the formation of a gelatinase B/TIMP-1/MMP complex, indicating that the inhibitory N-terminal domain of TIMP-1 is still available for interaction in the progelatinase B/TIMP-1 complex (Ogata et al., 1995).

Inhibition of the activated gelatinase B, on the other hand, occurs through interaction between the N-terminal domains of TIMP-1 and the active site of the enzyme, as C-terminal deletion mutants of TIMP-1 retain their inhibitory activity against gelatinase B (Murphy et al., 1991). C-terminal deletion mutants of gelatinase B, lacking the hemopexin and collagen type V domains, are less effectively inhibited by TIMP-1, indicating that the C-terminal part is also involved (O'Connell et al., 1994). The N-terminal domains seem to be responsible for high-affinity interaction with TIMP-1 with a dissociation constant in the nanomolar range. In contrast, the C-terminal domains are responsible for low-affinity interaction with a dissociation constant in the micromolar range (Olson et al., 1997). Interaction of gelatinase B with TIMP-2 is mediated by the N-terminal domains of the enzyme and not by the hemopexin domain, as deletion of the latter does not affect the binding of gelatinase B. Moreover, the inhibition of gelatinase B by TIMP-2 is less effective than by TIMP-1 (O'Connell et al., 1994). Also, no interactions of TIMP-2 with progelatinase B were observed (Olson et al., 1997). TIMP-3 is an insoluble ECM-bound MMP-inhibitor with, like TIMP-2, and both possesses a higher affinity for gelatinase A than for gelatinase B. It can bind to both pro-gelatinases and activated gelatinases, and the carboxyterminal domains of both enzymes are important for the interaction with these inhibitors (Butler et al., 1999).

2.2.7.2   Synthetic MMPs Inhibitors (MMPIs)

2.2.7.2.1   First-generation MMPIs

The classification for MMPIs includes the so-called first-generation MMPIs, which are pseudopeptide derivatives based on the structure of the collagen molecule at the site of initial cleavage by interstitial collagenase, and the second-generation MMPIs, which are non-peptide compounds with selective activity against individual MMPs.

Although, for many years complexes with known inhibitors were intensively studied, the inhibition mechanism of MMP-9 is poorly understood. Due to the extraordinary interest in the therapeutic intervention in cancer, over a hundred small low- molecular-weight MMP inhibitors have been designed and synthesized (Whittaker et al., 1999). For example, zinc coordinating groups that have been utilized include hydroxamates (CONH-OH), carboxylates (COO$^-$), aminocarboxylates (NHCOO$^-$), thiols (SH), and phosphinic (phosphinyls) (PO$_2{}^-$) acid derivatives.

Among these, the most widely used in clinical trials was the synthetic, hydroxamate-based inhibitor Batimastat (BB-94) developed by British Biotech (Figure 12). Batimastat was the first synthetic MMP inhibitor studied in humans with advanced malignancies, based on the cleavage site in collagens (Whittaker et al., 1999). Unfortunately, Batimastat is a non-orally bioavailable compound because of its extremely poor water solubility. Structural modifications of Batimastat resulted in synthesis of Marimastat (BB-2516) which was the second most intensive investigated inhibitor of MMPs (Figure 13). In contrast to Batimastat, it was the first orally available MMP inhibitor unfortunately not advanced to phase III clinical trials. These compounds inhibit MMPs potently and specifically.
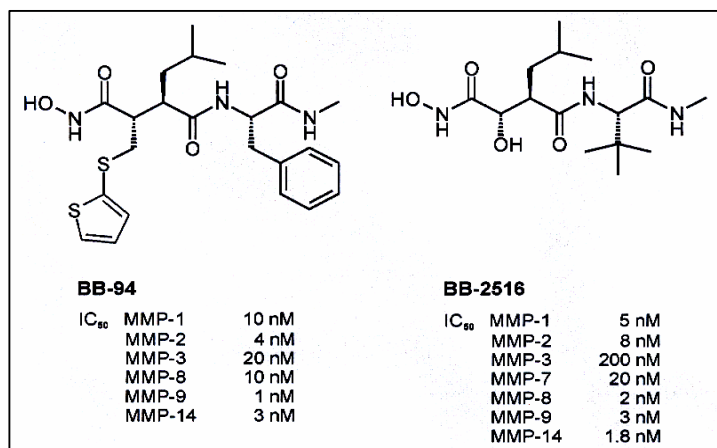
Figure 12. Structures of inhibitors: Batimastat (BB-94) and Marimastat (BB-2516) with inhibition constant (IC$_{50}$) for selected MMPs.

2.2.7.2.2   Next-generation MMPIs

In order to develop non-peptidic MMPIs with a more selective inhibitory profile, a new concept of inhibitor design has been followed. The disclosure of CGS-27023A (Figure 13), a small non-peptide MMPI in the mid-1990's represented a major advanced with this concept. The obvious potential of a small molecule inhibitor to overcome the pharmacokinetic problems associated with peptides, such as poor absorbtion and metabolic lability, attracted the interest of a large number of research groups and has led to several promising compounds based on the sulfonylamino hydroxamic acid scaffold.
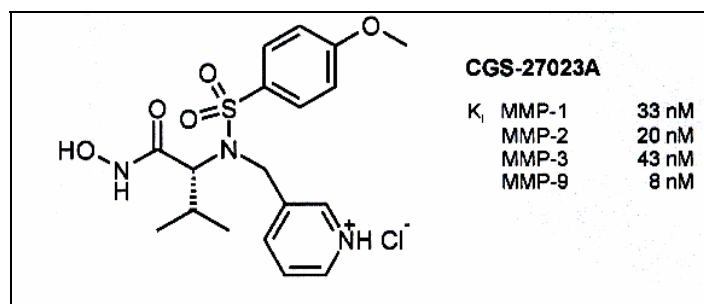
Figure 13. Structure of CGS-27023A, a next generation sulfonylaminohydroxamic acid inhibitor with inhibition constants (K$_i$) for selected MMPs.

Related compounds have also been independently identified by other research groups through "High-Throughput-Screening" (HTS). In general, these inhibitors have a Zinc Binding Group (ZBG) like hydroxamic acid or thiol and a group capable of acting as a Hydrogen Bond Acceptor (HBA), such as sulfone or ketone, both separated by two atoms (Figure 14).
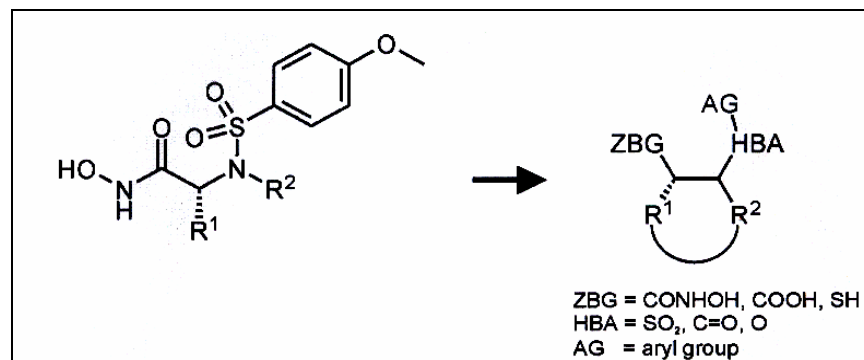
Figure 14. Development of non-peptide MMPIs based on the sulfonyl amino hydroxamic acid scaffold.

The HBA group is typically substituted with an aryl group (AR) which interacts with the S_1' site. In general, the size of this constituent determines the selectivity; monophenyl groups usually cause broad-spectrum inhibition, while larger biaryls, which are often linked through an oxygen, provide selective activity to MMPs with a deep S_1' pocket. Since the R^2 residue usually projects towards the open solvent pocket, a short tether can be attached between R^1 and R^2 to form a small ring.

Representative examples of this series of MMPIs are the biphenylbutyric acid derivative Tanomastat (BAY-129566) developed by Bayer and the heterocyclic sulphonamide Prinomastat (AG-3340) developed by Agouron, Pfizer (Figure 15). Tanomastat is the only MMPI under clinical investigation that is a carboxylic acid. It possesses higher specificity towards MMP-2, MMP-3 and MMP-9, unfortunately the development of this inhibitor was abandoned, because no positive effects could be revealed in human in a clinical phase-III trial (Whittaker et al., 1999; Wojtowicz-Praga et al., 1997). Prinomastat is a rather selective gelatinase inhibitor, which targets MMP-2 and MMP-9, collagenase-3 and stromelysin-1 exhibiting K_i-values in the picomolar range.
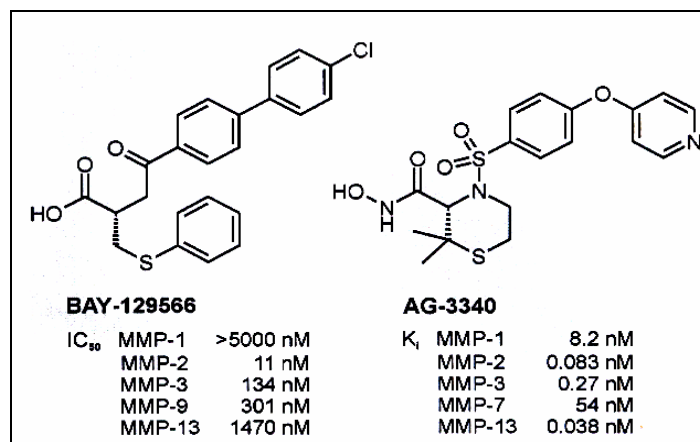
Figure 15. Next generation MMPIs reported to be evaluated in clinical trials. Tanomastat (BAY-129566) and Prinomastat (AG-3340) with IC_{50} and K_i values for selected MMPs, respectively.

Other selective active site inhibitors of gelatinases have been synthesized e.g., N-sulfonylamino acid derivatives (Tamura et al., 1998). They are orally bioavailable and effectively suppress tumor growth in mouse models, but their inhibitory profile towards other MMPs has not been elucidated yet (Tamura et al., 1998). Moreover, inhibitors with a dithiol structure have been identified as selective gelatinase inhibitors (Bernando et al., 2002). Unfortunately, the dithiol moiety in these chemicals induces an irreversible conformational change in the gelatinases (Bernando et al., 2002).

2.2.7.2.3   Bivalent Inhibitors

Even though numerous studies have demonstrated the importance of MMP-9 in cancer and atherosclerosis, and despite many inhibitor studies, no inhibitor was sufficiently specific and efficient for MMP-9.

Determination of the overall tertiary structure of full length MMP-9 has provided important information for the structure-directed design of new enzyme inhibitors directed toward the catalytic site. It has also given us hints for the development of potentially highly selective bifunctional inhibitors capable of differentiating between gelatinases (MMP-9 and -2) and the other enzymes of the MMP family (Elkins et al., 2002).

Indeed the gelatinases 2 and 9 differ from other MMPs mainly by the presence of the three fibronectin type-II (FnII) like domains which are thought to mediate gelatin binding. In the crystal structure of human ProMMP9 (PDB accession code: 1l6j) the three FnII domains aggregate at the tip of the elongated catalytic domain. The propeptide is bound to one side of the catalytic domain while its extended N-terminus reaches out to one of the three FnII domains from the active-site cleft of the catalytic domain where the three helices of the prodomain are clustered. The gap between the third FnII domain and the compact propeptide domain is filled by a bridge of amino acids between the first part of the construct, Val[29], and the first residue of the first helix, Thr[40]. The most relevant feature of this bridge is that on the N-terminal side of the gap, the side chain of Phe[31] is packed against the hydrophobic side chains of residues Trp[372], Phe[379] and Trp[385] of the third FnII domain, as shown in Figure 16.
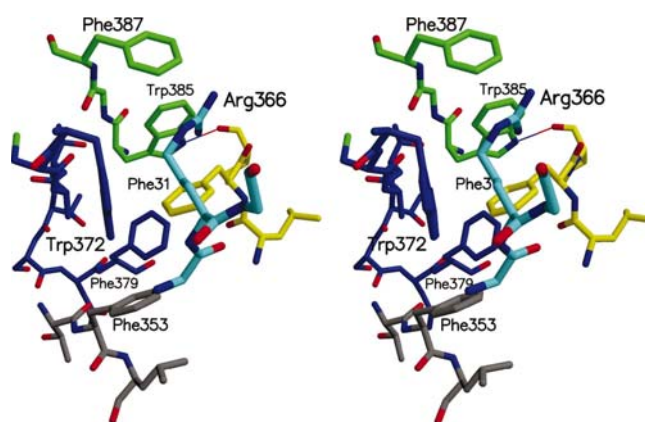
Figure 16. Stereoview of Phe[31] of the Propeptide (light green) that interacts with a cluster of aromatic side chains in the third FnII domain (Elkins et al., 2002).

The design of potential bivalent inhibitors was directed by this interaction between Phe[31] and the aromatic cluster. Modelling experiments suggest that it might serve as anchoring motif, which could introduce a selectivity point for inhibitors specifically designed for gelatinases and would be less potent toward other classes of MMPs.

Most likely, the gain in affinity and selectivity of a bivalent interaction of an inhibitor, compared to a monovalent one, is additionally achieved by exploiting the entropy effect (Mammen, 1998).

Nowadays, two bivalent inhibitors for thrombin based on amidinophenylalanines were synthesized. Finally, in1999 the X-ray structure of the complex was solved and confirmed the expected bivalent binding site (Steinmetzer et al., 1999). Two years later, homobivalent inhibitors were modelled and constructed for human beta-tryptase (Schaschke et al., 2001). The main advantage of bivalent inhibitors is their high selectivity for the target enzyme that can be achieved utilizing the principle of multivalency.

2.3   Membrane-type 1 matrix metalloproteinase (MT1-MMP)

2.3.1   General properties of MT1-MMP

MT1-MMP (MMP14) shares a common domain structure with other MMP family members, including a pre/propeptide, a catalytic domain, a hinge region (linker-1), a hemopexin (Hpex) domain (C319–C508), a stalk (linker-2) region, a transmembrane domain, and a cytoplasmic tail. (Sato et al., 1994; Seiki et al., 2002; Zucker et al., 2003; Itoh et al., 2002) (Figure 17).

Similar to other MMPs, the enzyme is produced as a zymogen and requires an activation step to remove the propeptide proteolytically (Nagase et al., 1997; Seiki et al., 1999). MT1-MMP possesses a basic amino acid motif of RRKR[111] at the end of the propeptide which is cleaved by furin or related proprotein convertases (Sato et al., 1996; Yana et al., 2000). The activation of MT1-MMP takes place during secretion in the Golgi (Mazzone et al., 2004) and the active enzyme is localized on the cell surface.
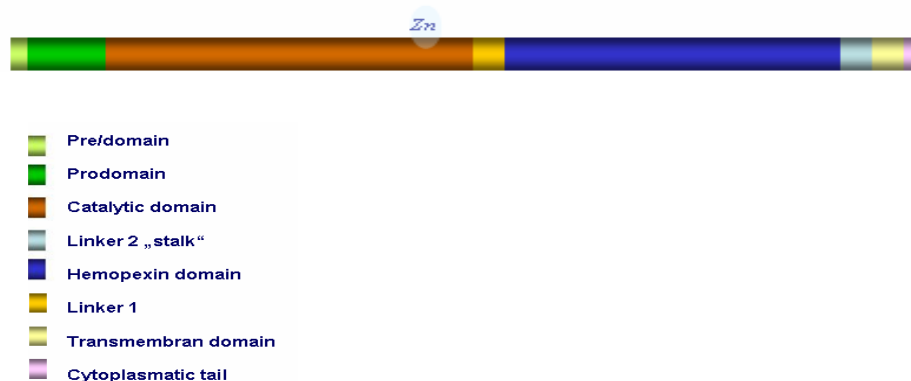
Figure 17. The schematic representation of full length MT1-MMP.

The MT1-MMP displays activity against a variety of extracellular matrix (ECM) proteins including collagen I, II and III (Hotary et al., 2000), laminins 1 and 5 (Koshikawa et al., 2000), aggrecan (Buttner et al., 1998; Fosang et al., 1998), fibrin and fibronectin (Hiraoka et al., 1998; Itoh et al., 2002), vitronectin and lumican (Li et al., 2004). MT1-MMP also activates other MMPs, such as proMMP-2 (Sato et al., 1994) and pro-MMP-13 (Knäuper et al., 1996). Moreover, MT1-MMP cleaves several cell surface proteins such as CD44 (Kajita et al., 2001), transglutaminase (Belkin et al., 2002), low density lipoprotein receptor - related protein LRP (Rozanow et al., 2004), α$_v$ integrin (Deryugina et al., 2002a) and syndecan-1 (Endo et al., 2003) (Figure 18).
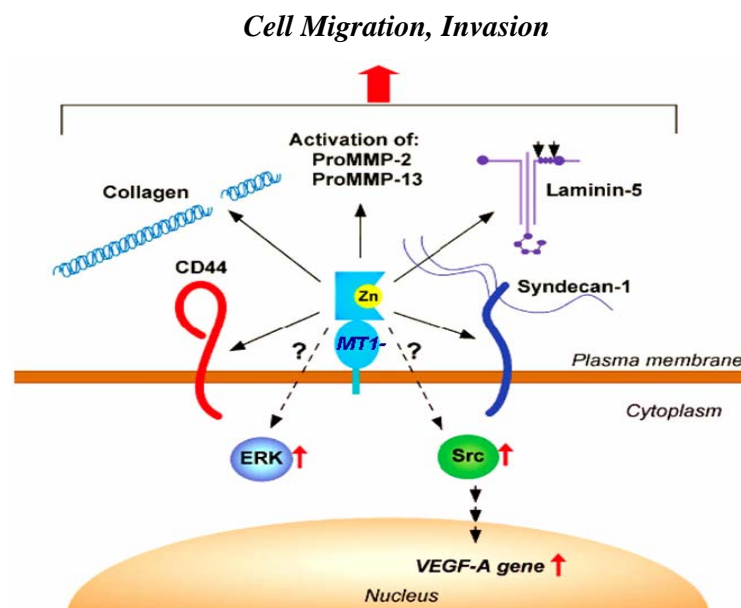
Figure 18. Biological functions of MT1-MMP which promote cell migration and invasion.

2.3.2   MT1-MMP as an important pericellular modifier

2.3.2.1   Cell surface localization of MT1-MMP

When cells migrate in tissue, degradation of ECM barrier is essential, but only in the direction of migration, because the ECM is also an important scaffold. To achieve such focal degradation, cells localize their MT1-MMP at lamellipodia, the migration front of the cells (Sato et al., 1997; Itoh et al., 2001; Mori et al., 2002). This localization is

achieved by interaction of MT1-MMP with CD44 through the Hpx domain of the enzyme and stem region of CD44 (Mori et al*.,* 2002).

MT1-MMP is associated indirectly with *F-actin*, because CD44 in turn is associated with *F-actin* through its cytoplasmic domain by interacting with Ezrin/Radixin/Moesin proteins (Naot et al., 1997).

The interaction of MT1-MMP with CD44 through the Hpx domain of the molecule is also required for CD44 shedding by the enzyme (Suenaga et al., 2004).

It has been also shown that MT1-MMP is colocalized with β1 integrin (Ellerbroek et al., 2001; Wolf et al., 2003). It is not clear whether this is due to a direct or indirect interaction, but these reports suggest that MT1-MMP and ß1 integrin are functioning in the same area on the cell surface.

2.3.2.2   Functions of MT1-MMP

One of the important functions of MT1-MMP is its collagen degradation activity. Collagen is a major ECM component that plays an important role in maintaining tissue architecture and in forming a stable scaffold for cells. Collagen is resistant to most proteinases at neutral pH apart from collagenolytic MMPs (i.e., MMP-1, MMP-2, MMP-8, MMP-13, and MT1-MMP) (Visse et al., 2003). All collagenolytic MMPs cleave interstitial collagen at a specific site, ¾ away from the N-terminus, which then initiates denaturation of triple helical collagen into gelatin, rendering it susceptible to other proteinases (Visse et al., 2003). Among the collagenases MT1-MMP is unique in that it is membrane-tethered (Holmbeck et al., 2004).

MT1-MMP is also important during migration of cells in a collagen matrix. It has been shown that only MT1-MMP can promote cellular invasiveness into collagen I matrix in epithelial cells and fibroblasts (Hotary et al., 2000; Sabeh et al., 2004). Other soluble collagenase MMPs, such as MMP-1, MMP-2, MMP-8, and MMP-13, cannot promote invasion even though they are secreted as an active form under the experimental conditions used (Hotary et al., 2000; Sabeh et al*.,* 2004).

Interestingly, pericellular collagen degradation is essential not only for invasion, but also for tumor cells to grow within a collagen-based 3-D matrix (Hotary et al., 2003). Again, only MT1-MMP as a collagen-degrading enzyme was found to play a critical role (Hotary et al., 2003). The effect of MT1-MMP is specific to 3-D cultures, suggesting that it is acting through pericellular degradation of collagen matrix. Soluble collagenase MMPs (MMP-1, MMP-2, and MMP-13) cannot substitute for MT1-MMP, and without MT1-MMP tumor cells cannot proliferate (Hotary et al., 2003). Though MT1-MMP was originally thought to be involved only in cancer cell invasion for metastasis, these findings suggest that MT1-MMP may also play a role in promoting tumor progression.

Initially, the enhanced invasiveness by MT1-MMP expression was thought to be due to enhanced pericelular ECM degradation allowing cells to migrate through. However, it has became evident that "clearing a path" is not the only mechanism. It was found that shedding of CD44 from the cell surface by MT1-MMP enhances cell migration on a hyaluronan-based 2-D matrix (Kajita et al., 2001). CD44 is a widely expressed major hyaluoran receptor, which interacts with the cytoskeleton through its cytoplasmic domain (Naot et al., 1997).

MT1-MMP is also an important promoter of angiogenesis. Angiogenesis is a formation of new vessels from existing vessel and provides a mechanism to establish blood supply. It is playing an important role in wound healing process, tumor growth, and progression of rheumatoid arthritis. Angiogenesis itself is a process of cellular invasion by endothelial cells. Endothelial cells need to detach from neighbouring cells, invade into stromal tissue, proliferate, and generate a tube structure. During this process, endothelial cells need to degrade basal lamina, fibrin and collagen enriched stromal tissue. Previous reports have shown that MMP-2 (Brooks et al., 1998), MMP-9 (Bergers et al., 2000), and their cognate cell surface receptors such as αvβ3 integrin (Brooks et al., 1998; Silletti et al., 2001) and CD44 (Yu et al., 1999) play a critical role in this process, but Chun (Chun et al., 2004), recently reported that plasmin, MMP-2, MMP-9, β3 intergin, and CD44 are not essential for angiogenesis, in contrast to MT1-MMP.

MT1-MMP also promotes angiogenesis by means other than stimulation of endothelial cell invasion. Expression of MT1-MMP in tumors stimulates angiogenesis in vivo by stimulating vascular endothelial growth factor (VEGF) synthesis from the tumor cells

(Deryugina et al., 2000b; Sounni et al., 2002). The underlying mechanism is not clear, but MT1-MMP activity on the cell surface presumably modifies the immediate microenvironment, which triggers a cell-signalling pathway to produce VEGF-A, that is specifically unregulated by MT1-MMP (Sounni et al., 2004).

MMP-2 degrades type IV collagen, a major component of the basement membrane. As cancer cells needs to transverse the basement membrane to achieve invasion and metastasis, the activation of proMMP-2 by MT1-MMP seams to be a critical step (Seiki et al., 2003). Over-expression of MT1-MMP enhances cellular invasiveness during *in vitro* experiments with Matrigel, a reconstituted basement membrane (Sato et al*., 1994).

2.3.3   Regulation of MT1-MMP; controlling cell functions

2.3.3.1   Inhibition of MT1-MMP activity

Since MT1-MMP is expressed on the cell surface as an active form, inhibition is one of the critical steps to regulate its activity. MT1-MMP is inhibited by the endogenous inhibitors TIMP-2 (Fernandez-Catalan et al., 1998), TIMP-3, and -4, but not by TIMP-1 (Will et al., 1996; Bigg et al., 2001). This TIMP-1 insensitive nature is common to all transmembrane type MT-MMPs (e.g., MT2-, MT3-, and MT5-MMPs) and allows them to work under conditions where high levels of TIMP-1 are present. Another inhibitor for MT1-MMP is *RECK* (reversion-inducing-cysteine rich protein with Kazal motifs), a GPI-anchored glycoprotein (Oh et al., 2001). RECK was originally discovered as a tumor invasion suppressor gene with dual functionality: suppressing MMP-9 expression and inhibiting its enzyme activity (Takahashi et al., 1998). Later, it was also found to inhibit the proteolytic activity of MT1-MMP and MMP-2 (Oh et al., 2001).

2.3.3.2   Proteolytic processing

It has been shown that the 60 kDa active MT1-MMP undergoes further processing to a 44–45 kDa species by MMP-2 or MT1-MMP itself (Lehti et al., 1998; Stanton et al., 1998; Toth et al., 2002). This removes the catalytic domain of MT1-MMP making it inactive, and is a mechanism of downregulation. A high level of 45 kDa form coincides

with high proMMP-2 activation whereas no proMMP-2 activation occurs when the 45 kDa form is not detected besides full length mature MT1-MMP on the cell surface (Lehti et al., 1998; Stanton et al., 1998). Thus, MT1-MMP can be ''functionally active,'' and as a result undergoes further processing, becoming ''functionally inactive''.

This phenomenon suggests that there may be a step which regulates the functional activity after expression of the mature enzyme on the cell surface, and one of the possible mechanisms to achieve this could be a homooligomer complex formation of the enzyme (Osenkowski et al., 2004). In some cells, the whole ectodomain of MT1-MMP was shown to be shed (Toth et al., 2002; Harayama et al., 1999; Toth et al., 2004). The cleavage occurs in the linker-2 region and releases functional MT1-MMP from the cell surface (Toth et al., 2004), which may act as a soluble proteinase in the extracellular milieu.

2.3.3.3   Regulation of MMP-2 activation

ProMMP-2 activation and its regulation is an important step for cancer cells to invade into basal lamina, which has been extensively studied. This process is not a simple interaction of proMMP-2 and MT1-MMP, but involves its endogenous inhibitor TIMP-2 as enhancer (Strongin et al., 1995). MT1-MMP on the cell surface forms a complex with TIMP-2 through the catalytic domain of the enzyme and the N-terminal inhibitory domain of TIMP-2 as an enzyme-inhibitor complex. The exposed C-terminal domain of TIMP-2 has an affinity for the Hpex domain of proMMP-2, resulting in the formation of an MT1-MMP-TIMP-2-proMMP-2 ternary complex (Strongin et al., 1995). Formation of this complex is absolutely essential and proMMP-2 activation does not occur without TIMP-2 (Butler et al., 1998; Kinoshita et al., 1998; Wang et al., 2000) (Figure 19).

Since MT1-MMP in this complex is inhibited by TIMP-2, another MT1-MMP free from TIMP-2 is required to carry out the activation of proMMP-2. To arrange another molecule of MT1-MMP next to the ternary complex of MT1-MMP-TIMP-2-proMMP-2, MT1-MMP forms a homo-oligomer complex through its Hpex domains and/or transmembrane/cytoplasmic domains (Itoh et al., 2001; Lehti et al., 2002). In this complex one of the MT1-MMP molecules acts as a receptor and the other acts as an

activator, forming a proMMP-2 activation complex. This homo-oligomer complex formation is required for the activation process on the cell surface, because separating two MT1-MMPs by overexpressing a catalytic domain deletion mutant of MT1-MMP efficiently inhibits proMMP-2 activation (Itoh et al., 2001).

a)
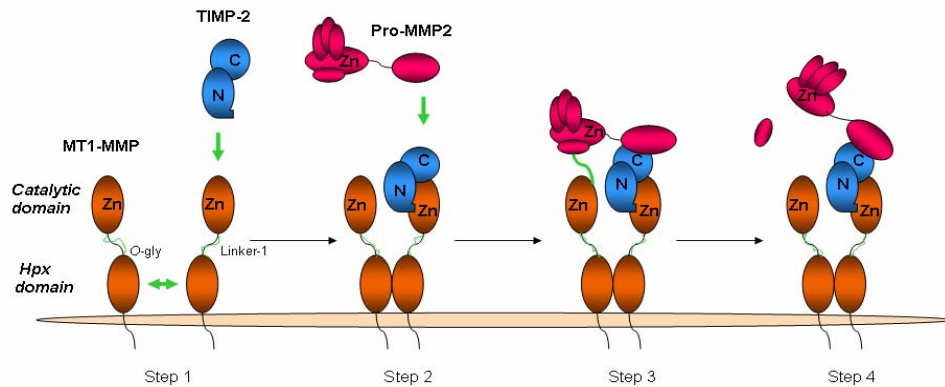
b)
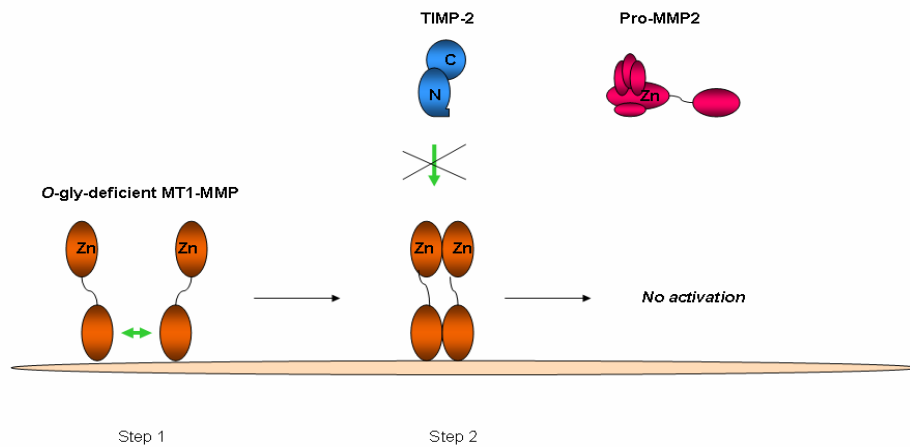
Figure 19. The model of pro-matrix metalloproteinase-2 (ProMMP-2) activation by membrane type-1 matrix metalloproteinase 1 (MT1-MMP), involving homodimer formation via the Hpex domains of MT1-MMP and TIMP-2 binding.

Also the replacement of the Hpex domain with other Hpex domains from MT4-MMP (Itoh et al., 2001) or MMP-2 (Cao et al., 2004) significantly inhibits the activation, presumably because the homo-oligomer complex can not be formed any more.

Another report demonstrates that an Hpex domain-deleted mutant of MT1-MMP activates proMMP-2 (Wang et al., 2004a), which may be attributed to the transmembrane/cytoplasmic domain-mediated interactions for the homo-oligomer complex formation (Lehti et al., 2002).

Nevertheless, Overall and coworkers (Overall et al., 2000) have suggested that MT1-MMP may not form homophilic dimer or oligomer complexes. They had investigated intermolecular interactions in the MMP-2 activation complex between the TIMP-2 C-domain and the MMP-2 hemopexin C-domain. Interestingly, using recombinant MT1-MMP hemopexin C-domain, no direct role for the dimer form of MT1-MMP in the cell surface activation of proMMP-2 was found. Moreover they have suggested, that the MT1-MMP hemopexin C-domain did not form homodimers nor did it bind the gelatinase A hemopexin C-domain, the C tail of TIMP-2, or full-length TIMP-2. Hence, the ectodomain of the remnant 44-kDa form of MT1-MMP appears to play little if any role in the activation of gelatinase A favouring the hypothesis that it accumulates on the cell surface as an inactive, stable degradation product.

Wang and co-workers (Wang et al., 2004) have provided direct evidence to show that the conserved hemopexin domain of MT1-MMP is not required for its activity toward MMP-2, yet is essential for MT1-MMP mediated invasion and growth in three-dimensional type-1 collagen matrix. Furthermore, deletion of the hemopexin domains in MT-MMPs does not impair their ability to activate proMMP-2.

Because growth and invasion in a three-dimensional model may correlate with tumor invasiveness *in vivo*, they (Wang et al., 2004) suggested that the hemopexin domains of MT-MMPs should be targeted for the development of anti-cancer therapies by employing screening assays developed for three-dimensional models rather than their enzymatic activity toward proMMP-2.

Chapter 3   Experimental Procedures

3.1   Molecular biology methods

3.1.1   Cloning

All the molecular biology methods described below were performed basically according to the standard procedure (Sambrook et al., 1989 and Shipley et al., 1996). All instruments and buffers used in experiments were sterilized with 70% ethanol or autoclaved as applicable. The *cDNA* of human full length MMP-9 was kindly provided by T. Pourmotabbed (Pourmotabbed et al., 1994).

3.1.1.1   Mini-catalytic domain of MMP-9 (miniMMP-9)

The fibronectin type II-like repeats of the 92-kDa gelatinase, which split the catalytic domain, were deleted by recombinant PCR. The region of the catalytic domain (CD) 5' close to the fibronectin type II-like repeats was amplified with the primers 5'-CTGTGCAT-GGATCCAAACTTTGA-3' and 5'-CGAGGAACAAACTGTATCCGACGCCCTTGCCC-AGGG- 3'. The introduction of the *NcoI* site in the 5' primer created an additional Met-Gly dipeptide at the N terminus in order to start translation at this point within the cDNA. The 3' region to the fibronectin type II-like repeats was amplified with the primers: 5'-CCCT-GGCAGGGCGTCGGATACAGTTTGTTCCTCG- 3' and 5'-CAACTCTCGAGTCAACC-ATAGAGGTGCCG- 3'. A stop codon was placed in the 3'- primer after residue 443, thereby eliminating the collagen type V and hemopexin-like domains.

The PCR products were purified using QIAGEN Kit and the two products were annealed to each other by virtue of the complementary design with the internal PCR primers and amplified using the outside primers. The final PCR products were digested with *NcoI* and *XhoI* and subcloned into the pET-14b vector (Novagen) for expression in *E. coli.* The resulting fragment coded for a protein lacking residues 217–390 of the parent molecule which encompass the three fibronectin type II-like repeats. Thus, the 92 CD contained residues 110–216 of the parent molecule fused to residues 391–443. Constructs were confirmed by DNA sequencing.

3.1.1.2   Pro-catalytic MMP-9 (Pro-MMP-9; ProMMP9ΔcollVΔpex)

For pro-catalytic MMP-9, specific primers of human MMP-9 were designed. Primer 1: 5'-GCAATTACTGATACCATGGCCCCCAGACAGCGCCAGTCCACCCTTG-3'
incorporates sequences for a unique *NcoI* site and an initiating methionine. Primer 2: 5'-GCGACGGCATCACTCGAGGTCGACTCAACCATAGAGGGCCGGATGCCATTCAC-GTCGTCC- 3' incorporates sequences for a stop codon and a unique *SalI* site. Using these two primers, a 1275 bp DNA fragment was obtained by polymerase chain reaction (PCR). These fragments were digested with *NcoI* and *SalI* restriction enzymes and ligated into the *NcoI* and *SalI* sites of the T7 expression vector, pET-28a (Novagen). The correctness of the sequence was confirmed by DNA-sequencing.

3.1.2   Plasmid Preparation and restriction analysis

Glycerol cultures of the transformed *E. coli* strain DH5α (Novagen) were grown overnight at 37° C in 150 ml LB medium with 100 µg/ml ampicillin. After centrifugation, plasmid DNA was extracted from the cells following the Qiagen Mini Prep Kit protocol and stored at –20 °C.

Plasmid DNA was incubated for 3 h with 1-2 U of the required restriction enzyme per µg DNA in the buffers recommended by the manufacturer.

3.1.3   Agarose Gel Electrophoresis

Agarose gel electrophoresis was used for separation and detection of DNA fragments of different lengths. To prepare an agarose gel a mixture of 0.7% agarose (*w/v*) (Biozym) with TAE-buffer was warmed in the microwave oven until the agarose was completely solubilized. Ethidium bromide was added to a final concentration of 0.5 µg/ml. The mixture was poured in an electrophoresis chamber, which had been previously sealed with custom-made dams. After solidification at room temperature, the gel was covered with TAE-buffer. The DNA samples were mixed with 6x gel loading dye buffer and pipetted in the corresponding gel wells. The gel was electrophoresed at constant 50 V and DNA bands were visualized under UV light ($\lambda = 254$ nm).

- TAE-buffer: 1.0 mM EDTA
                20 mM Acetic Acid
                40 mM Tris/HCl, pH 8.0

- 6x Gel Loading buffer: 0.2 g Bromophenol Blue
                0.2 g Xylene Cyanol
                10 ml 1x TAE-buffer
                80 ml Glycerin (87 %)

3.1.4   *E. coli* Transformation by Electroporation

50 µl electrocompetent cells were thawed on ice and mixed with 2 µl plasmid DNA. The cell/DNA mixture was pipetted into an electroporation cuvette (Biorad) at 4 °C. The cells were electroporated at 1650 V in a gene pulser. One ml LB medium was added to the electroporated cells and the suspension transferred into a culture tube was incubated by shaking for 1 h at 37 °C. The incubated cells were subsequently plated or further grown liquid cultures.

3.1.5   Cell Cultures; plate, liquid and glycerol cultures

For plate cultures, autoclaved LB medium with 15 g/l agar was cooled to 50 °C, mixed with 100 µg/ml ampicillin (or 30 µg/ml kanamycin) and poured into sterile plates. After solidification, plates were stored at 4 °C. For growing colonies, ampicillin-resistant bacteria were plated and incubated at 37 °C overnight.

Liquid cultures were prepared as follows: five ml autoclaved LB medium supplemented with 100 µg/ml ampicillin (LB/amp medium) were inoculated with a single colony picked from an agar plate. After overnight incubation at 37 °C, the resulting incubated pre-culture was used either for plasmid preparation or for inoculation of larger cultures in ratios of 1:100 to 1:1000.

For long term storage (6 months), 150 µl glycerin (87% *v/v*) was mixed in sterile conditions with 0.85 ml of an exponentially growing cell culture. The mixture was immediately shock-frozen in liquid nitrogen and stored at –80 °C.

3.2 Protein chemical and biochemical methods

3.2.1 Mini-MMP-9

3.2.1.1 Expression and refolding

The resulting mini-MMP-9 catalytic domain construct in pET-14b was transformed into the *E. coli* BL21 (DE3) strain (Novagen) for expression. Colonies were grown in 1 litter of Luria-Bertani (LB) media containing 100 µg/ml ampicillin to the logarithmic phase and induced with 0.4 mM isopropyl-1-thio-b-D-galactoside (IPTG) for 4 h.

After centrifugation, the pellet was resuspended in 50 ml of 50 mM Tris/HCl, pH 7.5, 10 mM $CaCl_2$, 30 mM NaCl and sonified 4 x 5 min on ice. Urea in the same buffer was added to a final concentration of 6 M, and the extract was rocked gently at 4 °C overnight, prior to centrifugation at 20,000 x g for 40 min. Subsequently, the sample was refolded by dialysis against stepwise urea concentration reduction (4 M, 2 M, and 1 M) in the same buffer containing 20 mM $ZnCl_2$ and 0.05% Brij 35 and finally against urea-free buffer (50 mM Tris/HCl, pH 7.5, 10 mM $CaCl_2$, 30 mM NaCl, 0.05% Brij 35, in which $ZnCl_2$ was omitted). Afterwards, the protein was dialyzed against 20 mM Tris/HCl, pH 7.5, 10 mM $CaCl_2$, and 30 mM NaCl buffer.

3.2.1.2 Purification and protein concentartion

The refolded protein was purified to homogeneity by affinity chromatography with the Sepharose-coupled hydroxamate inhibitor (Pro-Leu-Gly-NHOH) (Moore et al., 1986). This purification procedure allows selecting the properly folded catalytic domain of MMP-9. Then the protein was eluted from the column with a buffer containing 100 mM Tris/HCl pH 10.0 and dropped directly into 400 mM Tris pH 7.0 buffer. Each fraction was immediately pooled and concentrated for crystallization to 2.0 mg/ml.

Purified protein was concentrated using the centrifugation concentrators Centriprep for volumes of 15 ml or Centricon for volumes less than 2 ml (Millipore, Eschborn). The finally

concentrated protein samples were filtrated through an Ultrafree (Millipore, Eschborn) 0.22 µm membrane in order to remove suspended particles.

3.2.1.3   Determination of protein concentration

The UV absorption and the Bradford method were used to measure protein concentration. For proteins with known amino acid composition and size the molecular absorption coefficient can be calculated according to Pace et al., (1995). Aromatic amino acid residues strongly absorb UV radiation, especially tryptophan (maximum at 280 nm) followed by tyrosine (at 274 nm) (Brown, 1980). The absorption of the protein solution at 280 nm (A_{280}) is photometrically measured. The protein concentration was then calculated using the Lambert Beer's law:

$$A = \varepsilon \cdot c \cdot l$$

where A is the absorbance,

ε - absorption or extinction coefficient of the compound,

c – concentration (usually in units of molarity, mol/liter),

l – is the pathlength (in cm) of the light through the solution

The colorimetric Bradford method often used for protein concentration determination measures the maximum absorption for acidic solution of Coomassie Brillant Blue G-250 (Bradford 1976) which shifts from 465 nm to 595 nm upon binding to the protein. Both hydrophobic and ionic interactions stabilize the ionic form of the dye, causing a visible colour change. A calibration curve is prepared with bovine serum albumin (BSA) as a standard protein. The method was performed according to the recommendations of the suppliers of the Bio-Rad Kit.

3.2.1.4   Electrophoresis of proteins on SDS-polyacrylamide gels (SDS-PAGE)

The "discontinuous electrophoresis" according to Laemmli (1970) uses two gel layers of different composition: the upper stacking gel is a low percentage polyacrylamide gel of 5%

polyacrylamid AA (PAG) with a pH of 6.8 where the proteins are concentrated, the lower separation gel is a higher percentage of polyacrylamide gel e.g., 12% AA, with a pH of 8.8, where the proteins are separated. The percentage of sodium dodecyl sulphate (SDS) in both gels ensures that all proteins are denaturated and negatively charged so that the separation depends only on their size.

The separation gels applied were usually in the range of 15% or 12 % polyacrylamid to achieve better resolutions depending on the molecular mass of the proteins to be analyzed. The samples were always mixed with the same volume of sample buffer and heated for 2-5 min at 95 ºC. For analysis of the total protein content before and after expression, about 10^8 cells were pelleted, resuspended in 10 µl of sample buffer and heated as described above. In addition, a sample containing a protein mixture of known composition (molecular weight marker; Broad Range SDS-Marker, BioRad, Munich) was included in all experiments to determine molecular masses of proteins in the neighboring lanes. Electrophoresis was performed at 100 V for the stacking gel and at 150 V (or 200 V) for the separation gel. The proteins were visualized by Coomassie Blue staining (Schägger *et al.,* 1987), which enables the detection of microgram amounts. Finally, destaining buffer was used to wash repeatedly the gels until the background Coomassie was completely removed.

- 1x Loading Dye Buffer (for 5ml):   0.31 ml 1 M Tris/Cl, pH 6.8

    0.1% Bromophenol Blue

    1.0 ml 10% SDS

    0.58 ml 87% Glycerol

    0.25 ml *ß*-mercaptoethanol

    2.9 ml H_2O

- Separating Gel (for 8 gels): 20 ml 1.5 M Tris/Cl, pH 8.8

    32 ml 30% AA/0.8% Methylene bis-AA

    24.4 ml H_2O

    0.8 ml 10% SDS

    0.8 ml 10% APS (added immediately before mixing)

    32 µl TEMED (added immediately before mixing)

- Stacking Gel (for 8 gels): 3.75 ml 1.0 ml Tris/HCl pH 6.8

    5.1 ml 30% AA/0.8% Methylene bis-AA

                    20.4 ml H_2O

                    0.3 ml 10% SDS

                    0.3 ml 10% Ammonium peroxodisulfate, APS (added
                    immediately before mixing)

                    30 μl TEMED (added immediately before mixing)

- Running Buffer: 0.1% (*w/v*) SDS

                    25 mM Tris-HCl, pH 8.3

                    200 mM Glycine

- Staining Solution: 0.1% Coomassie Brilliant Blue R-250

                    12.5% (*v/v*) Acetic acid

                    25% (*v/v*) Ethanol

- Destaining Solution: 2.5% (*v/v*) Acetic acid

                    25 (*v/v*) Ethanol

3.2.1.5   Protein Transfer and Western Blots

Proteins were transferred from a non stained polyacrylamide gel to a polyvinylidenfluoride
(PVDF) membrane by electroblotting in a Trans-Blot transfer cell (Towbin et al., 1979).
Prior to use, the hydrophobic PVDF membrane was submerged in 60% methanol solution
for 1 min, shortly washed with distilled water and incubated in transfer buffer for 5-20 min.
The blotting layer sequence in the transfer cell was from bottom (positive electrode) to top
(negative electrode) as follows:

- 9 sheets of Whatman 3MM paper (Maidstone, UK) prewetted in
  transfer buffer (1 min),
- 1 sheet of PVDF membrane (pretreated as described above),
- the polyacrylamide gel,
- 6 sheets of Whatman 3MM paper prewetted in transfer buffer.

Protein transfer and fixation to the PVDF membrane were carried out by electroblotting for
1.5 h with 50 mA (approximately 0.8 mA/cm^2). The membrane was stained for 1 min in the
membrane staining solution, washed with the membrane destaining solution and air-dried.

- Transfer Buffer: 25 mM Tris/HCl, pH 8.0

    20 mM Glycine

    20% Methanol

- Membrane Staining Solution: 0.1% Coomassie Brilliant Blue R-250

    10% Acetic acid

    50% (*v/v*) Methanol

- Membrane Destaining Solution: 7% Acetic acid

    30% (*v/v*) Methanol

3.2.1.6   Protein analytical work

3.2.1.6.1   N-terminal amino acid sequencing

To demonstrate the identity of the purified recombinant protein, N- terminal amino acid sequencing was performed. For this purpose the protein band was eluted from the PVDF membrane and subjected to Edman degradation (Edman et al., 1967) coupled to RP-HPLC in an automatized procedure as described by Hewick (Hewick et al., 1981).

The HPLC analysis and the amino acid sequence determination of protein samples was performed by Dr. Mann, at the Max-Planck-Institute for Biochemistry, Martinsried.

3.2.1.6.2   Mass spectroscopy

Mass spectrometry (MS) allows high-accuracy determination of the ion mass in the gas phase based on the measurement of their mass-to-charge ratio. Analyte ions can be transferred to the gas phase from liquid or solid samples through techniques such as electrospray or MALDI (matrix assisted laser desorption ionization). The matrix assisted laser desorption ionization is a soft technique that allows the mass determination of large biological molecules such as proteins, since the molecule being ionized does not fall apart or break-up during the process (Karas and Hillenkamp, 1990).

The molecular masses of purified protein samples were determined by MALDI mass spectrometry, which was gently carried out by E. Weyher-Stinge (Department for Organic Chemistry, Max-Planck-Institute for Biochemistry, Martinsried).

3.2.1.6.3   Circular dichroism

Far-UV circular dichroism (CD) spectra were recorded with a J-715 spectropolarimater (JASCO, Tokyo, Japan) at a protein concentration of 0.2 mg/ml in an 0.02 cm cuvette. The protein was dialyzed over night against a buffer containing 20 mM Tris/HCl, pH 7.5, 10 mM $CaCl_2$ and 30 mM NaCl. Near-UV CD spectra were recorded in a 1 cm cuvette. For higher accuracy the protein concentration was determined by UV spectroscopy. For interpretation of the CD-spectra the program CDNN (Bohm et al., 1992) was used.

3.2.1.7   Kinetic measurement

3.2.1.7.1   Theoretical aspects of protease-inhibitor interactions

Substances that decrease an enzyme's activity are known as inhibitors. *Irreversible* inhibitors normally form covalent bonds with the enzyme. *Reversible* inhibitors are characterized by the formation of equilibrium between the complexed and the free form of enzyme (E) and inhibitor (I).
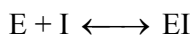
$$E + I \longleftrightarrow EI$$

This equilibrium is characterized by the inhibition constant,

$$K_i = \frac{[E] \cdot [I]}{[EI]}$$

which is the dissociation constant of the enzyme–inhibitor complex.

Reversible inhibitors

Most inhibitors studied in this work are reversible inhibitors. Competitive inhibitors bind to the active site of the enzyme in place of the substrate if the concentration of bound inhibitor [EI] is negligible with respect to the total concentration of the inhibitor, reversible inhibition can be described by the classical equation:

$$\frac{V_i}{V_o} = \frac{1}{1 + \dfrac{[I_t]}{K_{i(app)}}} \qquad \text{where} \quad K_i = \frac{K_{i(app)}}{[S]/K_M + 1}$$

$[S]$-   initial substrate concentration

K_M-   Michaelis Menten constant

K_i-   real inhibition constant

V_i-   activity of the reaction in the presence of inhibitor

V_o-   initial activity in the absence of inhibitor

$[I_t]$-   total concentration of inhibitor (free and bound)

$K_{i(app)}$-   apparent inhibition constant at substrate concentration $[S]$

Irreversible inhibitors

Formation of the irreversible, covalent enzyme-inhibitor complex EI* proceeds via at least one intermediate non-covalent enzyme-inhibitor complex, according to the mechanism as follows:

$$E + I \xleftrightarrow{\quad K_i \quad} EI \xrightarrow{\quad k_2 \quad} EI^*$$
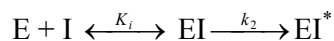
where K_i is the dissociation constant for the intermediate complex and k_2 is the first order rate constant for the formation of EI*, the inactive enzyme-inhibitor complex.

3.2.1.7.2   Activity assay of Mini-MMP-9 *in vitro*

The proteolytic assay performed in this work was based on the cleavage of fluorogenic peptide *Substrate 1* (Bachem AG) amidated at their C-terminus, Dnp-Pro-(ß-

cyclohexyl)Ala-*Gly-Cys*(Me)-His-Ala-Lys(N-Me-Abz)-NH$_2$ where Nma-N-methylanthra-nilic acid is a fluorophore and a Dinitrophenyl-Dnp group as a quenching component. The cleavage site is the peptide bond between Gly and Leu.

The enzyme activity was measured continuously in a spectrofluorimeter using a thermostated one cell sample fluorimeter with an excitation wavelength at 280 nm and emission wavelength at 340 nm. The substrate was used at a final concentration of 10 µM in a total 500 µl reaction mixture. The corresponding assay buffer (200 mM NaCl, 50 mM Tris/HCl, 5 mM CaCl$_2$, 20 µM ZnSO$_4$, 0.05% Brij 35, pH 7.6) and the substrate were mixed and equilibrated at 25 ºC. The enzyme reaction was started by addition of the purified enzyme to the mixture of buffer/subtrate or buffer/subtrate/selective inhibitor (at the time t=0 min).

3.2.2   Pro-MMP-9

3.2.2.1   Expression

For expression in *E. coli*, a few clones were transformed into the BL21 (DE3) expression strain (Novagen). For induction, a single colony was picked from a freshly streaked plate, inoculated into 20 ml LB containing 30 µg/ml kanamycin and incubated overnight with shaking at 37 ºC. 1.0 ml of the overnight culture was then added to 1000 ml LB medium plus kanamycin and incubated by shaking at 37 ºC until the OD$_{595}$ reached 0.6 to 0.7. IPTG from a 100 mM stock was added to the culture with a final concentration of 0.4 mM. During incubation, aliquots were taken at 2, 3, 4 and 6 h following IPTG induction. Samples were placed on ice for 5 min and the cells were then harvested by centrifugation at 5000 g for 5 min at 4 ºC. The supernatant was removed and the cell pellet was used for SDS-PAGE. The remainder of the cells were stored at -80 ºC for further analysis.

3.2.2.2   Purification and refolding

The *E. coli* cell pellet was suspended into 200 ml of 25 mM Na$_2$HPO$_4$, 150 mM NaCl pH 7 (PBS) and sonicated 4 x 5 min on ice. After centrifugation at 16,000 *x* g for 90 min, the pellet was suspended using the tissuemizer into 250 ml of PBS containing 10 mM DTT, 1

mM EDTA and processed through the cell disrupter once. Following centrifugation at 26,000 g for 30 min, the washed lysate pellet was solubilized using the tissuemizer in 200 ml of freshly prepared 8 M urea, 25 mM Tris/HCl, 10 mM DTT, 1 mM EDTA, pH 7.5. The suspension was stirred overnight at room temperature on a stir plate, and then centrifuged at 26,000 x g for 30 min. The supernatant containing solubilised denatured pro-MMP-9 was filtrated using a 1.2 mm PVDF, a low-protein-binding membrane (Millipore). The filtrate was assayed for protein concentration according to the method of Bradford using the Bio-Rad protein-assay reagent and bovine serum albumin (Pierce) as a standard reference. The denatured protein solution (1.3 mg/ml, 200 ml) was applied at a linear flow rate onto a Resource Q column, (Pharmacia) pre-equilibrated in 8 M urea, 25 mM Tris/HCl pH 7.5 (buffer A). Following a wash to baseline OD_{280} with buffer A, bound pro-MMP-9 was eluted at a linear flow rate (2 ml/min) using a 10 column volume gradient (60 ml) of buffer A containing 0.25 M NaCl pH 7.5. Column fractions (2 ml) containing pro-MMP-9 were pooled based on purity as judged by a 12 % acrylamide SDS-PAGE gel. The pooled pro-MMP-9 protein was slowly added dropwise to a stirred room-temperature solution of 20 mM Tris/HCl, 200 mM NaCl, 5 mM $CaCl_2$, 1 mM $ZnCl_2$, 0.7 M L-arginine, 10 mM reduced (GSH) and 1 mM oxidized (GSSG) glutathione pH 7.5 to yield a maximum of 15 µg/ml protein in solution. After stirring overnight at room temperature, the solution was concentrated to one third of the total volume with a YM-20 membrane (Amicon). After filtration the enzyme concentration was determined. The enzyme was dialyzed overnight against 5 l of 20 mM Tris/HCl, 100 mM NaCl pH 7.5 buffer at 4 ºC. If required the enzyme was additionally purified on Superdex 75 column, pre-equilibrated in 50 mM Tris/HCl, 100 mM NaCl and 10 mM $CaCl_2$ pH 7.5 buffer.

3.2.2.3   Functional characterization

3.2.2.3.1   Kinetic measurement

The proteolytic assay performed in this work was based on the cleavage of the Fluorogenic Peptide Substrate 1, Mca-P-L-G-L-Dpa-A-R-NH_2 (Biotech R&D Company). The peptide substrate contains a highly fluorescent 7-methoxycoumarin group that is efficiently quenched by resonance energy transfer to the 2,4-dinitrophenyl group. The cleavage site is the peptide bond between Gly and Leu. The enzyme activity was measured continuously in

a spectrofluorimeter using a thermostated sample plate reader with excitation at 320 nm and emission at 405 nm. The substrate was used at a final concentration of 10 μM and the protein at a concentration of 0.5 nM in a total 200 μl reaction mixture. The corresponding assay buffer (200 mM NaCl, 50 mM Tris/HCl, 5 mM $CaCl_2$, 20 μM $ZnSO_4$, 0.05% Brij 35, pH 7.6) and substrate were mixed and equilibrated at 25 °C. The enzyme reaction was started by addition of the purified enzyme to the mixture of buffer/substrate/selective inhibitor at the time t=0 min.

3.2.2.3.1.1 Trypsin and APMA activation assay

The activation of *pro*-MMP-9 was performed by Trypsin and by *p*-aminophenyl-mercuric acetate (APMA). APMA from a 10 mM stock solution in dimethylsulfoxide (DMSO) was added to MMP-9, to a final concentration of 1 mM. The mixture was incubated at 37 °C for 2 to 24 hours. Trypsin (solved in 20 mM Tris/HCl, 150 mM NaCl, 10 mM $CaCl_2$, pH 7.5) activation assays were performed in protein buffer (20 mM Tris/HCl, 100 mM NaCl, pH 7.5) with trypsin at a concentration of 10 μg/ml. The mixture was incubated for 2 to 24 hours at room temperature. The concentration of active MMP-9 was determined prior to the proteolytic assay performed for mini-MMP-9 (described in 3.2.1.7.2) and by SDS-PAGE.

3.2.2.3.1.2 Inhibition assay

Inhibition assays were performed by using Fluorogenic Peptide Substrate 1, Mca-P-L-G-L-Dpa-A-R-NH_2 (Biotech R&D company) as substrate (see 3.2.2.3.1). The assay was performed in the buffer (200 mM NaCl, 50 mM Tris/HCl, 5 mM $CaCl_2$, 20 μM $ZnSO_4$, 0.05% Brij 35, pH 7.6) with a number of inhibitors, and Batimastat (BB-94) as a standard and three potential bivalent inhibitors: Al134 Peg_4, Al134 Peg_6 and Al134 Peg_8 synthesized in collaboration with Dr. A. Barazza/Prof. L. Moroder in the department of Organic Chemistry, MPI of Biochemistry, Martinsried. The assay buffer and substrate were mixed and equilibrated at 25 °C. The enzyme reaction was started by addition of the inhibitor to the mixture of buffer/substrate/purified and activated by APMA enzyme at the time t=0 min. The prodomain was cleaved by APMA at 37 °C and incubated for several hours. As a reference Batimastat was used in the concentration range of 0.1 to 10.0 nM. Respectively,

the three potential bivalent inhibitors were tested in the range of 0.1 to 50.0 nM of total volumne and the protein in the range of 0.5-1.0 nM.

3.2.3   MT1-MMP Hpex domain

3.2.3.1   Analysis of the oligomeric state in solution

The Hpex domain of MT1-MMP has been prepared and provided by Dr. Yoshifumi Itoh from the Department of Matrix Biology Kennedy Institute of Rheumatology, Faculty of Medicine, Imperial College, London.

It has been expressed in the human 293 embryonic kidney cells line as a catalytic domain, transmembrane/cytoplasmic domain-deleted mutant of MT1-MMP. During the secretion process, the pro-peptide has been processed by pro-hormone convertases, thus the secreted protein does not contain a pro-domain. A FLAG-tag (DYKDDDDK) has been inserted immediately downstream of the propeptide, therefore, the FLAG is located at the very N-terminus of the purified protein.

The Hpex domain of MT1-MMP was stored in 50 mM Tris/HCl pH 7.5, 150 mM NaCl, 10 mM $CaCl_2$, 0.02% NaN_3, TCN and dialysed against 20 mM Tris/HCl pH 7.5 for further experiments.

In order to investigate the oligomeric state of MT1-MMP Hpex domain in solution, gel filtration experiments and analytical sedimentation equilibration runs were conducted.

3.2.3.1.1   Gel filtration chromatography

Gel filtration chromatography was performed at room temperature using a Superdex 75 HR 10/30 column (1 x 30 cm, Amersham-Pharmacia, Freiburg) connected to the Äkta FPLC (Amersham Pharmacia Biotech AP, Uppsala, Sweden). The column was calibrated with globular protein size standards (Fluka, Neu-Ulm; BioRad, München, Germany). The protein standards used for calibration were as follows: bovine γ-globulin (158 ka), albumin (67),

ovoalbumin (44 kDa), chymotrypsin (25 kDa), equine myoglobin (17 kDa), ribonuclease (13,7 kDa) and cyanocobalamin (Vitamin B-12) (1.35 KDa).

MT1-MMP Hpex samples in concentrations between 0.1 and 0.4 mM in the buffer, 20 mM Tris/HCl pH 7.5 were incubated at 25°C for 15 min and then applied in a maximum volume of 100 μl aliquot to the column and eluted at a flow rate of 0.5 ml/min. The void volume (V_o) was determined with chymotrypsin (25 kDa; Fluka, Neu-Ulm, Germany), the total volume of the liquid phase (V_t) with buffer. The apparent M_r values were extracted from plots of log (M_r) against volume (V_t) of the buffer;

$$K_{av} = \frac{(V_e - V_o)}{(V_t - V_o)}$$

(where V_e is the analyse elution volume).

3.2.3.1.2   Molecular weight determination by analytical ultracentrifuge analysis; Sedimentation Velocity and Sedimentation Equilibrium

The analytical ultracentrifugation is one of the most versatile, rigorous and accurate methods for determining the molecular weight of a protein or other macromolecule. There are two basic types of experiment performed with the analytical ultracentrifuge.

In the sedimentation velocity experiment, an initially uniform solution is placed in the cell and a sufficiently high angular velocity is used to cause relatively rapid sedimentation of the solution towards the cell bottom. This produces a depletion of solute near the meniscus and the formation of a sharp boundary between the depleted region and the uniform concentration of sedimenting solution. The rate of movement of this boundary can be measured and leads to the determination of the sedimentation coefficient, *s*, which depends directly on the mass of the particles and inversely on the frictional coefficient, which is in turn a measure of effective size. Measurement of the rate of spreading of a boundary can lead to a determination of the *diffusion coefficient, D*, which depends on the effective size of the particles:

$$D = \frac{RT}{NF}$$

where R is the gas constant,

T the absolute temperature.

The ratio of the sedimentation to diffusion coefficient gives the molecular weight:

$$M = \frac{s^0 RT}{D^0(1 - v\rho)}$$

where M is the molar weight of the protein,

v its partial specific volume,

ρ is the solvent density.

The superscript zero indicates that the values of s and D, measured at several different concentrations, have been extrapolated to zero concentration to remove the effects of interactions between particles on their movement (Freifelder et al., 1970; Van Holde et al, 1975).

In sedimentation equilibrium experiments, a small volume of an initially uniform solution is centrifuged at a somewhat lower angular velocity than is required for a sedimentation velocity experiment. As the solution begins to sediment towards the cell bottom and the concentration at the bottom increases, the process of diffusion opposes the process of sedimentation. After an appropriate period of time, the two opposing processes approach equilibrium, and the concentration of the solute increases exponentially towards the cell bottom. Measurement of the concentration at different points leads to the determination of the molar weight of the sedimenting solute. It can be shown that, for a single, ideal, nonassociating solution:

$$M = \frac{2RT}{(1 - v\rho)\omega^2 x d(\ln c)/dr^2}$$

where M is the protein molar weight (in g/mol),

ω the angular velocity of the rotor,

c the concentration of the solute (in g/L) at a radial distance,

r the distance from the axis of rotation.

This means that a plot of log (concentration) *versus* (radius)^2 for a single, ideal solute at sedimentation equilibrium yields a slope proportional to the molar weight. Alternatively, one can fit the data of *c versus r^2* to find the least squares best estimate of *M*(1 - *v* ρ).

Sedimentation velocity and sedimentation equilibrium runs were carried out on an analytical ultracentrifuge (model E; Beckman instruments, Inc., Fullerton, CA) equipped with electronic speed and temperature control and photoelectric scanner. The buffer used in all the sedimentation experiments contained 20 mM Tris/HCl pH 7.5. The density of this buffer was measured with a pycnometer at 20°C.

Experiments were carried out by Dr. G. Wiegand (Department of Organic Chemistry, Max-Planck-Institute for Biochemistry, Martinsried).

3.3   Protein crystallography methods

3.3.1   Mini-MMP-9

3.3.1.1   Crystallization

The catalytic domain of the MMP-9 mutant (E402Q) inhibitor complexes were crystallized by the sitting drop vapour diffusion technique. Crystallization trials were carried out in CrysChem plates (Charles Supper Company, Natick, USA) at 20 ºC. To cover a broad spectrum of buffers, precipitation agents and salts, crystal screenings were performed using the House Factorials (in-house made crystal screen) and several Crystallization Kits (Hampton Research, Laguna Hills, USA). Promising conditions were optimized independently varying several parameters (e.g., pH, protein concentration, salt concentration, additives) as well as by trying different protein to solution drop ratios.

3.3.1.2   Co-crystallization of miniMMP-9 complexes with different inhibitors

For co-crystallization experiments 10 mM stock solutions of the inhibitors were prepared by dissolving them in different solutions. The inactive E402Q mutant was co-crystallized with the following synthetic inhibitors:

- the barbiturate inhibitor 5-(4-phenoxyphenyl)-5-(4-pyrimidine-2-yl-piperazin-1-yl)-pyrimidine-2,4,6-trione *(RO206-0222),* provided by Dr. H.W. Krell, Roche, Penzberg; it was dissolved in 10% of DMF and 90% of Na_2CO_3;

- the phosphinate inhibitor [2-[1-Carbamoyl-2-(1*H*-Indol-3-yl)-ethylcarbamoyl]-3-(3-phenyl-isoxasol-5-yl)-propyl]-phenyl-phosphinic acid *(AM409),* provided by Dr. V.Dive, Saclay/A. Yotakis, Athens; it was well soluble in H_2O;

- the carboxylate inhibitor 3-(1*H*-indol-3-yl)-2-(4'-iodo-biphenyl-4-sulphonylamino)-propionic acid *(An1),* provided by R. Oltenfreiter, Gent; dissolved in DMSO;

- the hydroxamic acid inhibitor, 2-Amino-3,3,3-trifluoro-*N*-hydroxy-2-(4-phenoxy-benzenesulfonylmethyl)-propionamide *(MS560),* provided by Dr. M. Zanda, Milano; it was disolved in DMF;

- the hydroxamic acid inhibitor, 3-(4-methoxyphenylsulfonyl)-4,4-difluoro-*N*-hydroxybutanamide *(MJ24),* provided by Dr. M. Zanda, Milano; it was disolved in DMF.

An aliquot of 1 μl of protein/inhibitor solution in 20 mM Tris/HCl, pH 7.5, 10 mM $CaCl_2$, 30 mM NaCl buffer containing 2 mg/ml protein and 0.5 mM of each inhibitor was mixed with 1 μl of reservoir buffer. The final crystallization conditions read as follow:

- for the **RO206-0222** inhibitor 0.1 M citric acid/NaOH pH 5.0, 3.0 M NaCl;

- for **AM409** 0.1 M Tris/HCl pH 8.0, 3.0 M NaCl;

- for **An1** 0.1 M Hepes/NaOH pH 8.0, 4.0 M NaCl;

- for **MS560** 0.1 M Hepes/NaOH pH 7.0, 3.0 M NaCl;

- for **MJ24** 0.1 M Citric Acid pH 4.0, 3.0 M NaCl.

3.3.1.3   Data collection and structure determination

Crystals appeared after 4-12 weeks incubation at room temperature. They were transformed to solutions of the mother liquor after adding 20% ethylen glycol and flash frozen in a nitrogen gas stream at 100 K. Data sets between 2.0 and 2.2 Å resolution were collected using synchrotron radiation of the wavelength (λ) of 1.05 Å at the beamline BW6 of the Deutsches Elektronen Synchrotron (DESY in Hamburg, Germany), employing a Mar Research CCD detector. All crystals belong to the tetragonal space group $P4_12_12$ with two molecules of 18 kDa in the asymmetric unit. This corresponds to the solvent content of 54.8 to 56.0 % (v/v).

All datasets were indexed and integrated using the programs DENZO/SCALEPACK (Otwinowski and Minor, 1993) or MOSFLM6.11 (Leslie, 1991). Molecular replacement solutions were found with the program MOLREP (CCP4; Bailey, 1994) using the published coordinates of MMP-9 (PDB ID code: 1GKD). Rigid body, calculations of the electron density maps, simulated annealing, energy minimization, R factor and refinement were performed with the program CNS (Brunger et al., 1998). Model building was done using the program MAIN (Turk, 1996). Subsequent cycles of rebuilding and refinement finally yielded models with crystallographic R values in the range between 22.1 and 23.3 and for R free between 25.8 % and 28.1 %. PROCHECK was used for the validation of the stereochemistry of the models (Laskowski et al., 1993).

3.3.2   Molecular replacement; Introduction

An "easy" way to obtain a first model of a protein can be followed if the structure of this protein with an homologous amino acid sequence has already been established. The structure of this homologous protein is be served as a very first model that can be subsequently refined. This procedure is based on the observation that proteins, homologous in their amino acid sequence, have a very similar folding of their polypeptide chain (Huber et al., 1985).

The problem is to transfer the known protein molecular structure from its crystalline arrangement to the crystal of the protein for which the structure is not yet known. The

solution is the molecular-replacement/Patterson-Search method (Rossmann and Blow 1962). In the rotation step the spiral orientation of the known molecule with respect to the other is determined while in the next step the translation needed to superimpose the now correctly oriented molecule onto the other molecule, is calculated (Agarwal et al., 1985).

The basic principle of the molecular replacement method can be described as follows: The Patterson map is a vector map; vectors between atoms in the real structure show up as vectors from the origin to maxima in the Patterson map. If the pairs of atoms belong to the same molecule, then the corresponding vectors are relatively short and their points are found not too far from the origin of the Patterson map. For homologous molecules the Patterson map it is not exactly equal but very similar. Therefore, the self-Patterson vectors can supply the rotational relationship between the known and unknown molecular structures. From the cross- Patterson vectors the translation vectors required for moving the molecules to their correct position can be derived (Engh et al., 1991).

3.3.2.1   The Rotation Function

The angular relationship between identical units within one asymmetric unit *(self-rotation function)* or between equal or closely related molecules in two different crystal forms *(cross-rotation function)* can be derived from the X-ray data (Arndt et. al., 1977, Crowther et al., 1972).

The self-Patterson peaks all lie in a volume around the origin with a radius equal to the dimension of the molecule. If a number of identical molecules lies within one asymmetric unit, the self-Patterson vector distribution is exactly the same for all these molecules, except for a rotation that is same as their non-crystallographic symmetry in real space. Therefore, if the Patterson function is superimposed on a correctly rotated version, maximum overlap between the two Patterson maps will occur. Similarly for two different lattices, the two different Patterson maps must be superimposed to maximum overlap by a rotation of one of the two maps.

A rotation of the axes has the same effect as a rotation of the structure in the opposite direction. If the structure rotates, its Patterson map rotates in the same way. Applying the

rotation [C] to the Patterson function P(u) with the rotated Patterson function $P_r(u_r)$, an overlap function R of P(u) with the rotated Patterson version, $P_r(u_r)$, at the same crystal lattice *(self-rotation function)* or a different crystal lattice *(cross-rotation function)* is defined as:

$$R(\alpha, \beta, \gamma) = \int_U P(u) x P_r(u_r) du$$

U is the volume in the Patterson map where the self-Patterson peaks are located.

The product of R depends on the rotation angles (related to [C]) and will have a maximum value for correct overlap. P(u) and $P_r(u_r)$ must now be superimposed and P(u) x $P_r(u_r)$ calculated for every position u within U then the integral must be taken to obtain R(α, β, γ):

$$R(\alpha, \beta, \gamma) = \frac{1}{V^2} \sum_h \sum_h |F(h)|^2 |F([C]h')|^2 \ x \int_U \exp[-2\pi(h + h')u] du$$

For the rotation method it is important that all reflections are present because the calculation of the rotation function basically depends on the rotation of a Patterson map, which is mainly determined by strong reflections. Another point to consider is the resolution range of the data used in the calculations of the rotation function. Low resolution data can be excluded because they are rather insensitive to the rotation; moreover they are determined to an appreciable extent by the solvent region. High resolution data are more discriminating but are also more sensitive for the model.

The shape and size of the region U is assumed to be spherical. Its radius can be chosen equal to, or somewhat less than the diameter of the molecule. In the calculation of the rotation function, the known molecule is put into a large artificial unit cell having no crystallographic symmetry (space group P1). The dimensions of the cell should be such that all cross-vectors are the longer than the diameter of the molecule. Instead of working with the X-ray data of the crystal structure of the known molecule, the calculated structure factors of the artificial lattice must be tried. The original model can be truncated by deleting

side chains, doubtful parts, or modified properly trying different relative orientations of the domains of the molecule.

3.3.2.2   The Translation Function

For the final solution of the molecular replacement method a translation required to overlap one molecule onto the other in real space must be determined, after it has been oriented in the correct way with the rotation function. The known molecule is moved through the asymmetric unit and structure factors are calculated and compared with the observed structure factors by calculating an R-factor or correlation coefficient as a function of the molecular position.

$$R = \frac{\sum\limits_{hkl} \left\| F(obs) \right| - k \left| F(calc) \right\|}{\sum\limits_{hkl} \left| F(obs) \right|}$$

The standard linear correlation coefficient C is

$$C = \frac{\sum\limits_{hkl}(\left| F(obs) \right|^2 - \overline{\left| F(obs) \right|}^2) x (\left| F(calc)^2 \right| - \overline{\left| F(calc)^2 \right|})}{\left[\sum\limits_{hkl}(\left| F(obs) \right|^2 - \overline{\left| F(obs) \right|^2})^2 \sum\limits_{hkl}(\left| F(calc) \right|^2 - \overline{\left| F(calc) \right|^2})^2 \right]^{1/2}}$$

The advantage of this correlation coefficient over the R-factor is that it is scaling insensitive. During R-factor search calculations, one need not start calculating the F(calc) values from atomic coordinates every time the molecule is shifted, but instead calculate phase shifts for each set of the molecules related by crystallographic symmetry. The result from the rotation function can be refined by changing the rotation parameters in small steps.

In a more straightforward method than trial and error search, a translation function is calculated that gives the correlation between a set of cross-Patterson vectors for a model structure and the observed Patterson function. Cross-Patterson vectors in this context mean vectors in the Patterson map derived from vectors between atoms in two molecules in the model structure related by a crystallographic symmetry operation [C]+ d. In space group P1,

in which no crystallography symmetry exists, the origin can be chosen everywhere and this has no influence on the absolute value of the structure factor.

The final form of the translation function is a Fourier summation in which the coefficients are known:

$$T\ (t) = \sum_{h} \left| F_{obs}(h) \right|^{2} \cdot F_{M}(h) F_{M}^{*}(h[C]) \exp\left[-2\pi h \cdot t \right]$$

Unwanted background in the translation function is caused by self-Patterson vectors (vectors between atoms within a molecule) and by ignoring the Patterson vectors between molecules other than those under consideration. Self-Patterson vectors can easily be eliminated from the observed Patterson map, assuming that the known and unknown molecules have the same structure and, therefore, the self-Patterson vectors.

In the two-step procedure, first the calculation of the rotation function and subsequently the translation function, the latter usually causes more problems than the first. For example, the search model differs too much from the unknown structure, or the highest peak in the rotation function does not correspond to the correct orientation.

Several methods have been proposed to improve this situation:

a) Combine the translation search with a limited systematic variation of the orientation parameters using the R-factor or the correlation coefficient as criterion. This method has been described and successfully used by Fujinaga and Read (1987) using the standard linear coefficient.

b) Refine the search model and its orientation after the rotation, but before translation search *(Patterson correlation refinement)*. This second method was developed by Brünger (Brünger et al., 1991; 1992), who introduced two techniques for increasing the success in finding the correct translation of the search model. First he calculates a normal rotation function; peaks close together are clustered to a single peak. He selects not only the highest peak in the rotation function but a number of peaks and calculates the standard linear correlation coefficient between the squares of the normalised observed and calculated structure factors, as a function of the coordinates of the centre of gravity of the search model and its symmetry mates. This three-dimensional search for the optimal coordinates is done for each of the selected orientations and the orientation that gave the highest value for the correlation coefficient is then chosen for

the translation search. If this search is unsuccessful, the highest peaks for the rotation function are again selected, but now, before a translation search is carried out, the search model and its orientation are adjusted by energy minimisation. A single copy of this search model is put into a triclinic cell, identical in geometry to the crystal unit cell and in an orientation derived from the rotation function. The translation function is then of no relevance because of a change of the magnitudes of the structure factors.

c) Combination of existing phase information from isomorphous replacement with the translation function *(phased translation function)* is another approach. The method is based on overlapping the density electron map computed with the prior phase information, with the electron density map of one copy of the search model correctly oriented in the unit cell. The criterion is the linear correlation coefficient.

d) Zhang and Matthews (Zhang et al., 1990) proposed a modified rotation function if part of the structure is known (addition and subtraction strategy). This method can improve the quality of the rotation function as well as the translation function. For solving the rotation function of the unknown part with the addition strategy, the Patterson function of the known part is added in its correct orientation to the Patterson function of the search model for the unknown part. This modified Patterson is calculated as a function of [C] and compared with the observed Patterson. In the subtraction method the Patterson function of the known part is subtracted from the observed Patterson and solved as a function of [C]. If then the orientation of the molecule or subunit or part it is known, the rotation result can best be improved by incorporating the subtraction strategy, which will reduce noise in the rotation function.

e) Navaza (Navaza et al., 1994) has written a molecular replacement program *AmoRe* which incorporates several features, such as the exploration of many potential solutions and already existing knowledge of the models. It reformats the data from the new crystal form, generates structure factors from the model, calculates the rotation function and the translation functions, and applies rigid body refinement to the solutions.

3.3.3   MT1-MMP Hpex domain

3.3.3.1   Crystallization

The human MT1-MMP Hpex domain was crystallized using the sitting-drop vapor-diffusion technique. 1 µl of protein at a concentration of 5.0 mg/ml (in 20 mM Tris/HCl, pH 7.5) was

mixed with 1µl reservoir buffer, 2.1 M Malic Acid pH 6.0, 40 % v/v acetone. The crystals appeared after a few days at room temperature.

3.3.3.2   Data collection and structure determination

For data collections, crystals were transferred into cryobuffer (20 % Perfluoropolyether PFO-X125/03) and were flash frozen under a stream of nitrogen gas at 100 K. Data were collected using synchrotron radiation at the beamline BW6 of the Deutsches Elektronen Synchrotron (DESY, in Hamburg, Germany), employing a Mar Research CCD detector at the wavelength (λ) of 1.050 Å,. The diffraction data were processed and scaled by the programs DENZO/SCALEPACK. They diffracted to 1.8 Å belonging to the trigonal space group $P3_121$ containing one molecule in the asymmetric unit. The molecular replacement was performed with the program *PHASER* (Randy J. Read et al., 2004) using a monomer of The hemopexin domain of MMP9 (PDB ID code: 1ITV). One monomer was located in the asymmetric unit. For electron density maps calculations, a rigid body and positional refinement were performed using CNS (Brunger et al., 1998). Model building was performed using the program MAIN (Turk, 1996). Subsequent cycles of rebuilding and refinement finally resulted in a model with a crystallographic *R* value of 21.0 % and *R* free of 21.7 %. PROCHECK was used for stereo chemical coordinate validation (Laskowski et al., 1993).

Chapter 4   Results

4.1   Wild type mini-MMP-9 and the mutant E402Q

4.1.1   Protein purification and characterization

For the isolation of the mini matrix metalloproteinase-9, *E. coli* bacteria were cultured in a 12 liter fermentor (see paragraph 3.2.1.1). The amount of cells obtained was 15 g of wet weight.

The affinity chromatography purification step (3.2.1.2), 3.0 mg of highly active mini-MMP-9 was obtained from 15 g of cells. The protein eluted as a single peak from the hydroxamate inhibitor (Pro-Leu-Gly-NHOH), -coupled Sepharose column and the SDS-PAGE revealed highly pure enzyme with the expected molecular mass of 18 kDa (see Figure 20). The purity for both wild type and mutant was more than 95 %.
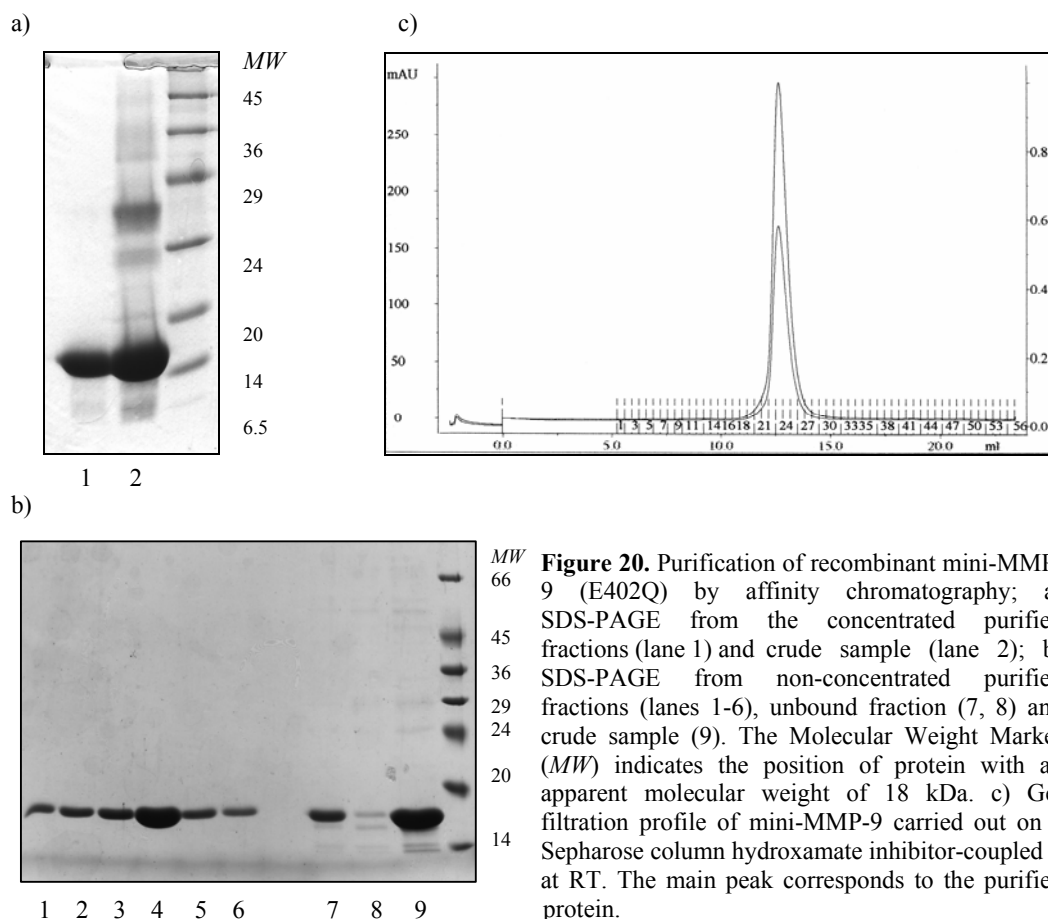
a)   c)

b)

Figure 20. Purification of recombinant mini-MMP-9 (E402Q) by affinity chromatography; a) SDS-PAGE from the concentrated purified fractions (lane 1) and crude sample (lane 2); b) SDS-PAGE from non-concentrated purified fractions (lanes 1-6), unbound fraction (7, 8) and crude sample (9). The Molecular Weight Marker (*MW*) indicates the position of protein with an apparent molecular weight of 18 kDa. c) Gel filtration profile of mini-MMP-9 carried out on a Sepharose column hydroxamate inhibitor-coupled at RT. The main peak corresponds to the purified protein.

Wild type and mutant were characterized by N-terminal sequencing (Experimental Procedure 3.2.1.6.1). The N-terminal sequencing identified the N-terminus of mini-MMP-9 GFQTFEGDLK which was preceded by the residues CAM. The result of the N-terminal sequencing was CAMGFQTFEGDLK.

The Mass Spectroscopy showed a molecular mass for the purified protein E402Q sample of 18318.0 Da compared with a theoretical valued 18316.3 Da. The same measurements were performed for the wild type enzyme.
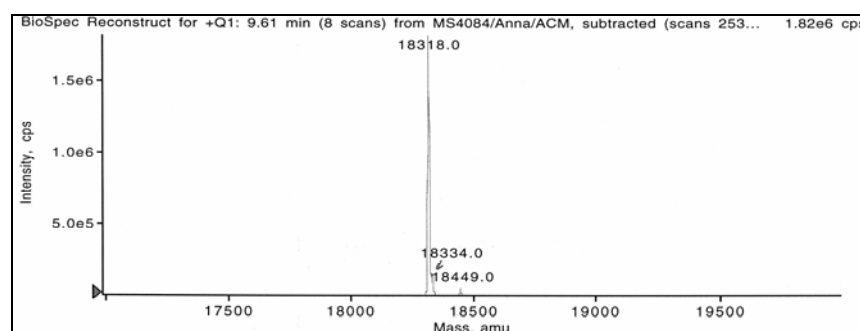

Figure 21. The Mass spectroscopy of the (E402Q) mutant miniMMP-9.

The circular dichroism spectroscopy was used to determine the fractions of secondary structure content of wild type as well as the mutant mini-MMP-9 (section 3.2.1.6.3). The spectrum indicates a mixture of helical, β-sheet, and random coil structure (Finkelstein et al., 1977; Figure 22). The helical content was extrapolated from the CD spectrum using the program CDNN (Bohm et al., 1992). The analysis of the spectrum using the CDNN method suggests a helix content of 3.7%, a β-sheet content of 52.2%, 19.3% of β-turn and 35.3% random coil of (Table 1).
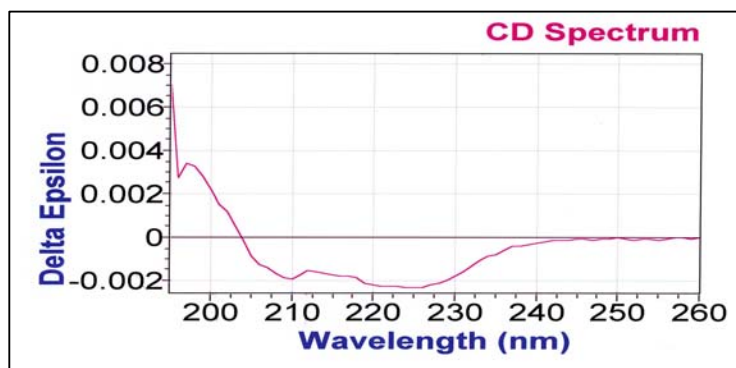

Figure 22. Circular dichroism spectrum of miniMMP-9. The protein sample was used in a concentration of 0.2 mg/ml in 20 mM Tris/HCl, pH 7.5, 10 mM $CaCl_2$, and 30 mM NaCl.

	210-260 nm
Helix	3.7%
Beta sheet	52.2%
Beta turn	19.3%
Random coil	35.3%

Table 1. Secondary structure elements calculated from the miniMMP-9 CD-spectrum, compared with the expected values.

4.1.1.1 Kinetic measurements

The enzyme activity of wild type mini MMP-9 was measured fluorometrically with an excitation wavelength at 280 nm and an emission wavelength at 340 nm. *Substrate 1* (Dnp-Pro-(ß-cyclohexyl)Ala-*Gly-Cys*(Me)-His-Ala-Lys(N-Me-Abz)-NH$_2$) was used at a final concentration of 10 µM in a total 500 µl reaction mixture (3.2.1.7.2). For several inhibitors like e. g. MS560 (2-Amino-3,3,3-trifluoro-*N*-hydroxy-2-(4-phenoxy-benz-enesulfonylmethyl)-propionamide) and SR39, IC$_{50}$ *values* were determined (see Table 2). The SR39 is an analogue of MS560, with only the amino group being substituted by a methyl group. As the reference, Batimastat (BB-94) was used.
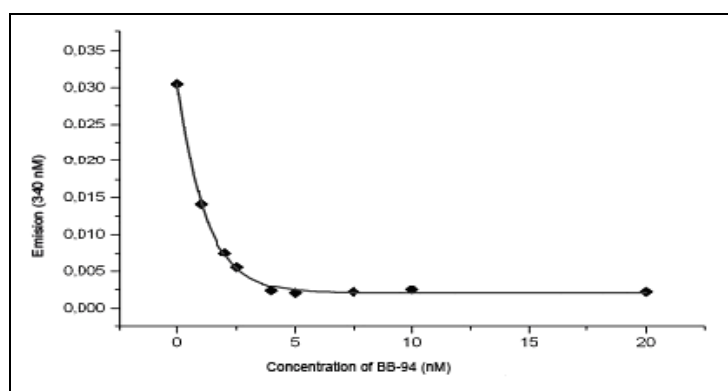

Figure 23. MiniMMP-9 inhibition curve of BB-94 inhibitor as a reference. The enzymatic reaction was performed with the fluorogenic substrate *Substrate 1* in a fluorimeter.
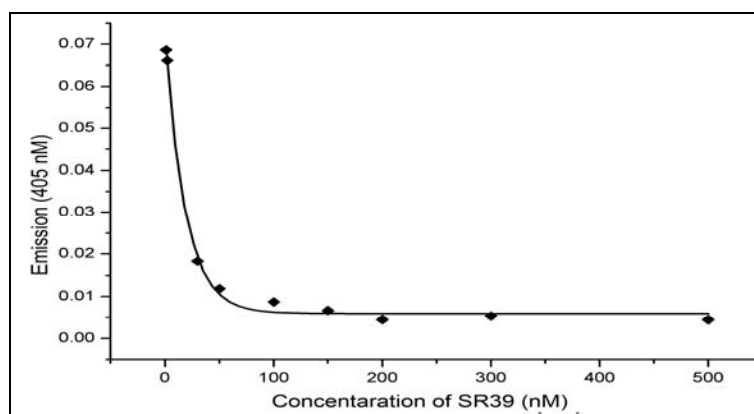
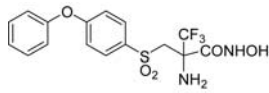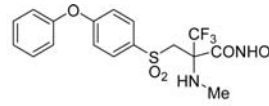**Figure 24.** MiniMMP-9 inhibition curve of the SR-39 inhibitor.

Inhibitor	IC_{50}
BB-94	~ 1.0 nM
MS560	~ 5.4 nM
SR39	~ 20 nM

Table 2. IC_{50} *values* for inhibitors of miniMMP-9.

4.1.2   Protein crystallization and data collection

The initial crystallization trials were carried out using commercial and homemade incomplete factorial solutions at 20 °C. In general, the crystals obtained at this temperature were quite big and of good quality. The crystals of the mutant mini-MMP-9/RO-206-0222 inhibitor complex grew within a few days. The optimized growing time for other crystals at 20°C was one week to two months, reaching the dimensions of roughly 0,2 * 0,1 * 0,1 mm. The final crystallization conditions read as follows:

- for the **RO206-0222** inhibitor 0.1 M citric acid/NaOH pH 5.0, 3.0 M NaCl;

- for **AM409** 0.1 M Tris/HCl pH 8.0, 3.0 M NaCl;

- for **An1** 0.1 M Hepes/NaOH pH 8.0, 4.0 M NaCl;

- for **MS560** 0.1 M Hepes/NaOH pH 7.0, 3.0 M NaCl;

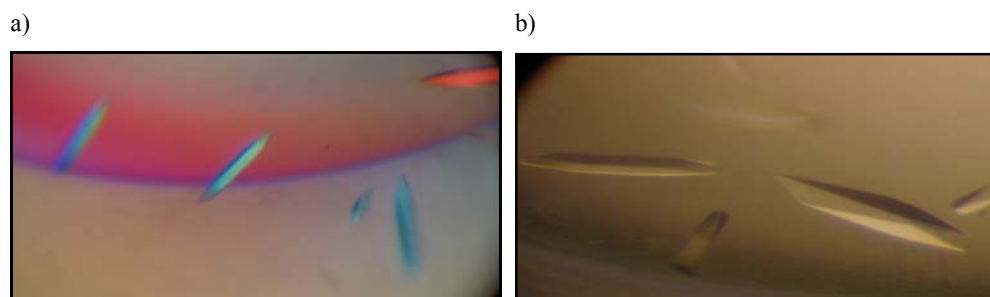- for **MJ24** 0.1 M Bicine pH 9.0, 3.0 M NaCl.

a)   b)

Figure 25. Crystals of miniMMP-9 (E402Q) in complexes with inhibitors: a) RO206-0222; b) AM409.

In searching for a cryoprotectant solution, the crystal mother solution was supplemented with increasing amounts of ethylene glycol. An amount of 20% ethylene glycol made flash cooling possible. After freezing in the nitrogen stream, the crystals diffracted to 2.0, 2.2 and 2.8 Å using synchrotron radiation (Figure 26).
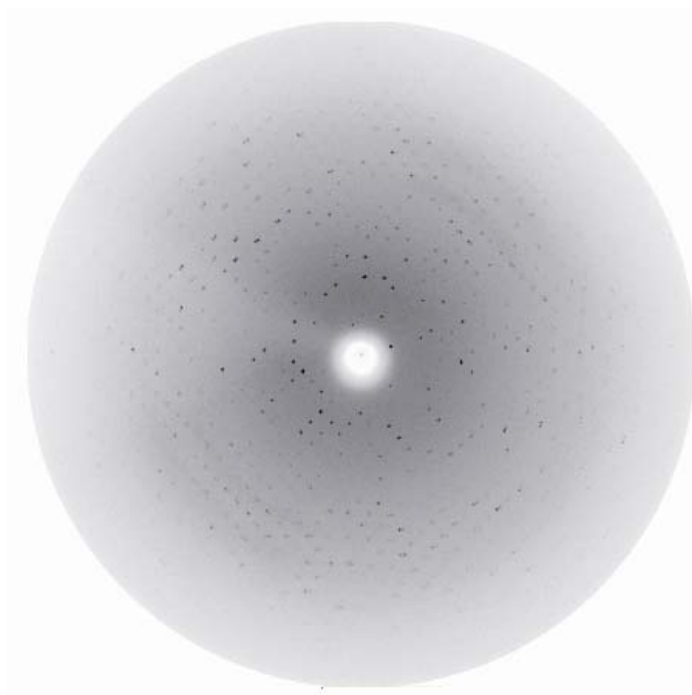

Figure 26. Diffraction image of the mini-MMP-9/RO206-0222 crystal. The image was recorded on a MarCCD detector on beamline BW6 at DESY, Hamburg. The detector edge corresponds to a limiting resolution of 1.95 Å using X-ray wavelength of 1.05Å.

All crystals belonged to space group $P4_12_12$ having very similar unit cell dimensions (see Table 3). The asymmetric unit comprises two molecules, and with a Matthews's coefficient of $V_m = 2.0$ to 2.9 $Å^3$/Da corresponding to solvent content is 54.8 to 56.0 % (see Table 3).

4.1.3   Phasing and Refinement

The structure of mini-MMP-9 was solved by the Patterson search method using the homologous MMP-9 active site inhibitor-mutant complex (PDB accession code: 1GKD). The search model consisted of a protein dimer, with non-conserved residues replaced by alanine, comprising both subunits and the cofactors Ca^{2+} and Zn^{2+}. Molecular replacement solutions were found with the program MOLREP according to the described procedure (see Experimental Procedures; 3.3.1.3) The refinement finally revealed models with crystallographic R_{factor} values in the range between 21.5 to 23.3 and with R_{free} values between 25.5 to 28.7. PROCHECK (Laskowski et al., 1993), used for coordinate validation, confirmed the good stereochemistry of the models with five different inhibitors in the active sites (Refinement statistics; Table 3).

The complete main chains of both monomers and the vast majority of side chains, except for some surface-exposed flexible residues, were completely enveloped in the final *$2F_o$-F_c* electron density map when contoured at 1σ. The final models contained all residues of the protein, except the first six N-terminal amino acids of the molecule B and the three or two C-terminal amino acids of the both molecules, respectively. In addition about 200 water molecules, 4 zinc, 8 to 10 calcium and 1 to 5 chloride ions were included in each model (Table 3).

Data collection and refinement statistics

Data Collection

Crystal content	mini-MMP- 9 /**RO-206-0222**	mini-MMP-9 /**AM-409**	mini-MMP-9 /**An1**	mini-MMP-9 /**MS560**	mini-MMP-9 /**MJ24**
Space group	$P4_12_12$	$P4_12_12$	$P4_12_12$	$P4_12_12$	$P4_12_12$
Cell constants (Å)					
a	55.23	55.85	55.19	55.72	55.42
b	55.23	55.85	55.19	55.72	55.42
c	259.20	259.89	260.36	260.45	260.79
Resolution range (Å)	20.0-2.0	20.0-1.95	20.0-2.0	20.0-2.0	20.0-2.8
Unique reflections	29510	28695	29627	22101	10832
I/σ	26.8	20.5	31.8	30.2	48.3
Linear R-fac	0.052	0.042	0.086	0.050	0.063
Completeness (%)	94.0	89.5	96.5	87.0	94.6

Refinement

Reflection used for refinement	27670	26125	27571	19604	9339
Working set	26317	24861	26236	18654	8845
Resolution range (Å)	20.0-2.0	20.0-1.95	20.0-2.0	20.0-2.0	20.0-2.8
[b]R_{factor} (%)	21.8	22.4	23.3	21.8	21.5
[c]R_{free} (%)	25.1	25.7	28.0	26.6	28.7
Protein molecules	2	2	2	2	2
Matthews coefficient (Å^3/Da)	2.7	2.8	2.0	2.8	2.9
Solvent content (%)	54.8	56.0	55.0	55.8	56.0
Residue number per au	314	310	310	307	307
Water molecules per au	215	186	232	237	168
Zinc ions per au	4	4	4	4	4
Calcium ions	10	10	10	8	10
Chlorine ions	5	4	4	-	1
R.m.s.d. [c] from ideal geometry					
Bond lengths (Å)	1.238	1.19	1.10	1.21	1.18
Bond angles (º)	0.006	0.007	0.007	0.008	0.009
Φ, Ψ angle distribution					
Preferred (%)	88.2	88.3	87.8	86.7	87.8
Add. allowed	10.3	9.8	10.6	11.8	10.6
Disallowed	0.8	0.0	0.4	0.0	0.0

[b]$R_{factor} = \Sigma_{hkl} ||F_{obs}| - |F_{calc}|| / \Sigma_{hkl} |F_{obs}|$

[c]R_{free} is the R-value calculated with 5 % reflections not used in refinement.

Table 3. Data collection and refinement statistics for mini-MMP-9 (E402Q) with the barbiturate inhibitor RO206-0222, the phosphinic acid inhibitor AM409, the carboxylate An1, the hydroxamic acid inhibitors MS560 and MJ24.

4.1.4   Description of the structures; Mini-catalytic domain with different inhibitors

4.1.4.1   The principal features of the MMP-9 catalytic domain

The major characteristics of the truncated catalytic domain of MMP-9, catMMP-9Δfib, catMMP-9ΔfibE402Q (shortly: mini-MMP-9) have been previously described in detail (Rowsell et al*.,* 2002). Like the catalytic domain of all "classical" MMPs (Bode & Maskos, 2003), miniMMP-9 essentially consists of a five stranded ß-sheet and three α-helices, exhibiting the shape of an oblate ellipsoid, with a notch at its flat surface representing the active-site cleft (Fig. 27). In the standard orientation, the cleft harbouring the catalytic zinc separates a bigger "upper" N-terminal domain from a smaller "lower" C-terminal domain. The active-site cleft extends horizontally across the domain surface and has the capacity to bind peptide substrates from left (N-terminus) to right (C-terminus). The main upper domain consists of a central highly twisted five stranded ß-sheet, flanked by three surface loops on its convex side and by two long regular α-helices on its concave side. The polypeptide chain starts in the active-site cleft, with Phe110 being the first ordered residue in the crystal structures. The chain runs around the molecule to pass β-strand sI, α-helix hA, β-strands sII and sIII, before entering the MMP-characteristic S-loop, which is fixed via the tetrahedrally liganded "structural zinc" and a calcium ion to the underlying β-sheet. Then it turns into the cleft-sided, antiparallel "bulge-edge" strand sIV, where it sandwiches a second calcium ion between the sIV-sV and the sII-sIII loop. The chain passes the central strand sV, binds a third calcium ion, runs through the large open sV-hB loop, and enters the long horizontally extending "active-site helix" hB, which provides the first (His401) and the second catalytic zinc liganding imidazole (His405) of the metzincin-characteristic HEXXHXXGXXH zinc binding motif (Bode et al., 1993) as well as the "catalytic" Gln402. Helix hB ends at Gly408, where the chain bends providing the third catalytic zinc ligand (His411), runs through a wide right-handed open spiral terminating in the tight 1.4-turn called "Met-turn" between Ala417-Leu-Met-Tyr420. Finally it turns back to the surface to enclose with its "S1' wall-forming segment" Pro421-Ile422-Tyr423-Arg424-Tyr425 a surface cleft becoming the S1' "pocket", runs through the wide, relatively short "specificity loop", and ends up in the C-terminal α-helix hC.

It is noteworthy that the N-terminus of this MMP-9 construct is first visible in the electron density from Phe110 onwards, four residues after the real N-terminus Gly106.

The following residues run along the cleft in prime side direction (to the left in Fig. 27) i.e., opposite to a bound peptide substrate (see Figure 27), taking a similar track as in pro-MMP-9 (Elkins et al., 2002). The Phe110 side chain inserts into the hydrophobic S3 pocket formed by His190, Phe192 and Tyr179, probably fixing the following segment to the cleft, in this way interfering with productive binding of larger substrates. An "accurately" tailored N-terminal MMP-9 segment starting with Phe107 would presumably nestle into a hydrophobic surface groove on top of helix hC, below the active-site cleft, and would form with its N-terminal α-ammonium group a salt bridge on the protein surface with the side chain carboxylate of Asp434, giving rise to the "superactivity" phenomenon observed in the collagenases (Nagase, 1997; Reinemer et al., 1994; Lang et al., 2006).
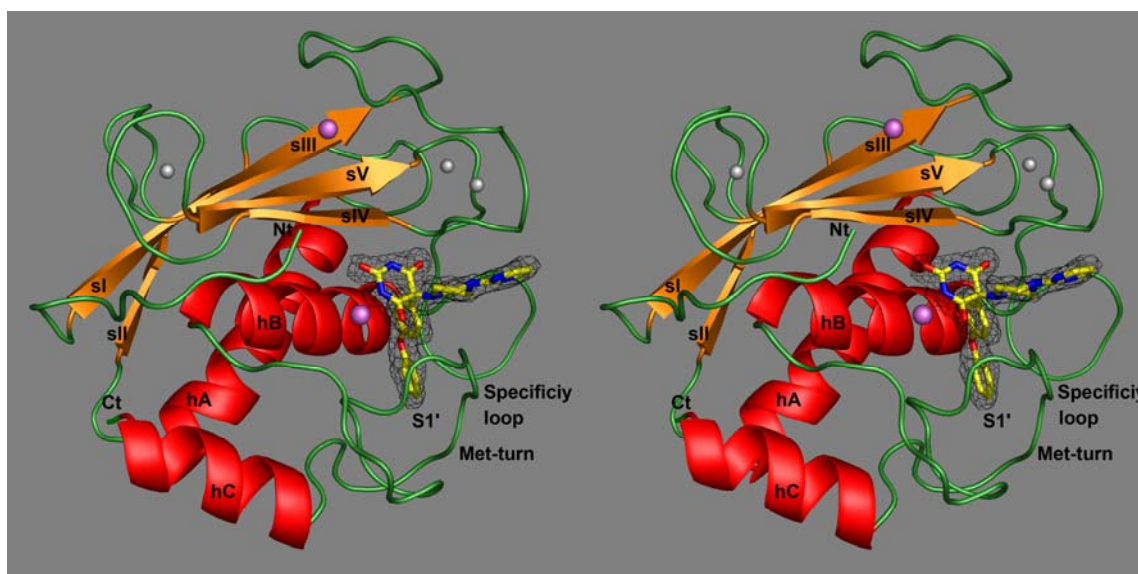

Figure 27. Ribbon representation of the MMP-9 catalytic domain shown in standard orientation together with the RO206-0222 inhibitor (with experimental electron density contoured at 1σ) bound in the active centre. Strands (orange) and helices (red) are labelled with Roman numerals and letters respectively. Additionally the Met-turn, the specificity loop, and the S1' specificity pocket are highlighted. The catalytic and the structural zinc (centre and top) and the three flanking calcium ions are shown as magenta and grey spheres. N-terminal and C-terminal are highlighted too.
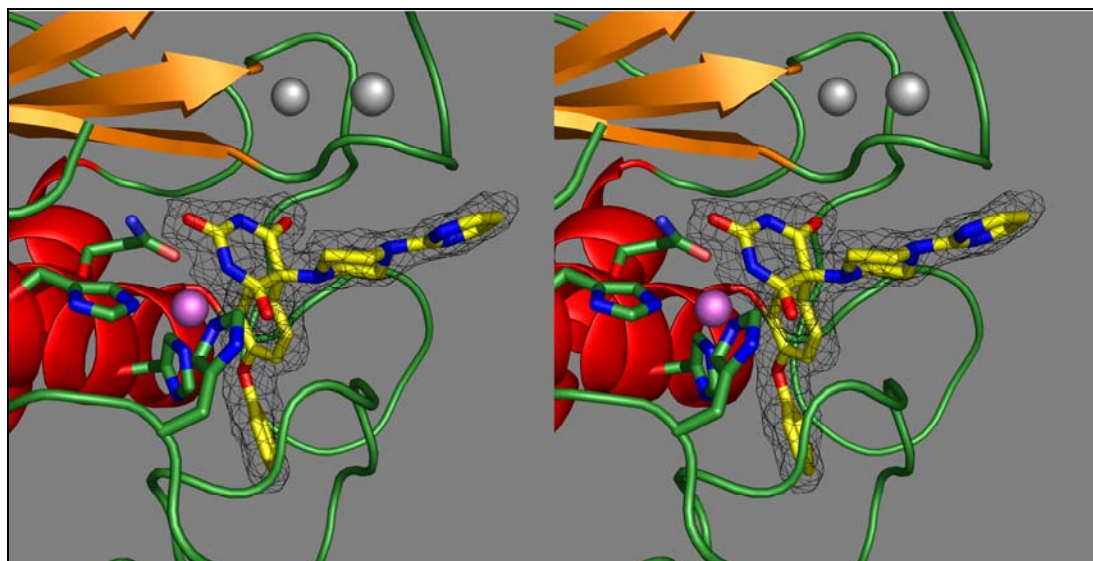
74

Figure 28. Schematic representation of the active centre of MMP-9 shown in standard orientation together with the RO-206-0222 inhibitor (with experimental electron density contoured at 1σ) bound in the active centre (three histidins His401, His405, and His411, and Glu402). The catalytic zinc and two calcium ions are shown in magenta and grey.

4.1.4.2   MMP-9-barbiturate inhibitor interaction (RO206-0222)

The RO206-0222 inhibitor 5-(4-phenoxyphenyl)-5-(4-pyrimidine-2-yl-piperazin-1-yl)-pyrimidine-2,4,6-trione, is based on barbituric acid and is doubly substituted at C_5 with phenoxyphenyl and pyrimidine-piperazin moieties (see Figure 29c). The central 2-hydroxypirimidine-4,6-dione ring of the barbiturate inhibitor mimics the interaction of the hydroxamate-derived batimastat (Grams et al., 1995). It chelates the catalytic zinc via one of the nitrogens (N_3) of the pyrimidine group and rigidly orients both C5 substituents into the S1' and S2' subsite, respectively. Together with the three liganding histidine nitrogens of the enzyme, it constitutes a tetragonal coordination sphere around the zinc. The Zn^{2+}-N3 coordination has favourable distances of 2.11 and 2.07 Å in the two molecules of the asymmetric unit.

The flanking oxygens O2 and O4 (3.29/3.26 and 2.95/2.81 Å) rather belong to the second coordination shell, so that the catalytic zinc can be considered to be almost perfectly tetrahedrally coordinated by the hydroxyl oxygen O2 and the imidazole Nε2 atoms of the three liganding His residues (2.22/2.26, 2.16/2.19 and 2.28/2.28 Å). The hydroxyl oxygen O2, positioned where the catalytic water is expected for peptidic substrates is placed above the carboxamide group of the "catalytic" Gln402, but is too far away (3.18

and 3.08 Å) and badly oriented to form good hydrogen bonds. The polar H1-N1-C6=O6 atoms of the barbiturate mimics the P1'-S1' antiparallel main chain interactions of a peptide substrate, with N1-H1 and C6=O6 forming favourable hydrogen bonds to the Ala189 carbonyl (2.63/2.50 Å) and Leu188 NH and Ala189 NH (2.85/2.77 and 3.41/3.17 Å), respectively. The C4=O4 carbonyl group, instead of contributing to binding, touches Pro421 of the S1' wall-forming segment (3.19/3.32 Å distant from the proline Cα), whose side chain and carbonyl group it pushes out of their normal position. This well defined Pro421 carbonyl group is (different to all other MMP complexes (see Figs. 30a and 31a and 32a and 33a) and, e.g., ligand-free adamalysin (Gomis-Rüth et al., 1993)) oriented towards the bulk water. This carbonyl rotation is even more enigmatic in that in the "up" orientation it could form a perfect hydrogen bond to the proximal NH group of the piperazine ring. It should be mentioned that the same Pro421-422 peptide rotation had been found in an MMP-8 complex with RO200-1770, a closely related barbiturate (Brandstetter et al., 2001).

In contrast to the polar interactions made by the barbiturate ring, interactions mediated by the two C5 substituents are predominantly hydrophobic (Fig. 29a). The plane of the proximal phenyl ring of the phenoxyphenyl moiety, extending into the S1' pocket is perpendicular to that of the barbiturate ring, with the C6-C5-C11-C12 and the C4-C5-C11-C12 dihedral angles in optimal staggered geometry. This phenyl ring almost stacks on the imidazole ring of His401, and is further surrounded by the Pro421-Met422 segment, the Val398 side chain and the Gln402 carboxamide, whose oxygen touches its edge (3.20/3.11 Å), probably making favourable polar interactions. Similar favourable charge-charge interactions are possible between the ether oxygen and the phenol ring of Tyr423, which borders the S1' pocket. The distal phenyl ring, arranged somewhat kinked but oriented nearly perpendicular to the proximal phenyl ring, just fills the more distal part of the S1' pocket, surrounded by the side chains of Leu397, Leu418, and the Met422-Tyr423 main chain. In addition, its edge is directed towards the carbonyl groups of Leu418 (3.38/3.20 Å) and Arg424 (3.20/3.99 Å). The side chain of this Arg424 is weakly defined by electron density at Cβ, but is not traceable any longer. The space beyond the distal phenyl ring, further to the opposite exit of the S1' tube, is occupied by three ordered water molecules, which are already in contact with the bulk water. According to the electron density, the piperazine ring, which is loosely sandwiched
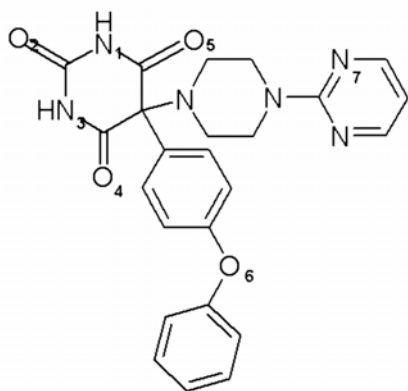
76

a)
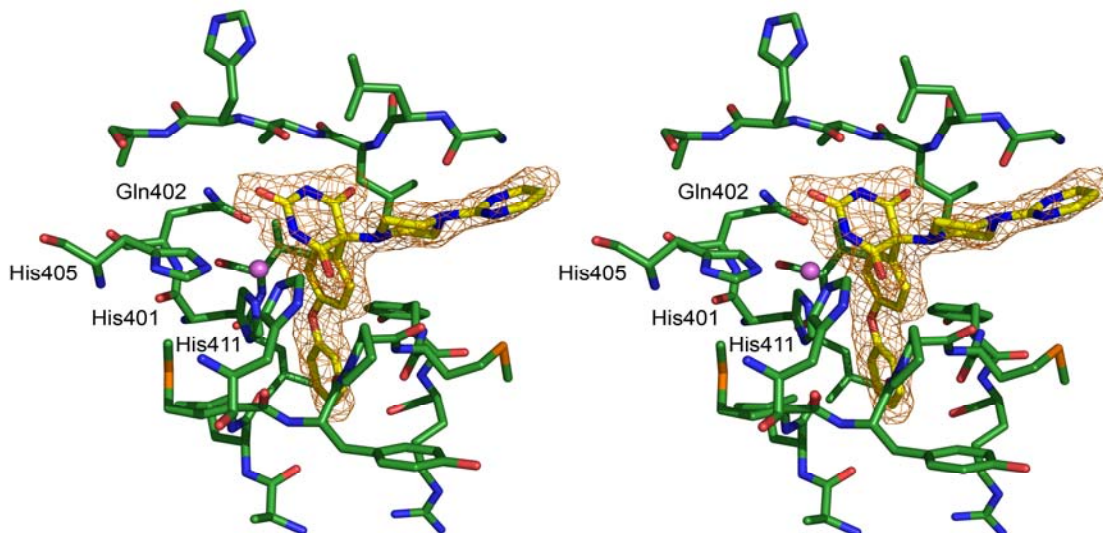
b)
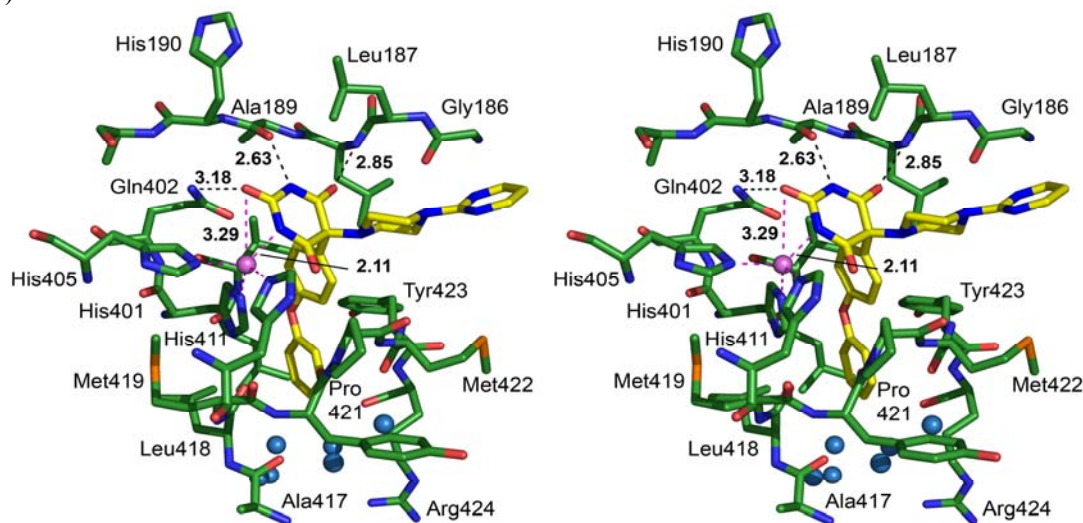
c)

Figure 29a. Stereo view of the active centre with electron density of a $2F_o$-F_c map around the RO206-0222 inhibitor (conture level 1σ).

Figure 29b. Stereo plot of the barbiturate inhibitor RO206-0222 bound to the active site cleft. Selected protein residues are rendered as stick representation and with a green sticks for carbon atoms. The inhibitor is coloured in yellow with oxygens as red and nitrogen as blue atoms. The main inhibitor-enzyme interactions with distances (for molecule A) are included.

Figure 29c. Chemical formula of RO206-0222 inhibitor.

between peptide groups Gly186-Leu187 and Pro421-Met422, unequivocally exhibits in both molecules the chair conformation (see Fig. 29a and 29b).

4.1.4.3   MMP-9-phosphinate inhibitor interactions (AM409)

The AM409 inhibitor [2-[1-Carbamoyl-2-(1*H*-Indol-3-yl)-ethylcarbamoyl]-3-(3-phenyl-isoxasol-5-yl)-propyl]-phenyl-phosphinic acid is a peptide which mimics the structure of the substrate in the transition state, where the water-attacked carbonyl group of the substrate coordinates the electrophilic zinc atom of the enzyme active site (Dive et al., 2004). The peptidic part of the inhibitor forms together with three imidazole nitrogens of His401, His405 and His411 five inter main-chain hydrogen bonds with the catalytic zinc (see Figure 30a and 30b), with the Zn^{2+}-Nε distances between 2.16-2.30 Å (Table 4). The phosphinate oxygens of the inhibitor are located asymmetrically; oxygen O1P is significantly closer to the zinc (2.05/1.95Å) than the second O2P (2.69/3.15 Å) and is additionally in hydrogen bond distance to the nitrogen of the "catalytic" Gln402 (2.95/2.86 Å).

The dominant interactions between inhibitor and enzyme are made by the phenyl-isoxazole group inserted into the S1' pocket and by the "right" side of the inhibitor chain (Indole-ethylcarbamoyl group). The phenyl isoxazole side chain extends into the S1' pocket, with both aromatic ring systems in perfectly planar position to one another, and with the hetero atoms pointing towards the "back" of the molecule. In accordance, the nitrogen and the oxygen of the isoxazole form rather weak vanderWaals interactions with Val398 (3.45/3.54 Å). In front, the Pro421-Tyr420 and Met422 segments make weak interactions with phenyl moiety and goes down to Arg424, whose the side chain is again rather badly defined beyond Cβ. From the left, the isoxazole stacks on imidazole ring of His401 (3.47/3.74 Å). Good symmetry is additionally observed for the oxygen of the isoxazole and Gln402 (3.81/3.85 Å).

The first carbonyl group of the "right" side of the inhibitor peptide bond is hydrogen-bonded with the main chain nitrogen of Leu188 (2.70/2.77 Å), while the NH and the carbonyl function of the terminal carboxamide group are hydrogen bonded with the carbonyl of Gly186 (3.12/3.31 Å) and the amide of Tyr423 (2.64/2.53 Å), respectively (Figure 30a). The P2'-indole side chain folds back on the inhibitor main chain and nestles
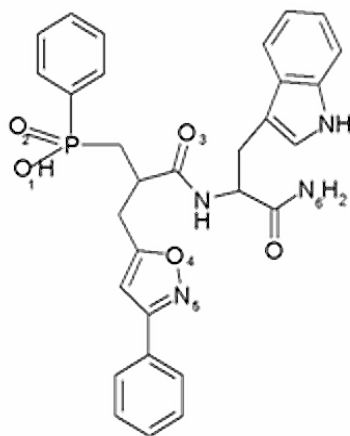
a)
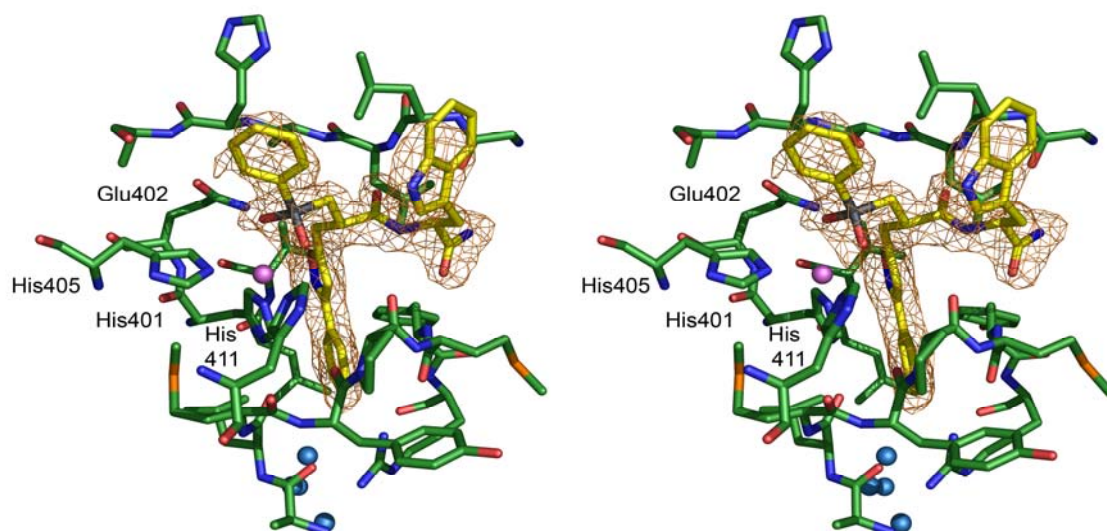
b)
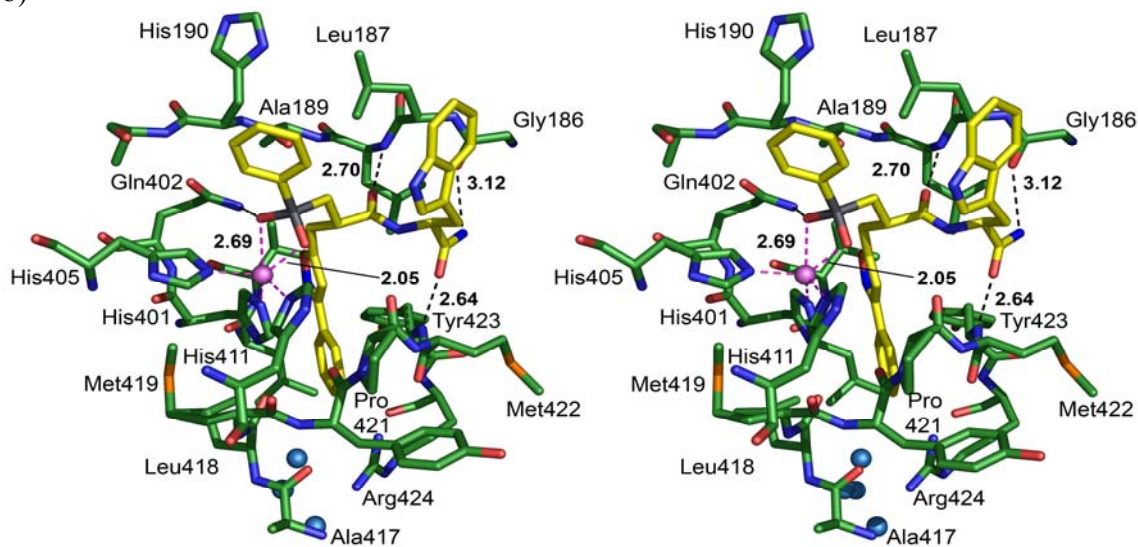
c)

Figure 30a. Stereo view of the active centre with electron density of a $2F_o$-F_c map around AM409 inhibitor (contoured at 1σ).

Figure 30b. Stereo plot of the phosphinic peptide mimic inhibitor AM409 bound to the active site cleft. Selected protein residues are rendered in stick representation with carbon atoms in green. The inhibitor is coloured in yellow with oxygens as red and nitrogen as blue atoms.

Figure 30c. Chemical formula of AM409 inhibitor.

loosely to the Leu187 side chain, adopting an "up" as well as a "down" orientation, as indicated by the electron density. In spite of this ambiguous orientation, this P2' indole side chain seems to considerably contribute to affinity, as shown by the strong (up to 100 fold) gain in inhibitory power in another series of structurally related phosphinates, when going from P2'-Ala to Trp (Vassiliou et al., 1999).

4.1.4.4   MMP-9-carboxylate inhibitor interaction (An1)

The carboxylic inhibitor An1 (Oltenfreiter et al., 2004), 3-(1*H*-indol-3-yl)-2-(4'-iodo-biphenyl-4-sulphonylamino)-propionic acid is labelled with the gamma-emitting radionuclide Iodine-123. Halogens in para position of the biphenyl ring, in general, increase the potency of the inhibitor against some MMPs (Skiles et al., 2001).

In the complex with mini-MMP-9, the inhibitor is well defined by electron density (see Fig. 31b). The terminal carboxylic group of the inhibitor An1 interacts in a similar asymmetrical manner with the catalytic zinc ion as the phosphinyl oxygens of AM-409 (Fig. 31) and coordinates it via both oxygens O1 (2.18/2.10Å) and O2 (2.64/2.69Å). The catalytic zinc is thus penta-coordinated, with the imidazoyl Nε2 atoms of the three liganding His residues (2.23/2.15/2.23 and 2.23/2.25/2.26 Å) forming the base and both oxygens placed at the tip.

The indole moiety binds, as the phenyl group of AM409 inhibitor, likewise into the S1 cleft, with the Trp group exhibiting a D configuration at Cα. The sulphonamide oxygen O3 (Fig. 31a, c) forms hydrogen bonds to the main chain NH groups of the bulge segment Leu188-Ala189 and to a fixed water, respectively (2.76/2.70Å; 3.20/3.02Å). The sulphonamide nitrogen of the inhibitor peptide is too distant from the hydrogen of Ala189 to form a bond (3.99/4.06 Å).

According to the electron density (Fig. 31b), the indole-yl moiety being α-substituted in R-configuration extends into the S1 subsite, making only loose contacts with the cleft rim. The significantly larger IC$_{50}$-values of compounds with a Val compared with the Trp side chain (Oltenfreiter et al., 2005a) indicate that this interaction is nevertheless of importance for the affinity. The biphenyl moiety extends into the S1' cavity completely filling it. Both phenyl rings are rotated against each other for ~45°, i.e., they considerably
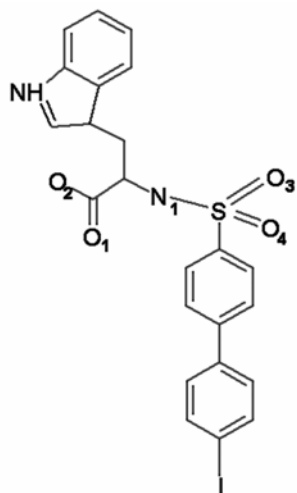
a)
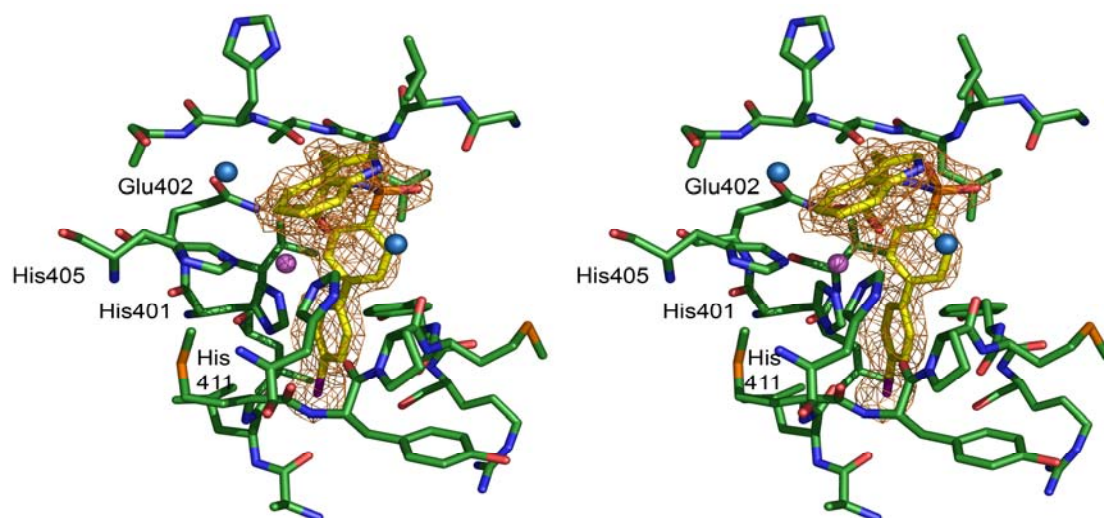
b)
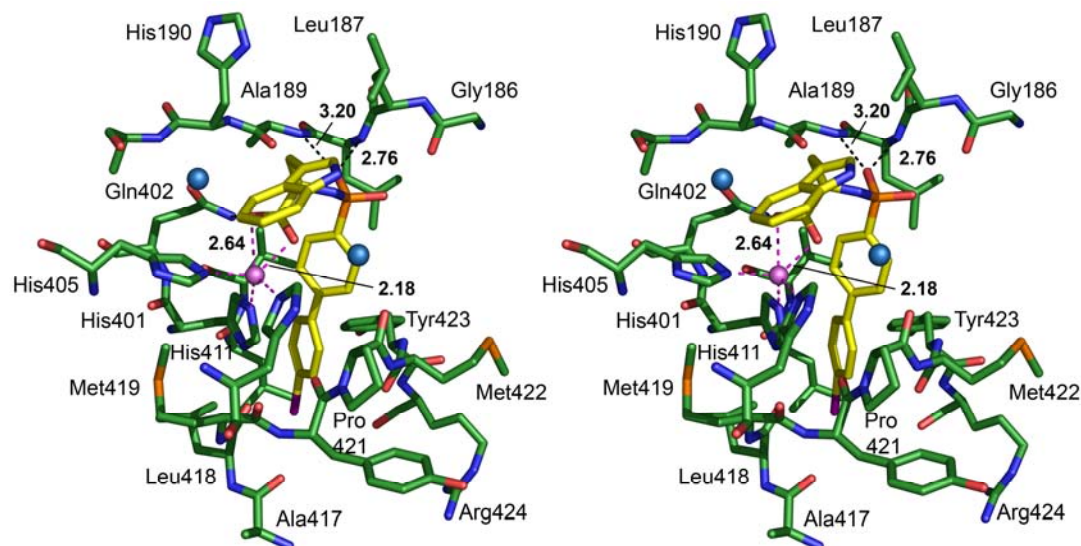
c)

Figure 31a. Stereo view of the active centre with electron density of a $2F_o$-F_c map around the An1 inhibitor (contoured at 1σ).

Figure 31b. Stereo plot of the carboxylate inhibitor An1 bound to the active site cleft. Selected protein residues are displayed as stick representation and with green sticks for carbon atoms. The inhibitor is coloured in yellow with oxygens as red and nitrogen as blue atoms.

**Figure 31c.** Chemical formula of An1 inhibitor.

81

deviate from planarity, presumably in order to avoid contacts of the ortho hydrogens but also due to better S1' contacts. As a consequence, the proximal and in particular the distal phenyl ring stack obliquely on the His401 imidazole ring, besides making favourable edge-to-face and edge-carbonyl contacts with the Tyr423 phenole and the Tyr420 carbonyl group, respectively. The well-defined distal iodine, extending into the lower exit of the S1' pore, is in loose contact with the side chains of Leu397 and Leu418 and the Arg424 carbonyl group, and further surrounded by ordered solvent molecules.

### 4.1.4.5   MMP-9-hydroxamate inhibitor interaction (MS560)

The racemic hydroxamate inhibitor MS560 (2-Amino-3,3,3-trifluoro-*N*-hydroxy-2-(4-phenoxy-benzenesulfonylmethyl)-propionamide) has been designed to investigate the effect of a trifluoromethyl (Tfm) group substituted in α-position to the hydroxamate group of MMP inhibitors involved in cancer (Sinisi et al., 2005). The Tfm group is rather hydrophobic, but can accept hydrogen bonds. According to the crystal structure, the inhibitor binds the catalytic zinc ion like batimastat. Unequivocally, the inhibitor is bound with S-configuration at the α-carbon, in agreement with very recent measurements on homologous enantiomers lacking the additional amino group, so that the trifluormethyl group is in normal vanderWaals contact with the hydrophobic active-site cleft groups. Also, it is sandwiched between the third zinc ligand, the His411 imidazole group, the side chain of Leu187 and Ala189 provided by the bulge strand. Surprisingly, the other α-substituent, the polar amino group, is directed towards the Leu187 isobutyl group and contacts it at a very short vanderWaals distance (3.66/2.85 Å), pushing it away from its normal location. The sulfonyl oxygen (O3) makes similar contacts as observed for AM409 to atoms with Leu188 and Ala189 (2.98/2.85Å; 3.99/3.39Å). The second oxygen (O4) of the sulphonamide displays hydrogen interactions with Leu188 (3.91/2.85 Å) and with neighbouring water molecules (2.94/3.26 Å). The Zn^{2+}-O1 and Zn^{2+}-O2 (the hydroxyl oxygen) coordination have distances of 2.26/2.36 and 2.30/2.41 Å, respectively (Table 4). In addition, O1 interacts with the Nσ nitrogen of Gln402 with a hydrogen bond (2.92/3.07 Å) and with a neighbouring water molecule (2.96/2.75 Å).

The phenoxy-phenyl side chain of MS560 extends quite differently and less favourably into the S1' cavity (see Discussion and 51) than observed for the same side chain of
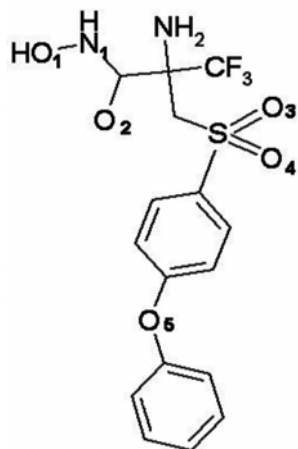
a)
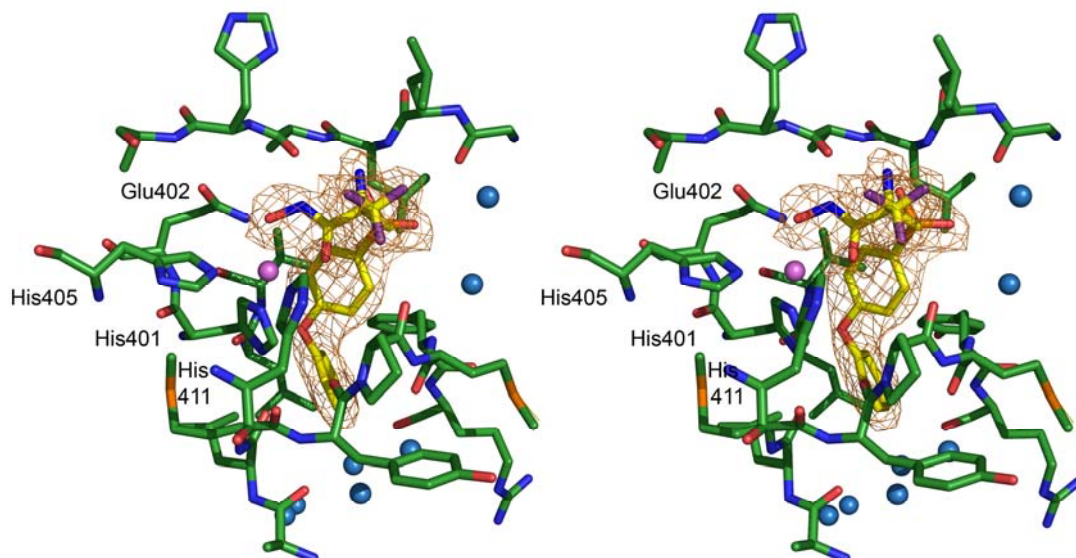
b)
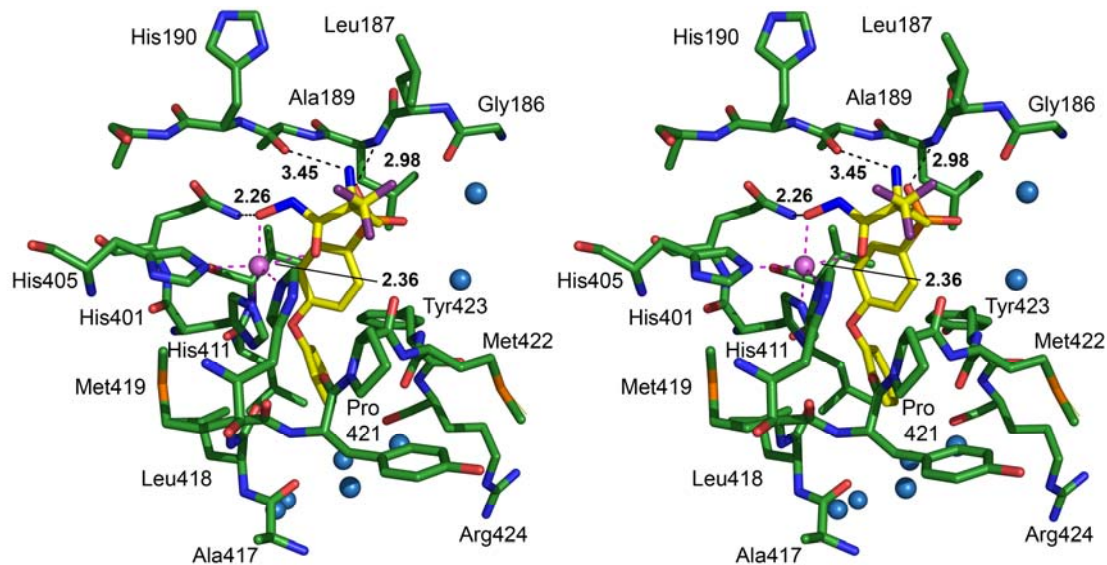
c)

Figure 32a. Stereo view of the active centre with electron density of a $2F_o$-F_c map around the MS560 inhibitor (contoured at 1σ).

Figure 32b. Stereo plot of the inhibitor MS560 bound to the active site cleft. Selected protein residues are rendered in stick representation with green sticks for carbon atoms. The inhibitor is coloured in yellow with oxygens as red and nitrogen as blue atoms.

Figure 32c. Chemical formula of MS560 inhibitor.

83

RO206-0222. Due to the different side chain extensions, the ether oxygen is in quite close and presumably unfavourable contact with the His401 Nδ1 (2.94/2.94 Å).

4.1.4.6   MMP-9-carboxylate inhibitor interaction (MJ24)

The MJ24 inhibitor 3-(4-methoxyphenylsulfonyl)-4,4-difluoro-*N*-hydroxybutanamide was designed like the previously described MS560, to investigate and better understand "fluorine effect". The inhibitor was based on the structurally very simple class of hydroxamate inhibitors bearing an arylsulfone moiety in γ-position (Groneberg et al., 2000; Salvino et al., 2000; Freskos et al., 1999) and showed nanomolar inhibitory potency against MMP-2, 3 and 13. The inhibitor binds the catalytic zinc ion via both oxygens of the carboxylate group quite symmetrically (2.47/2.88Å). Zinc is penta-coordinated with the imidazoyl Nϵ2 atoms of the three liganding His residues (2.40/2.32/2.20 and 2.28/2.35/2.31 Å). Unfortunately, this inhibitor is not as well defined by electron density as the previously described MS560. One of the oxygens from the carboxylate group is in hydrogen bond contact with the Gln402 N-H (3.01/3.55 Å). Additionally, the inhibitor interacts with the bulge-edge segment (N of Ala189 and C of Leu188) and accordingly with the wall forming segment (Pro421) by forming two (3.20/3.12 and 3.21/3.00 Å) and one (2.98/2.85 Å) good hydrogen bonds, respectively. One of the tasks of this structure analysis was to determine and show the configuration of the difluoromethyl group.

The methoxy-phenyl group is quite short and adapts well to the S1' cavity. Even thought this small group was inserted into the pocket, the Arg424 side chain is again not well defined and leaves the S1' channel open.

a)
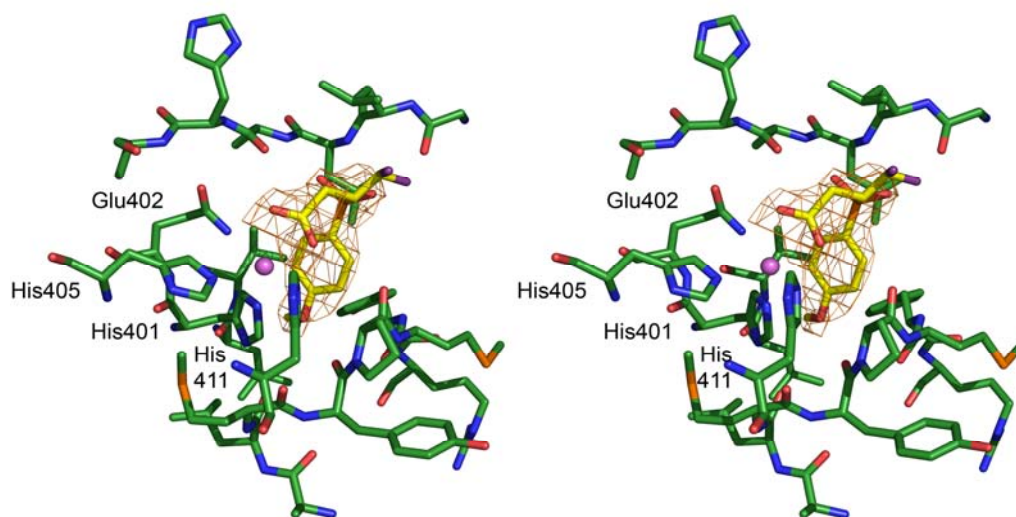
b)
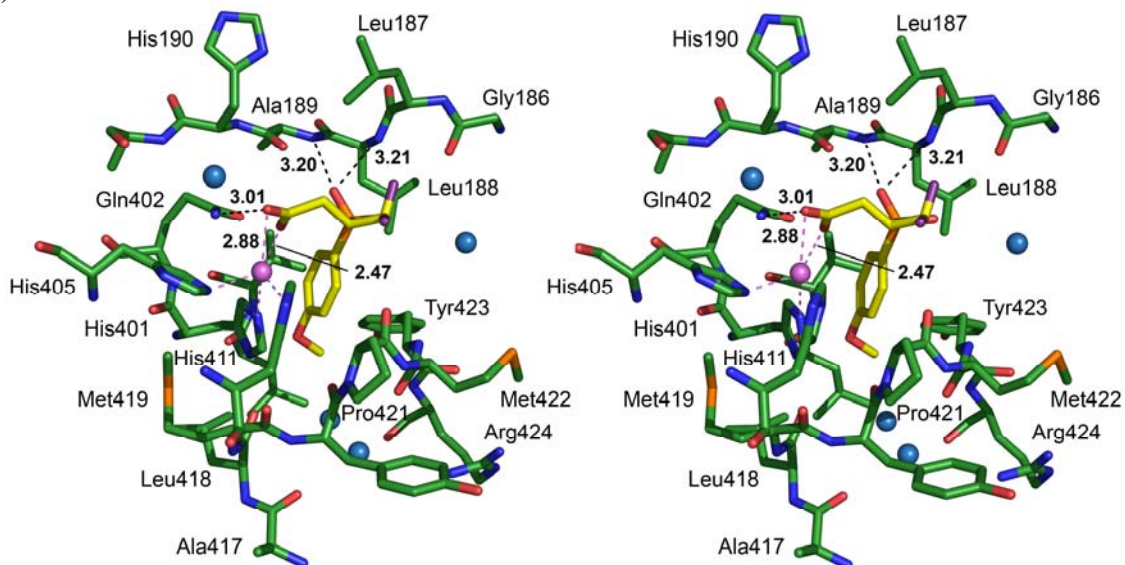
c)

Figure 33a. Stereo view of the active centre of miniMMP-9 (molecule B) with electron density of a $2F_o$-F_c map around the MJ24 inhibitor (contoured at 1σ).

Figure 33b. Stereo plot of the inhibitor MJ24 bound to the active site cleft of miniMMP-9 (molecule A). Selected protein residues are rendered in stick representation and with green carbon atoms. The inhibitor is coloured in yellow with oxygens as red and nitrogen as blue atoms.

Figure 33c. Chemical formula of MJ24 inhibitor.

Ligand-zinc distances at the active site of mini-MMP-9

RO260-0222; tetrahedral geometry

	Molecule A	Molecule B
Zn^{2+} -N_3	2.11 Å	2.07 Å
Zn^{2+} -Nε(401)	2.22 Å	2.26 Å
Zn^{2+} -Nε(405)	2.16 Å	2.19 Å
Zn^{2+} -Nε(411)	2.28 Å	2.28 Å
O_2 - Zn^{2+}	3.29 Å	3.26 Å
O_4 - Zn^{2+}	2.95 Å	2.81 Å
O_2 -N(Gln402)	3.18 Å	3.08 Å
N_1 -O(Ala189)	2.63 Å	2.50 Å
O_5 -N(Leu188)	2.85 Å	2.77 Å
O_5 –N(Ala189)	3.41 Å	3.17 Å
N_7 -O(Gly186)	3.58 Å	4.70 Å
O_4 –Pro(421)	3.19 Å	3.32 Å

AM409; trigonal bipyramidal geometry

	Molecule A	Molecule B
Zn^{2+} - O_1	2.05 Å	1.94 Å
Zn^{2+} - O_2	2.69 Å	3.15 Å
O_2 - N(Gln402)	2.95 Å	2.86 Å
Zn^{2+} -Nε(401)	2.26 Å	2.21 Å
Zn^{2+} -Nε(405)	2.16 Å	2.22 Å
Zn^{2+} -Nε(411)	2.25 Å	2.30 Å
O_3 –N(Leu188)	2.70 Å	2.77 Å
N_6 -O(Gly186)	3.12 Å	3.31 Å

An1; trigonal bipyramidal geometry

	Molecule A	Molecule B
Zn^{2+} - O_1	2.18Å	2.10Å
Zn^{2+} - O_2	2.64Å	2.69Å
O_2 - N(Gln402)	3.01 Å	3.42 Å
Zn^{2+} Nε(401)	2.23Å	2.23Å
Zn^{2+} - Nε(405)	2.15Å	2.25Å
Zn^{2+} - Nε(411)	2.23Å	2.26Å
O_3 - N(Ala189)	3.20Å	3.02Å
O_3 – N(Leu188)	2.76Å	2.70Å
N_1 – O(Ala189)	3.99Å	4.06Å

MS560; trigonal bipyramidal geometry

	Molecule A	Molecule B
Zn^{2+} - O_2	2.36Å	2.41Å
Zn^{2+} - O_1	2.26Å	2.30Å
O_1 - N(Gln402)	2.92Å	3.07Å
O_1 – H_2O	(H_2O_{104}) 2.96Å	(H_2O_{58}) 2.75Å
Zn^{2+} - Nε(401)	2.25Å	2.21Å
Zn^{2+} - Nε(405)	2.31Å	2.37Å
Zn^{2+} - Nε(411)	2.32Å	2.36Å
O_3 –N(Leu188)	2.98Å	2.85Å
O_3 –N(Ala189)	3.99Å	3.39Å
O_4 –N(Leu188)	3.91Å	2.85Å
N_1 –O(Ala189)	3.04Å	3.34Å
N –O(Ala189)	3.45Å	3.48Å
O_4 – H_2O	(H_2O_{169}) 2.94Å	(H_2O_{153}) 3.26Å
O_5 - N_α(His401)	2.94Å	2.94Å

MJ24; trigonal bipyramidal

	Molecule A	Molecule B
Zn^{2+} - O_2	2.47Å	2.42Å
Zn^{2+} - O_1	2.88Å	2.60Å
O_1 – N (402)	3.01Å	3.55Å
Zn^{2+} - $N\varepsilon(401)$	2.40Å	2.28Å
Zn^{2+} - $N\varepsilon(405)$	2.32Å	2.35Å
Zn^{2+} - $N\varepsilon(411)$	2.20Å	2.31 Å
O_3 –N(Ala189)	3.20Å	3.12Å
O_3 –N(Leu188)	3.21Å	3.00Å
O_4–N(Leu188)	-	3.19Å
O_4–C(Leu188)	3.50Å	-
O_5 - N_α(His401)	2.85Å	2.98Å

Table 4. Zn^{2+} coordination geometry and ligand-zinc distances at the active site.

4.2 Pro-catalytic MMP-9 (ProMMP-9ΔcollVΔpex)

4.2.1   Protein purification and characterization

For the isolation of the enzyme, the bacteria were cultured in a 3 liter fermentor, whereby the amount of cells obtained was 7.0 g wet weight (see paragraph 3.2.2.1).

Purification with anion exchange chromatography (3.2.2.2), yielded 65 mg of the denatured protein from 7.0 g of cells. The protein eluted as a single peak was slowly added drop wise to a stirred at room-temperature solution of refolding buffer (3.2.2.2), yielding a maximum of 15 µg/ml protein in solution. After overnight stirring, the protein was dialysed against 20 mM Tris/HCl, 100 mM NaCl pH 7.5 and concentrated yielding about 2.0 mg of refolded protein. Analysis by SDS-PAGE showed a molecular weight of 46 kDa for ProMMP-9ΔcollVΔpex, approximately equal to the expected molecular mass, with purity of about 80 % (Figure 34).

4.2.2   Activation of ProMMP-9 by trypsin, APMA, and by stromelysin-1

Wild type proMMP-9 was activated from the latent to an active form by cleavage of the N –terminal prodomain. This cleavage can occur either by a conformational change induced by limited auto-proteolysis of one or more sites within the pro-domain after partial unfolding with *p*-aminophenyl-mercuric acetate (APMA), by proteolytic cleavage with the serine proteinase trypsin (cleavage at Arg_{87}–Phe_{88}) or by cleavage through the metalloproteinase stromelysin-1.
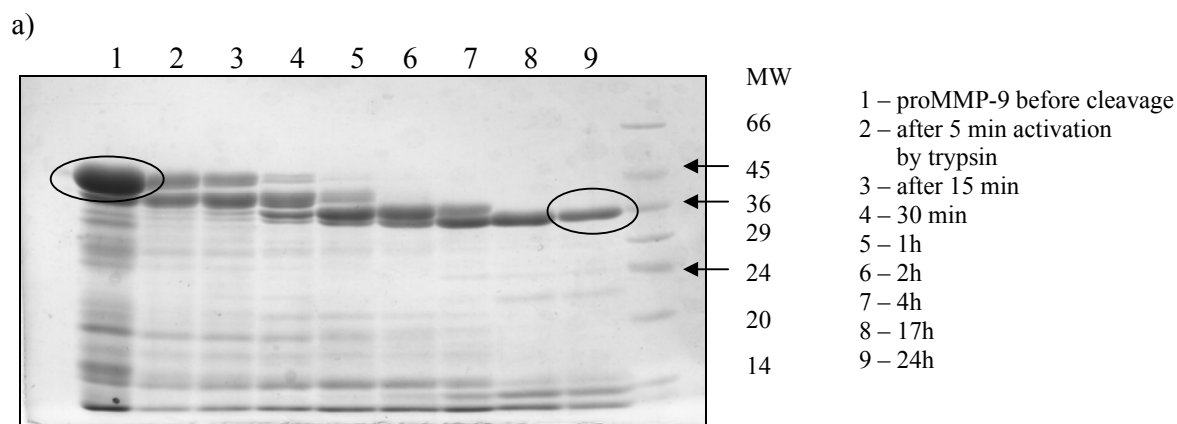
a)

Figure 34 a). Time course and effect of activation of wild-type proMMP-9 on SDS-gels by trypsin. 1.0 mg/ml protein were incubated in 20 mM Tris/HCl, 100 mM NaCl pH 7.5 containing 10 µg/ml trypsin at RT.
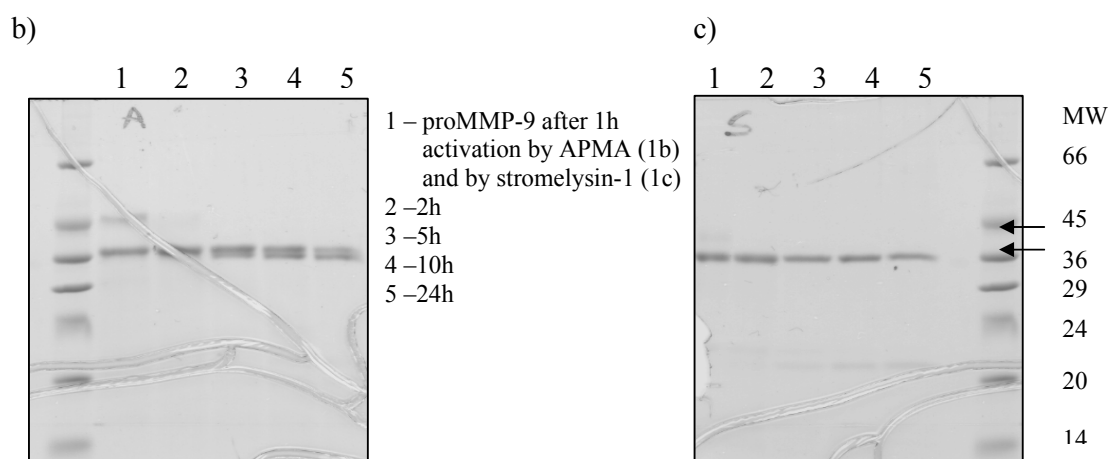
b)   c)

Figure 34 b). Time course and effect of activation of wild-type proMMP-9 on SDS-gels by APMA. 0.4 mg/ml protein were incubated with 1.0 mM APMA (with 5 mM Ca^{2+}) at 37°C;. **Fig. c)** by stromelysin-1, 0.4 mg/ml protein incubated with 16 µM stromelysin-1 at 37°C.

The processing was terminated at different time points by boiling the samples with SDS-gel loading buffer. Subsequently, aliquots were separated in 12% SDS-PAGE gels under reducing conditions. Treatment of proMMP-9 wild-type with trypsin in the absence of Ca^{2+} led to degradation of the enzyme (see Figure 34a). In order to determine the time course of the activation, 5 µl of the reaction mixture were removed at each time point, and the samples were incubated for various times (5, 15, and 30 min, 1 hour, 2, 4, 17, and 24 hours, respectively). SDS-PAGE analysis of proMMP-9 with trypsin treatment revealed cleavages in the pro-domain after a short time, followed by the generation of intermediates and finally the active enzyme (36 kDa) after 17 to 24 hours (Fig. 34a). The activation steps were confirmed by continuously measuring of the activity (see Fig. 35)

according to the activation assay described in paragraph 3.2.2.3.1.1. The proteolytic assay was performed following cleavage of the Fluorogenic Peptide Substrate 1 (Mca-P-L-G-L-Dpa-A-R-NH$_2$).

Treatment of proMMP-9 with APMA was initiated at 37 ºC in the presence of 5 mM Ca^{2+} (5 mM) (Pourmotabbed et al., 1995) followed by autoproteolytic processing of the enzyme to the stable form. As shown in Figure 34b, treatment of recombinant proMMP-9 generates active spices after 1 hour incubation. One day incubation resulted mostly in degradation products (see Fig 34b, line 5). In the absence of Ca^{2+}, the ProMMP-9 activation was not observed.

The incubation with stromelysin-1 at 37 ºC did not require the presence of Ca^{2+}. SDS-PAGE analysis revealed active enzyme after 1 hour treatment, which was stable even after 24 hours (Fig. 34c).
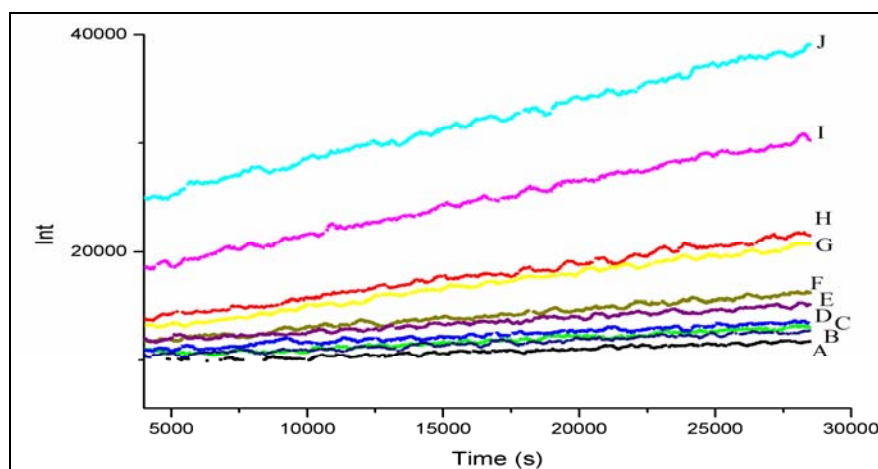

Figure 35. Activity control of proMMP-9 as an effect of activation after cleavage of the pro-domain by trypsin after: B-0min, C-5 min, D-15 min, E-30 min, F-1h, G-2h, H-4h, I-17h and J after 24 hours respectively; A- substrate without proMMP-9. The fluorogenic peptide *Substrate 1* was used in a concentration of 10 μM.

4.2.3   Inhibition of proMMP-9 by bivalent inhibitors

The bivalent MMP inhibitors should contain two distant head groups, one binding to the catalytic domain such as a hydroxamic acid, to coordinate the catalytic zinc, and another for binding via a flexible linker of appropriate length to a portion of the propeptide sequence centred on the Phe31 side chain in order to exploit the hydrophobic pocket of

the third FnII domain for exosite binding. A schematic representation of head and tail groups interacting simultaneously with the two distinct sites of the enzyme is depicted in Figure 36.
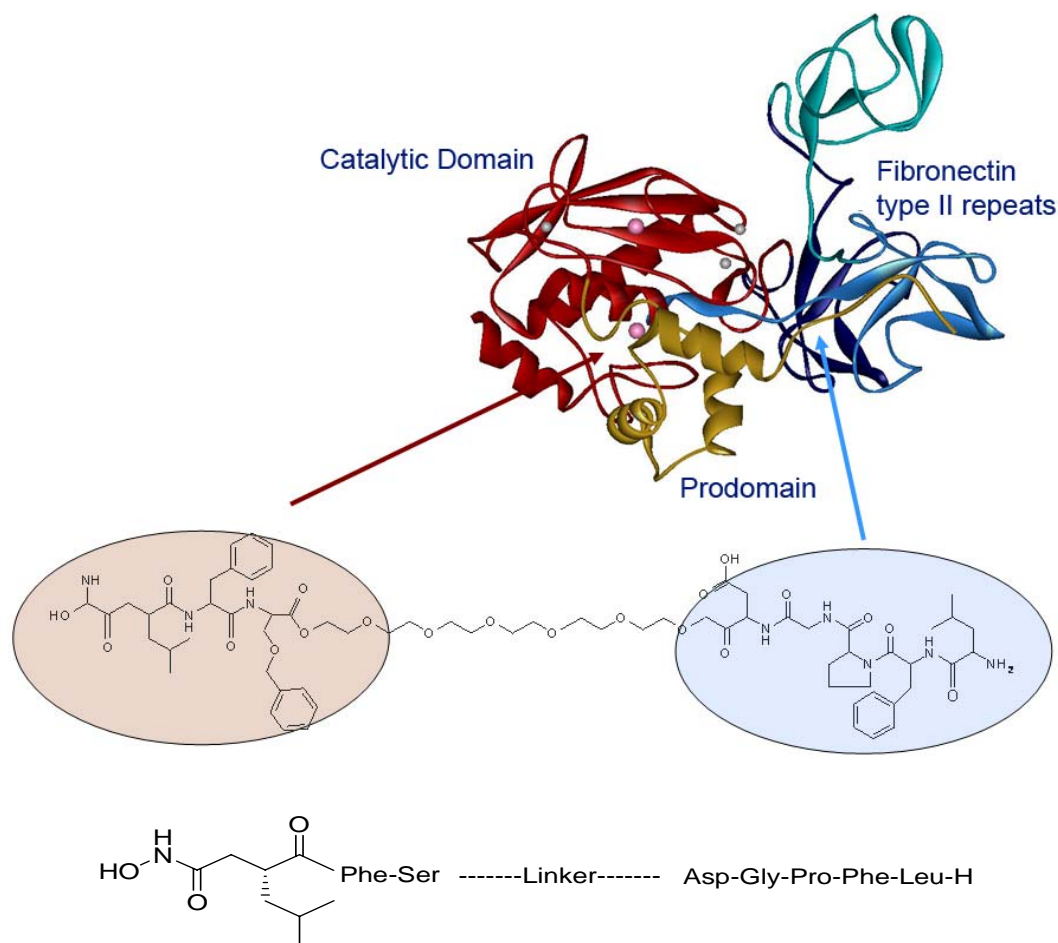

Figure 36. Schematic representation of the inhibitors designed and modelled on the crystal structure of proMMP-9. The catalytic domain is shown in red, the three FnII domains are in green, blue, and cyan, the Zn^{2+} ions are shown as a magenta spheres. The propeptide domain is yellow. The drawing shows the binding head for the catalytic domain (e.g., a hydroxamate moiety) and the pentapeptide (corresponding to the sequence surrounding Phe31) both connected by a flexible polyethylene glycol (PEG) linker.

For the Zn^{2+} binding head group, a pseudotripeptide was chosen with a hydroxamate as the metal chelating group. In analogy to batimastat, a phenyl residue was introduced in position P2′; the essential P1′ residue was the *i*But lateral chain (Leu) present also in batimastat, while in order to diminish binding affinities, the Cα of the hydroxamic acid was left unsubstituted. A Ser was introduced as P3′ residue, due to the good fit to the S3'subsite. As binding head group for the fibronectin exosite the pentapeptide portion Asp-Pro-Gly-Phe-Leu was chosen which is part of the proMMP-9 propeptide interacting with the Fibronectin II domain. The orientation of the two peptide sequences is

antiparallel, a fact which influences the choice of possible spacers. From flexibility and solubility considerations, and because of its modular character, a polyethylene glycol (PEG) spacer was selected to connect the two peptidic portions of the bivalent inhibitor.

PEG has several advantages, for example it is one of the best biocompatible polymers and possesses a multitude of useful properties (Zalipsky et al., 1995). It is soluble in both organic and aqueous media, lacks toxicity and immunogenicity (Dreborg et al., 1990), it is easily excreted from living organisms (Yamaoka et al., 1994), and resistant to degradation and modification (Mutter et al., 1971; Lu et al., 1993).

For our experiments three different bivalent inhibitors with varying linker length were designed. The first one contained four ethylene glycol blocks (Al134 (Peg$_4$)), the second one six (Al134 (Peg$_6$)), and the third one eight (Al134 (Peg$_8$)). The longer constructs, Al134 (Peg$_6$), and Al134 (Peg$_8$) were used as Ser(Bzl) derivative in the enzyme assays. However, modelling experiments and the binding modes of hydroxamate-type inhibitors to the catalytic domain of MMPs as derived from X-ray analysis strongly suggest a minimal role of this residue in the binding process.

4.2.3.1   Kinetic measurements

The three potential bivalent inhibitors Al134 Peg$_4$, Al134 Peg$_6$, and Al134 Peg$_8$ were assayed for their inhibitory potencies on two MMP-9 constructs: first the mini-MMP-9 and secondly proMMP-9, which was activated by APMA.

For the analysis of the hydroxamate head group of the bivalent inhibitors with the active centre, the mini-MMP-9 was used. With this enzyme very similar inhibitory potencies were determined for all three inhibitors (Table 5). The measurements clearly confirm a minimal interaction and thus interference of the spacer and FnII binding head with the catalytic site of the enzyme. As expected from considering the structure of the hydroxamate head group of the bivalent constructs, the affinities of all three inhibitors are slightly lower than those of batimastat (BB-94), taken as a hydroxamate-type reference inhibitor.
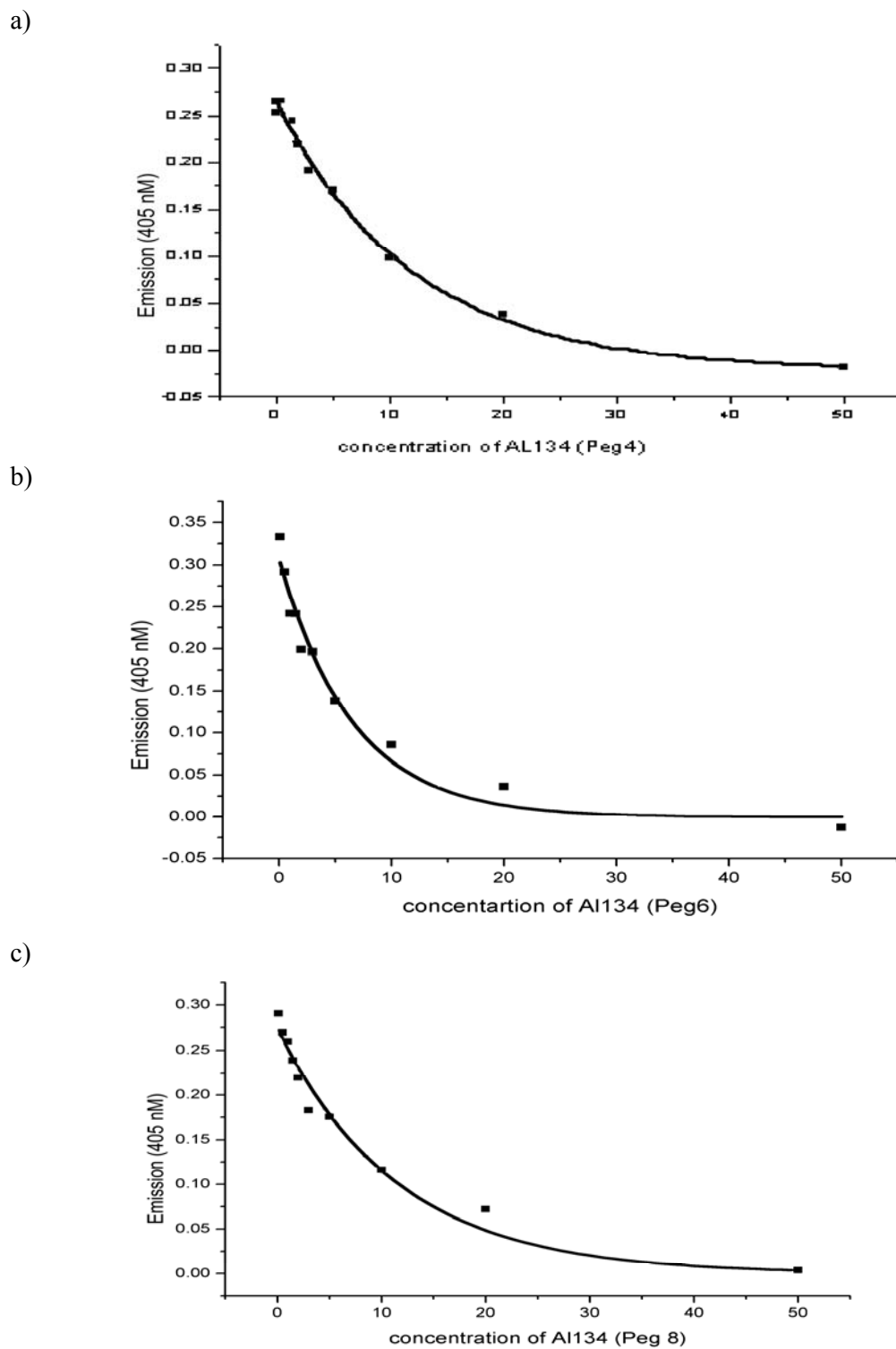
a)

b)

c)

Figure 37. Mini-MMP-9 inhibition curves with three potential hydroxamate inhibitors; a) Al134 Peg$_4$, b) Al134 Peg$_6$ and c) Al134 Peg$_8$. The fluorogenic peptide *Substrate 1* was used in a concentration of 10 µM. The three potential bivalent inhibitors were tested in the range of 0.1 to 50.0 nM of the total volume and the protein in the range of 0.5-1.0 nM.

94

Inhibitor	IC_{50}
BB-94	~ 1.0 nM
Al134 Peg$_4$	~ 11.8 nM
Al134 Peg$_6$	~ 6.5 nM
Al134 Peg$_8$	~ 12.0 nM

Table 5. IC_{50} *values* for three potential inhibitors for miniMMP-9 with: Al134 Peg$_4$, Al134 Peg$_6$, and Al134 Peg$_8$, and batimastat (BB94) for comparison.

To investigate the interactions of bivalent inhibitors with proMMP-9, different experiments were performed. Many fluorogenic assays with different conditions have been taken into account including, e.g., different activation profiles (by trypsin or by APMA), different temperatures and incubation times, and finally also some commercially available recombinant MMP-9 was used in experiments. One of the constructs chosen was the MMP-9 catalytic domain consist of residues Phe88-Pro438 (from BIOMOL Company), but unfortunately the enzyme was not stable enough for our experiments. The next construct was recombinant human MMP-9 (rhMMP-9), a 688 amino acid residue protein with a predicted molecular mass of approximately 77 kDa (Biotech R&D). Consequently, home made proMMP-9 and rhMMP-9 were used in final measurements. The *pro*-domain was cleaved by APMA and incubated at 37 ºC for several hours. The resulting inhibition constants (IC_{50} values) are listed in Table 6. In general, the IC_{50} values do not differ significantly for activation over 2 or 7 hours. Furthermore, there are differences observed in the respective IC_{50} values. The outcome remains the same for batimastat BB-94 (compare with mini-MMP-9), which Al134 Peg$_6$ looses affinity and Al134 Peg$_8$ nearly doubles affinity.

Inhibitor	IC_{50} for *pro*MMP-9 after 2h activation	IC_{50} for *pro*MMP-9 after 7h activation
BB-94	~ 0.87 nM	0.9 nM
Al134 Peg$_4$	~ 13.5 nM	14.1 nM
Al134 Peg$_6$	~ 17.5 nM	21.4 nM
Al134 Peg$_8$	~ 8.7 nM	6.7 nM

Table 6. IC_{50} *values* for three potential hydroxamate inhibitors of MMP-9 with: Al134 Peg$_4$, Al134 Peg$_6$, and Al134 Peg$_8$, and batimastat as control.

4.3   The MT1-MMP Hemopexin domain (Hpex)

4.3.1   Protein purification and characterization

The MT1-MMP hemopexin domain (Hpex MMP-14) has been prepared and kindly provided by Dr. Yoshifumi Itoh (Imperial Collage, London). MT1-MMP is involved in cancer related activation processes, which involve dimerization of the enzyme. There is a controversial discussion, whether a MT1-MMP homodimer forms via the Hpex domain (Itoh et al., 2001; Overall et al., 2000; Wang et al., 2004).

In order to investigate the oligomeric state of the MT1-MMP Hpex domain in solution, gel filtration experiments and analytical sedimentation and equilibration runs were conducted. Taking into account the salt concentration, two different experimental conditions were checked. In gel filtration experiments, on a Superdex 75 column, the protein was eluted with an apparent mass of 22 kDa, consistent with the molecular mass of the monomer, when the salt in the running buffer was omitted. When 150 mM NaCl was included, the protein was eluted with a molecular mass of 30 kDa on a Superose 12 column (profile not shown).

To monitor the different results, analytical sedimentation velocity and equilibration runs were also carried out considering the two different buffer conditions. The sedimentation velocity experiment was additionally performed with another protein, MMP-1 Hpex. Equilibrium runs provide an absolute method for the measurement of molecular mass.
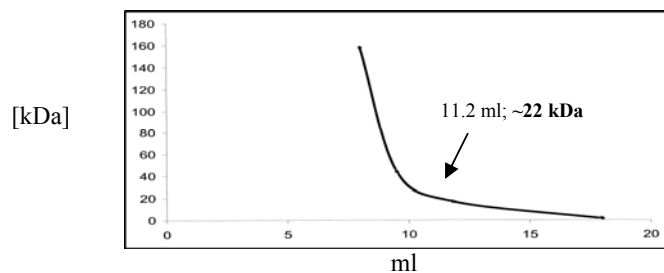
a)

b)

c)

[kDa]

11.2 ml; **~22 kDa**

ml
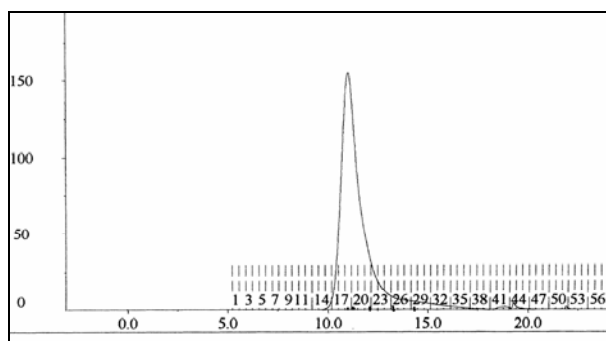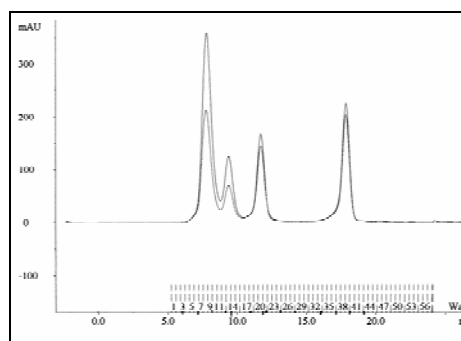
Figure 38 a). Gel filtration chromatography (20 mM TRIS/HCl, pH 7.5) for MT1-MMP Hpex domain eluted as a single peak from the Superdex S-75 column, detected at OD_{280}; **b).** Gel filtration for protein standards used in the calibration profile; bovine γ-globulin (158 ka), ovoalbumin (44 kDa), myoglobin (17 kDa), and cyanocobalamin (1.35 KDa); **c)** Calibration curve indicating the Molecular Weight (kDa) of MT1-MMP Hpex domain.

The results of these experiments confirmed the gel filtration runs. The sedimentation velocity in both buffers (with 150 mM NaCl and without salt) conditions showed a significant difference. For MT1-MMP Hpex analysed in a buffer without salt, the sedimentation coefficient was 2.49, and when 150 nM NaCl was included, the coefficient increased till 2.74 (Fig. 39 a and b), corresponding to molecular masses of roughly 20 kDa and 40 kDa, respectively. Unfortunately, the equilibration run was performed only in the buffer without salt. For MT1-MMP Hpex, the molecular weight of the domain was determined to about 20604 ± 500 Da (Fig. 40 a). As a reference, the MMP-1 Hpex domain yielded respectively 21684 ± 500 Da, corresponding to a monomer (Fig. 40 b). Taken together, our data indicates that Hpex of MT1-MMP undergoes dimerization in high salt concentration.

Finally, both techniques have confirmed the molecular mass of 22 kDa and of approximately 40 kDa under various buffer conditions. Apparently, the salt content of the solution determines the oligomeric state of Hpex MT1-MMP, i.e., either predominantly monomeric or dimeric.
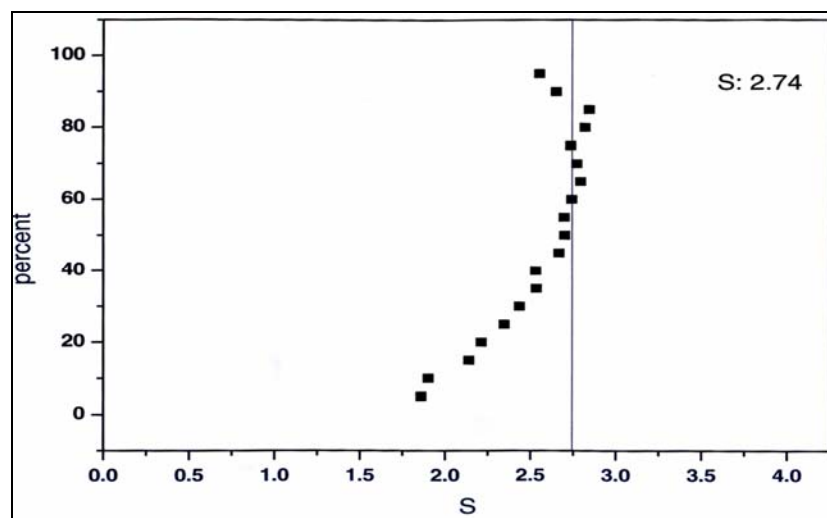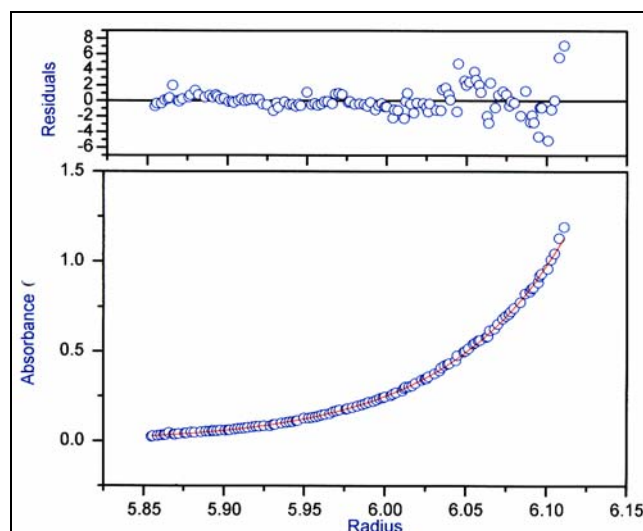
a)
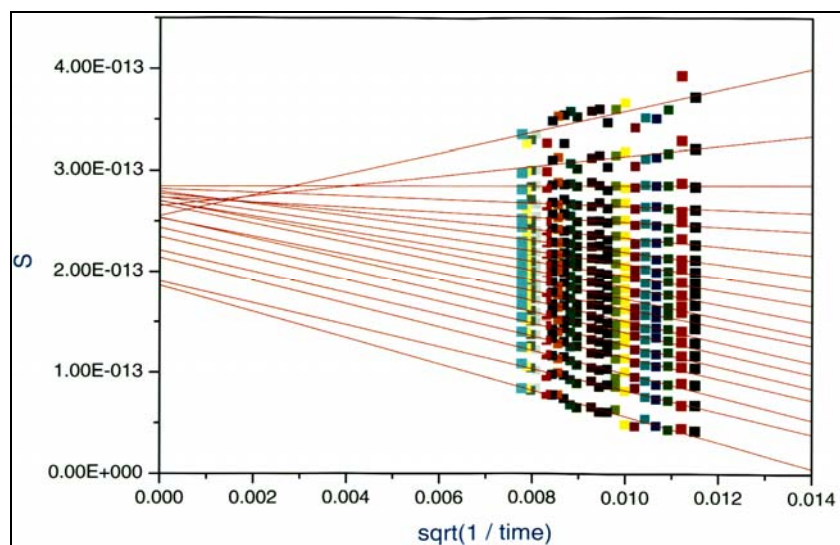
b)

Figure 39. Sedimentation velocity profiles for the MT1-MMP Hpex domain performed in 20 mM TRIS/HCl, pH 7.5, 150 mM NaCl; **a)** The profile indicating a mixture of monomer and dimer in solution; **b)** Sedimentation Coefficient S: 2.74 indicating dimers in the solution.
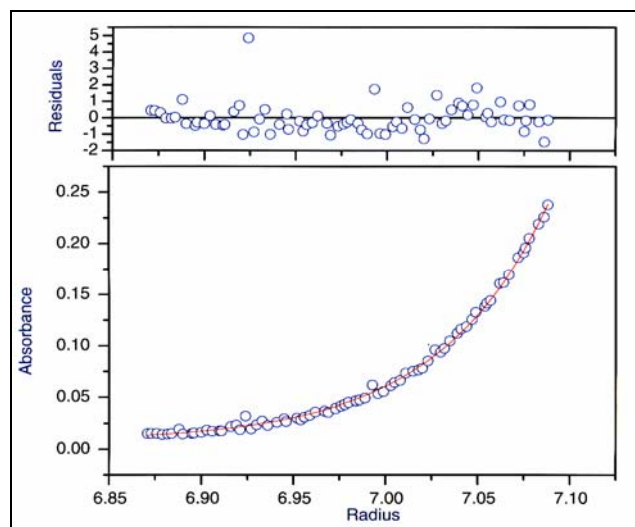
98

a)

b)

Figure 40. Equilibration profiles of analytical ultracentrifugation runs; **a)** for MT1-MMP Hpex, **b)** for MMP-1 Hpex. Experiments were performed in 20 mM TRIS/HCl, pH 7.5.

4.3.2   Protein crystallization and data collection

Prior to crystallization, the purified human MT1-MMP Hpex domain was concentrated up to 5.0 mg/ml by ultra-filtration in 20 mM Tris/HCl pH 7.5. The crystals belonged to space group $P3_121$ contain one molecule in the asymmetric unit with a Matthews coefficient of $V_m= 2.9$ Å^3/Da, corresponding to a solvent content of 57.0 %. Finally, a high resolution native data set with a limiting resolution of 1.8 Å was collected from a single crystal (see statistic displaed in Table 7).

Data Collection

Crystal content	MT1-MMP Hpex domain
Space group	P3$_1$21
Cell constants (Å)	
a	77.28
b	77.28
c	66.86
Resolution range (Å)	20.0 - 1.6
Unique reflections	27474
I/σ	32.1
Linear R-fac	0.052
Completeness (%)	99.0

Refinement

Reflection used for refinement	21682
Resolution range (Å)	20.0 - 1.8
Solvent content (%)	57.0
Protein molecules per asu	1
Residue number	194
Water molecules	131
Chlorine ion	1
Calcium ion	1
[b]R$_{factor}$ (%)	21.0
[c]R$_{free}$ (%)	21.7
R.m.s.d. [c] from ideal geometry	
Bond lengths (Å)	0.005
Bond angles (°)	1.259
Ramachandran plot	
Preferred (%)	83.1
Add. allowed	15.6
Disallowed	0.6

[b]$R_{factor} = \Sigma_{hkl} ||F_{obs}| - |F_{calc}||/\Sigma_{hkl} |F_{obs}|$

[c]R_{free} is the R-value calculated with 5% of reflections not used in refinement

Table 7. Data collection and refinement statistics for MT1-MMP Hpex domain.

4.3.3   Structure determination

The availability of the three-dimensional structure of the homologous Hpex domain of MMP9 (PDB ID code: 1ITV)) allowed to determine the MT1-MMP Hpex domain crystal structure. The corresponding maximum likelihood based molecular replacement was performed using the program PHASER (Read et al., 2004). The final refinement resulted

in a model with crystallographic R_{factor} and R_{free} values of 21.0 and 21.7, respectively. The final model had an excellent stereochemistry (refinement statistics in Table 7).

4.3.4   Description of the overall structure

The MT1-MMP Hemopexin Domain (Hpex; C-terminal domain CTD*)* belongs to the topological family of β-propeller domains, which encompasses proteins with several blades of β strands ranging from four to eight. All hemopexin domains conform to one type characterized by a fourfold propeller and show the overall shape of a disc or shallow cylinder. Those Hpex domains are composed of a succession of four structurally homologous hemopexin-type repeats of 35–45 residues, each repeat featuring a blade or β-leaflet, around a central pseudo fourfold axis. This axis exhibits a central funnel-like tunnel or shaft (see below), which traverses the molecule and in this way connects both flat disc surfaces (Gumis-Rüth; 2004) (see Figure 41).

Accordingly, this β-propeller domain has been formed by modular tetramerization of an ancestral β-leaflet in a circular manner, such that the fourth blade packs against the first. Each of the four constituting blades (I to IV) of the propeller is made up of a four-stranded antiparallel β-sheet (strands β1 to β4) of simple up-and-down connectivity or β-leaflet topology (Figure 41, 3D Structure). The blades are arranged in such a way that the sequentially and structurally first inner strands β1 within each blade are located with radially directed hydrogen bonds to the following strands that run along the shaft of the propeller. The blades accumulate an internal twist on going from one strand to its outer neighbour, such that the outermost strand is nearly perpendicular to the innermost. The direction of the β1 strands along the channel axis allows to distinguish between an 'entry side' (origin of the strand) and an 'exit side' (end of the strand) of the thick disc or squat cylinder. The resulting toroidal domain structure is tethered by an SS-bridge between the two terminal blades, which maintain domain integrity. Usually, the central shafts serve as ion-binding sites in all hemopexin domains. In general, hemopexin domains serve as crucial components in protein-protein and protein-substrate interactions.
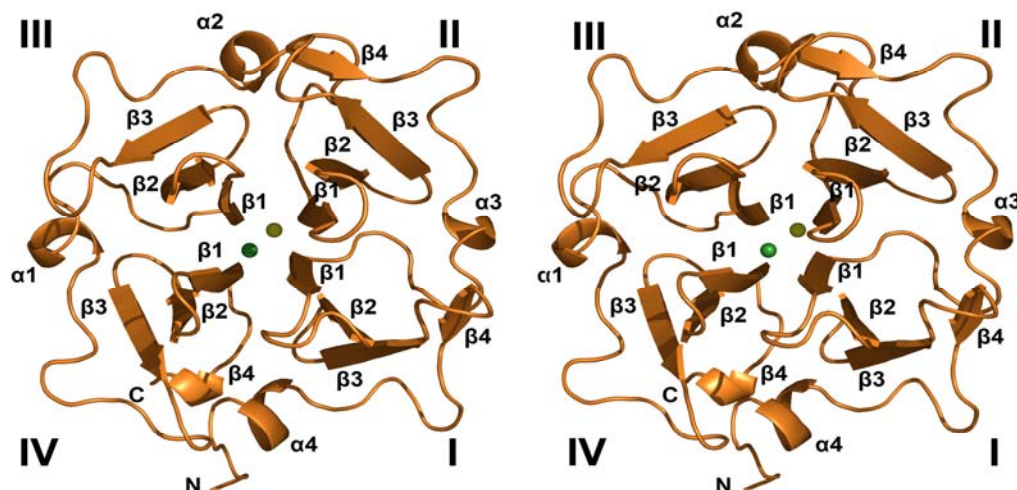
Figure 41. Stereo ribbon plot of the MT1-MMP Hpex domain. View of the 'entry side' of the channel trough disc. The four blades are labelled I to IV, as well as is each constituting β-strand (β1 to β4) and α-helix (α1 to α4). The sodium ion is shown as a yellow sphere, and chlorine as a green, respectively.

4.3.4.1   New evidence for dimerization of MT1-MMP Hpex domain

Although the MT1-MMT Hpex domain crystallized with one molecule in the asymmetric unit, two different possible dimerization sites have been found. The crystal structure shows that the dimerization is due to non-covalent interactions of the two Hpex domains, referred as molecule A and B. Those contacting molecules are generated by the symmetry operations of space group P3₁21. In the case of the symmetrical dimer, the interface between blades II/III and II/III is generated by the crystallographic symmetry operation (2 fold axis), that relates the two molecules by a 180 º rotation around an axis running tilted approximately by about 30 º to the propeller axes. Many contacting residues are involved and the strongest interactions are shown in Figure 42a. These interactions are contributed in the same way by both molecules, A and B. For example, Tyr436 of molecule A forms a hydrogen bond with Thr412 from the symmetry related molecule B (2.69Å) and vice versa. Furthermore, several hydrophobic and polar contacts are observed between the molecules, thus one can conclude that this interaction possesses an overall "mixed" character of protein interaction.

Additionally, a large non-symmetrical (asymmetrical) interaction was observed which appears to be a typical crystal contact. This contact between molecules A and B between blades I/II/III/IV and II/III is much more polar and charged compare with the

symmetrical interaction. It is essential and involves mostly hydrophilic residues. Moreover, many internal water molecules are observed, mainly accumulated in the centre of the cavity (see Fig. 42b). Surprisingly, they are not participating in the hydrogen bonds that connect the two Hpex domains.
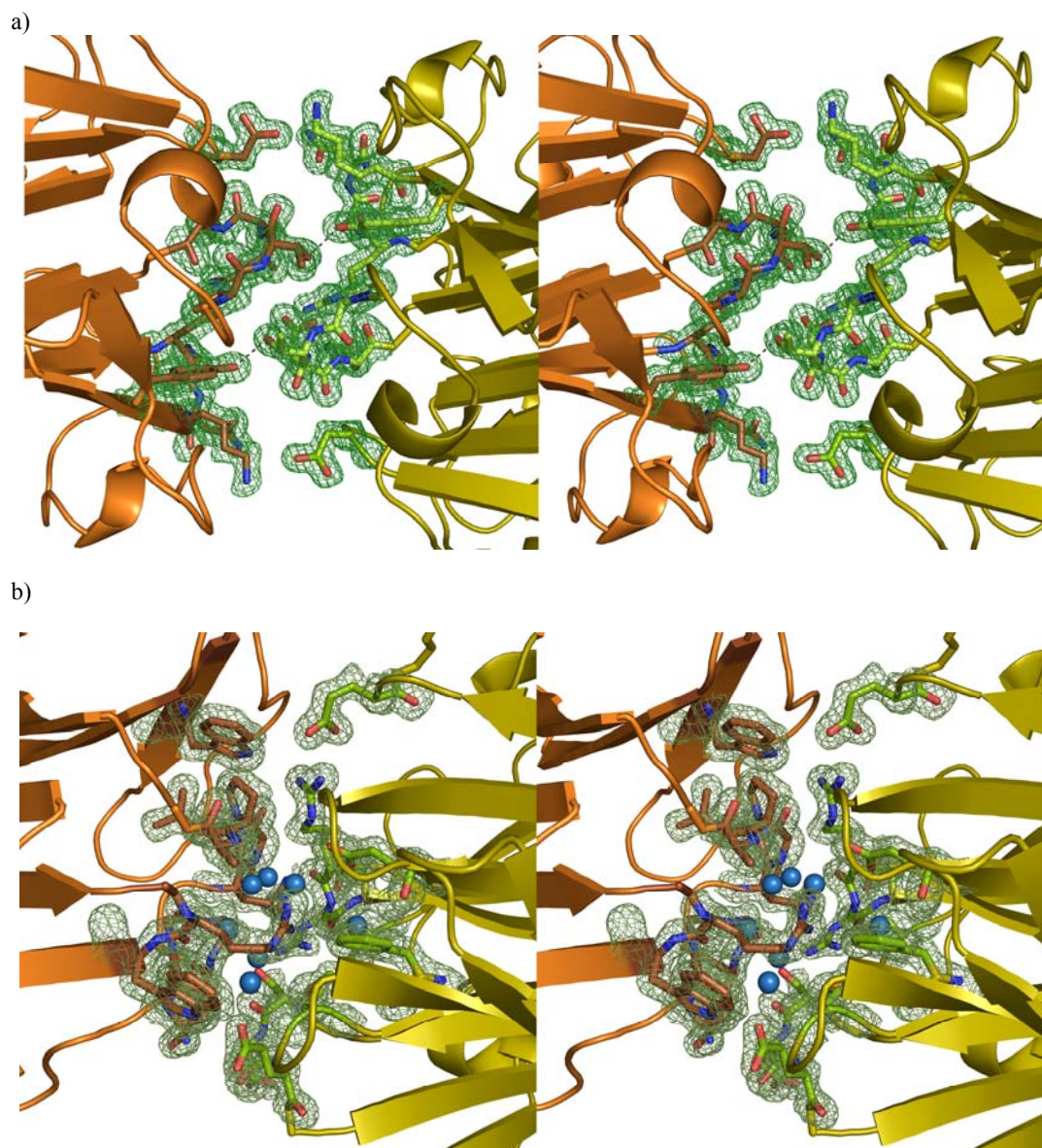
a)

b)

Figure 42. Detailed stereo view; a**)** at the symmetrical MT1-MMP-Hpex (molecule A) - MT1-MMP-Hpex (molecule B) dimer interface that is characterized by a crystallographic of $P3_121$ a two fold rotation. The interaction is mixed polar and hydrophobic. Involved residues are represented as stick models and covered by the electron density of $2F_o$-F_c map (contoured at 1σ) at 1.8 Å resolution; **b)** at the asymmetrical MT1-MMP-Hpex (molecule A) - MT1-MMP-Hpex (molecule B) dimer interface. This interface is characterized by a more hydrophilic interactions and less tight binding than in the case of the symmetrical dimer.

Apparently, one sodium ion binds to the exit side of the channel. It forms contacts with the carbonyl oxygen atoms of Asp416 (2.25 Å; blade II), Asn369 (2.35 Å; blade III), Thr370 (2.74 Å; blade III), and Arg464 (2.54 Å; blade I), and with one of the surrounding water molecules, Wat56 (2.61 Å). Additionally, deeper in a channel a well defined density was observed, which could be interpreted as a chloride ion. It is situated next to NH- of Ala371 (3.05 Å; blade III) and water Wat19 molecule (2.85 Å), while its charge may be compensated by the nearby sodium ion.

Chapter 5   Discussion

Cancer is a life-threatening disorder and one of the major health problems in our century. The investigated Matrix Metalloproteinase-9 (MMP-9, Gelatinase B) is a critical component of the angiogenic switch driving metastasis in various cancers. Additionally, it promotes other diseases like osteoarthritis, atherosclerosis or heart failure. In normal conditions, the MMP-9 proteolytic activity is tightly regulated by the endogenous tissue inhibitors of matrix metalloproteinases (TIMPs). Disruption of this MMP-TIMP balance leads to an excess of active MMP-9 which triggers deleterious events, mostly the degradation of all the main protein components of the extracellular matrix. In the case of cancer, inhibition of MMP-9 may prevent tumor growth. Therefore it is essential to design potent inhibitors in order to compensate for the loss of this regulatory mechanism.

Because of their association with a variety of diseases, the MMPs have received considerable attention as drug targets. Much of the effort in this area has focused on the design of small molecule antagonist with three primary features: 1) a catalytic zinc binding moiety, 2) a peptide mimetic and 3) a large hydrophobic moiety that fits into the deep S_1' pocket, present in most MMPs.

Even though many inhibitors have been studied, no one was sufficiently specific, and efficient for any individual MMP. In an attempt to clarify important determinants for the specific inhibition of MMP-9, we have analyzed the crystal structures of five different specific MMP-9 inhibitors. We have prepared the inactive E402Q mutant form of the truncated catalytic domain of human MMP-9, lacking both the fibronectin type II like and the C-terminal hemopexin domains, and have determined the 2.0 Å X-ray crystal structures of this recombinant mini-MMP-9 in complexes with the following catalytic zinc-directed synthetic inhibitors of different binding type: a phosphinic acid (AM409), a pyrimidine-2,4,6-trione (RO206-0222), a carboxylate (An1), a trifluoromethyl hydroxamic acid inhibitor (MS560), and a difluoro carboxylate inhibitor (MJ24).

5.1 Slow binding inhibitors of gelatinases

For our study several different inhibitors were available. For example, the very interesting SB-3CT, a novel slow-binding and transition state (mechanism) based synthetic inhibitor which was newly designed to be highly selective for gelatinases (MMP-2: K_i = 13.9 nM; MMP-9: K_i = 600 nM). X-ray absorption studies (Kleifeld et al., 2001) demonstrated that the catalytic zinc ion of MMP-2 is directly coordinated by the sulfur atom of the bound inhibitor in a monodentate manner to complete a tetrahedral coordination sphere at the zinc ion (Fig. 43). The design of such a mechanism-based inhibitor provides a novel approach for MMP inhibition by imparting or re-establishing the proenzyme structural motifs. In essence, the covalently attached inhibitor mimics the binding of the propeptide segment in MMPs, which is coordinated via a cysteine residue to the catalytic zinc ion by a similar binding via the thiolate group.
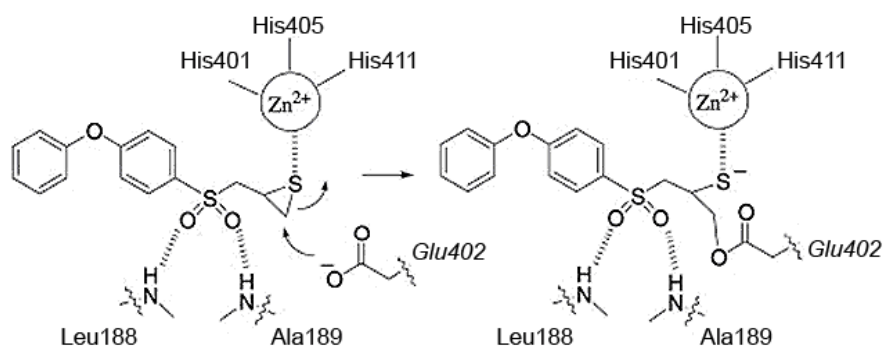

Figure 43. Proposed mode of MMPs inhibition by SB-3CT. Schematic representation of the proposed binding of SB-3CT, a mechanism based inhibitor, to the catalytic zinc ion in MMPs. The inhibitor is coordinated to the zinc ion via the thiolate of the thiirane group (adopted from Brown et al., 2000).

Overall, the results shown by Kleifeld and co-workers (Kleifeld et. al., 2001) suggest that the molecular coordination at the catalytic zinc site in the presence of SB-3CT is similar in the type of ligation, coordination number, and conformation to the proenzyme structure. In addition, all further analyses confirmed the modelling studies and the original proposed inhibition mechanism of MMPs by SB-3CT. Unfortunately, in our hands the crystals of miniMMP-9-SB-3CT complex never diffracted.

To solve the difficult problem of developing MMP inhibitors capable of differentiating the gelatinases MMP-2 and -9 from the other members of the MMPs family, the

structure-based design relying on the peculiar interaction of a propeptide portion in MMP-9 with a well delineated hydrophobic pocket of the third fibronectin domain was attempted. By exploiting the binding affinities of metal chelating groups at the active site and the exosite binding of a polypeptide portion to the fibronectin domain, the concept of bivalent inhibitors was pursued with three newly synthesized compounds: Al134 (Peg_4), Al134 (Peg_6), and Al134 (Peg_8) (see Fig. 44).
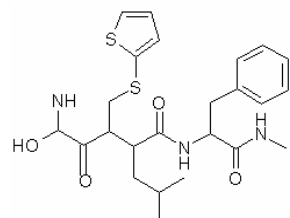
a)
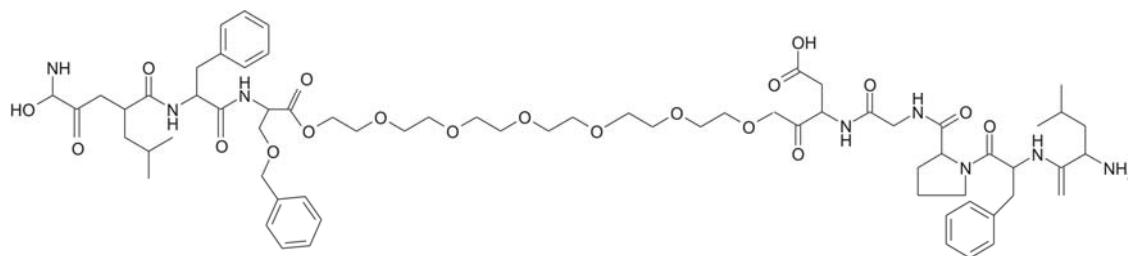
b)

Figure 44. Comparison of schematic chemical formulas: **a)** Bivalent inhibitor and **b)** Batimastat, BB-94.

For the isolated, truncated catalytic domain (miniMMP-9), similar inhibitory potencies of the three bivalent inhibitors were determined. However, the chemical differences to Batimastat may account for an overall 10-fold reduced inhibitory effect on the catalytic domain of miniMMP-9. Moreover, the almost identical IC_{50} values support the hypothesis of a minimal effect of the Ser(Bzl) group and of the polyethylene glycol spacer length on the binding affinities and, thus, interference with the catalytic site of the enzyme. As expected, the affinity of batimastat, taken as a monovalent hydroxamate-type inhibitor reference, was nearly unchanged when going from miniMMP-9 to full length MMP-9 (1.0 nM and 0.9 nM, respectively).

In contrast, one of the bivalent inhibitors, Al134 (Peg_8), exhibited a significantly increased inhibition of the full length MMP-9 with an IC_{50} drop from 12.0 nM to 6.7 nM. Al134 (Peg_4) displayed the same inhibition for miniMMP-9 and the full length

proteinase, while Al134 (Peg$_6$) even had a four fold decrease of inhibition of full length MMP-9.

Hence, one can assume that the bivalent inhibition concept for MMP-9 is working in principle. Obviously, the catalytic domain binding head has to be improved and probably designed exactly as in Batimastat. Additionally, the length of the PEG- linker could be optimized by using PEG$_7$, PEG$_9$, or PEG$_{10}$ units. Finally, the specificity of this novel inhibitor type should be tested with MMP-2.

5.2   The barbiturate ring as a chelator of the catalytic zinc

Barbiturates have been studied and applied as drugs for decades. They have been used as sedatives, narcotics and antiepileptic agents. Thus, they represent compounds with good bioavailability and biological compatibility. The barbiturate (pyrimidine-2,4,6-trion)-derivative RO206-0222 inhibitor has been previously described as highly specific for gelatinases (Grams et al., 2001).

Despite their apparent dissimilarity, the central barbiturate ring of the RO206-0222 inhibitor mimics the interactions of the inhibitor RO200-1770 for binding to MMP-8 (Brandstetter et al., 2001).
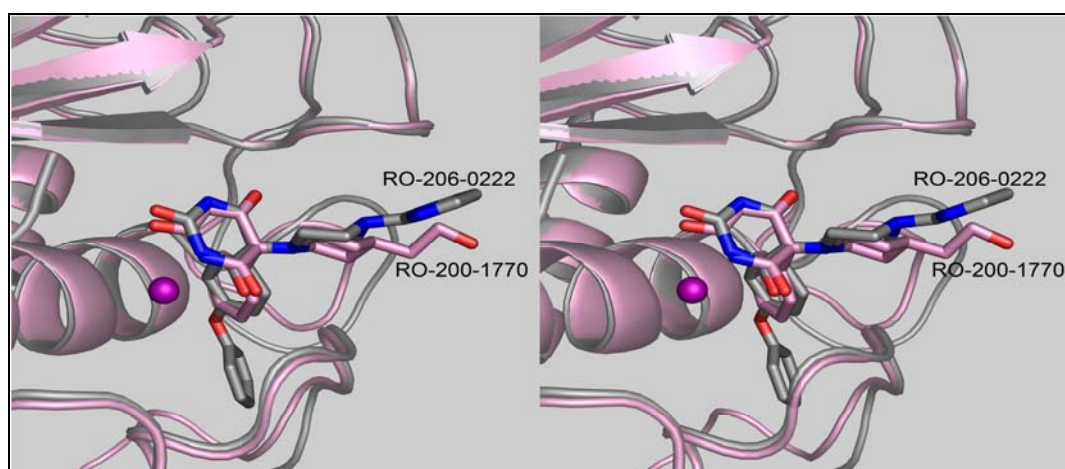

Figure 45. Stereo view of comparison of the MMP-8/RO200-1770 inhibitor (pink) and the MMP-9/RO206-0222 inhibitor (grey), depicted as stick models. The catalytic zinc is shown in magenta.

According to the electron density, the piperazine ring, which is loosely sandwiched between the peptide groups Gly186-Leu187 and Pro421-Met422, unequivocally exhibits in both molecules the chair conformation shown (see Fig. 45). In a related barbiturate compound (RO204-1924), the replacement of this piperazine by an isosteric piperidine ring (RO200-1770) leads to an increase in MMP binding, explained by higher desolvation energies for the piperazine binding (Brandstetter et al., 2001). The distal pyrimidine ring of RO206-0222 approximately arranged in the piperazine midplane extends into the bulk water, making quite weak contacts with Gly186. As indicated in Figure 45, investigation of the longer P1' group of RO206-0222 does not to be impaired by the apparently restricted S1' cavity of MMP-8 (Bode et al., 1994).

As shown in Fig. 46, RO206-0222 is not only a potent inhibitor against MMP-9, but also against MMPs-2 and 14 (and probably MMP-8, see Brandstetter et al., 2001), while the inhibition of MMP-1 is much weaker, giving rise to an extraordinary discrimination against MMP-1. These values certainly reflect the large S1' cavities of the former MMPs, and the restricted S1' pocket of MMP-1 and MMP-7, where the S1' cavity is delimited by the Arg or Tyr side chain at position 397 to a size allowing accommodation of medium-sized amino acid side chains only. The binding of inhibitors with longer P1' groups to MMP-1, also illustrated by experimental structures (Lovejoy et al., 1999), shows, however, that the Arg397 side chain, lacking the stabilizing hydrogen bond to Arg397 O, can be pushed out of its pocket site, under the cost of free binding energy. This is in agreement with results obtained for a series of related barbiturates, where the affinity and in particular the selectivity potential increased with the length of the P1' group (Grams et al., 2001; Brandstetter et al., 2001). As also mentioned by these authors, some of the binding effects of these barbiturates might be caused by the differential flexibility/plasticity with respect to the Pro421-422 peptide rotation, thereby explaining the decreased affinity for MMP-13.
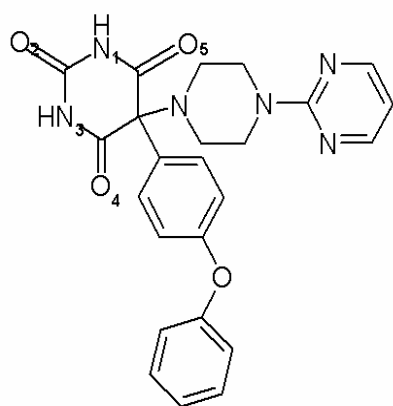
IC$_{50}$ [nM]:   **MMP-9:**   **2**
            MMP-1:   4310
            MMP-2:   5
            MMP-13:   245
            MMP-14:   9

Figure 46. Chemical formula of the RO206-0222 inhibitor with IC$_{50}$ values for selected human MMPs (Alrt et al., 2002).

5.3 The phosphinic peptide compounds as highly potent inhibitors

In the phosphinic peptide MMP inhibitors studied in this series, the isoxazole ring is used as a rigid scaffold to project various chemical groups in the right orientation able to interact with the S1' pocket. As shown in Fig. 47, AM409 is a powerful inhibitor not only for MMP-9, but also for MMPs-2, 8, 12, 13 and 14 (V. Dive, unpublished). This presumably reflects the similar binding to their open tunnel-like S1' cavities, whereas the other MMPs possess more restricted S1' pockets. In other phosphinate inhibitor series, developed by Devel and co-workers (2006), the phenyl-isoxazole-yl compounds were more potent inhibitors against most of these MMPs including MMP-9 than compounds further substituted in meta or para position. MMP-2 accepted compounds with longer P1' substituents even better. However, this might be explained by its even more open S1' pore. The weaker affinity towards MMP-3, on the other hand, might be due to the known rotability of the His424 side chain allowing closure of the S1' cavity (Dhanaraj et al., 1996). As expected, inhibition of MMP-1 and MMP-7, with Arg and Tyr residues at position 397 (MMP-9 nomenclature, see Fig. 48), respectively, by AM409 is much weaker, obviously due to the much stronger S1' blockage by these side chains. On the other hand, the low (sub)micromolar but still significant IC$_{50}$ values for MMPs-1 and 7 show that AM409 is still able to bind, presumably in that this phenyl-isoxazole-yl group penetrates the bottom of the S1' pocket by pushing these blocking side chains out of their "normal" position (Babine & Bender, 1997). Such an S1' perforation has been

experimentally shown for MMP-1 (Lovejoy et al., 1999). It is noteworthy that the strong inhibition of MMP-9 is in agreement with our finding that the Arg424 side chain does not occlude the S1' pocket of MMP-9. A similar argument holds for MMP-8, where the apparently blocking Arg side chain at position 426 (Bode et al., 1994) does not seem to hinder the unconstrained S1' perforation by the phenyl-isoxazole-yl (see Fig. 30 a and b) and longer P1' side chains (Devel et al., 2006).
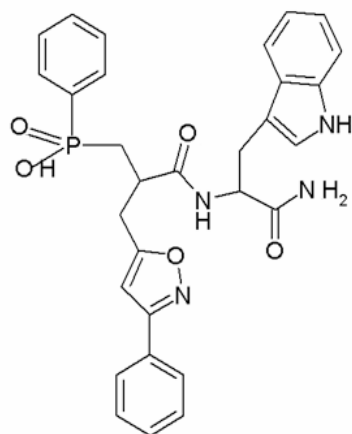
Ki [nM]:	**MMP-9:**	**1**
	MMP-12:	8.6
	MMP-13:	14
	MMP-14:	32
	MMP-8:	2.9
	MMP-2:	12
	MMP-3:	696
	MMP-1:	> 5μM
	MMP-7:	>>2.5μM

Figure 47. Chemical formula of the AM409 inhibitor with Ki values for selected human MMPs (V. Dive, unpublished data).
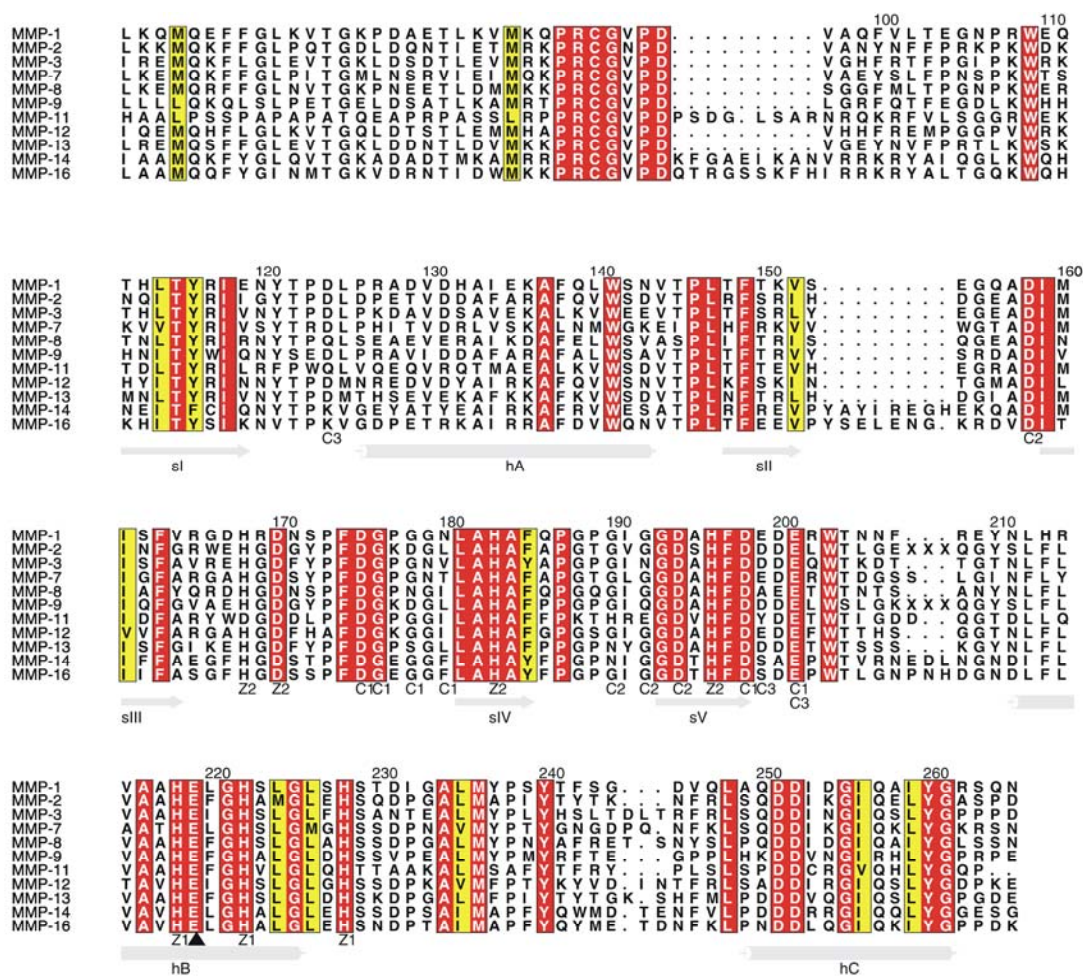
Figure 48. Sequence alignment of the catalytic domains of MMPs 1, 2, 3, 7, 8, 9, 11, 12, 13, 14, and 16 catalytic domains. The residue numbering is that of pre-proMMP-1. The location and extend of the α-helices and β-strands are represented by cylinders and arrows; strictly or strongly conserved residues are shown with red and yellow background respectively; special symbols denote residues involved in main and side-chain interaction with the catalytic (Z1), and the structural zinc (Z2), the first (C1), second (C2), and third calcium ion (C3) of the catalytic domains. Both gelatinases possess additional 175- and 176-residue fibronectin inserts in the gap between sV and hB, marked as xxx.

5.4 The function and influence of halogen substituted inhibitors

The distal iodine substituent of An1 is well defined in the miniMMP-9 complex, and extends into the lower exit of the S1' pore. It is in loose contact with neighbouring side chains of Leu397 and Leu418 and the Arg424 carbonyl group, and further surrounded by ordered water molecules. In general, halogens appended in para position to the biphenyl system increase the inhibition potency, but in particular improve the pharmacokinetics (Skiles et al., 2001).

As one can see in Fig. 49, the carboxylate inhibitor An1 discriminates between MMPs-2, 9, 14 and 16 (Oltenfreiter et al., 2004). The difference between MMP-2 and MMP-9 is, in view of the very similar active-site clefts of both proteinases, difficult to explain, but might be due to an unfavourable influence of the mobile Arg424 side chain of MMP-9, which in MMP-2 is replaced by the much less bulky Thr424 (Dhanaraj et al., 1999). As expected, the corresponding hydroxamic acid compound binds significantly more tightly, reflecting the superior coordination property of hydroxamic acids compared with carboxylic acids, due to a closer approach to an ideal trigonal-bipyramidal geometry predicted to be optimal by ligand field theory, but also because of lower desolvation free energy costs of the uncharged neutral hydroxamic acid group around physiological pH (see Grams 1995b). By contrast, carboxylate compounds, such as An1 in general discriminate more than hydroxamic acid compounds (Oltenfreiter et al., 2005b). This might be due to weaker restraints of the substituents in the carboxylate compound, allowing most likely a more freely adaptation to the S1' cavity.
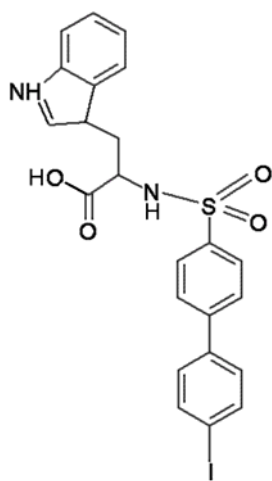
IC_{50} [nM]: **MMP-9:** **201**
MMP-2: 9.3
MT1-MMP: 859
MT3-MMP: 679

Figure 49. Chemical formula of the An1 inhibitor with IC_{50} values for selected human MMPs (Oltenfrieter et al., 2004).

The MS560 hydroxamic acid and the MJ24 carboxylate inhibitor have originally been designed to investigate the effect of tri- and bi-fluormethyl groups substituted in α-position of the hydroxamate and accordingly to carboxylate groups (Fig. 50) on the inhibition of MMPs involved in cancer (Sinisi et al., 2005). The task of this structure analysis was to determine the absolute configuration of the active compound, and to show the placement of those fluormethyl groups.
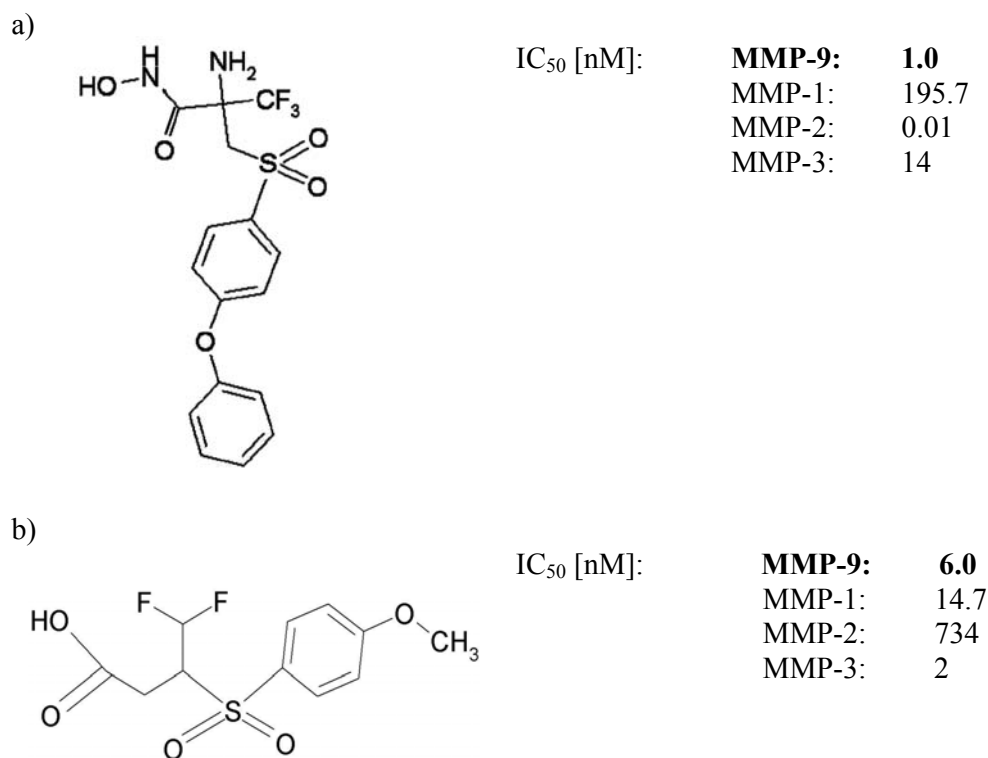
a)

IC$_{50}$ [nM]: **MMP-9:** **1.0**
MMP-1: 195.7
MMP-2: 0.01
MMP-3: 14

b)

IC$_{50}$ [nM]: **MMP-9:** **6.0**
MMP-1: 14.7
MMP-2: 734
MMP-3: 2

Figure 50. Chemical formulas of: **a)** MS560, and **b)** MJ24 inhibitors with IC$_{50}$ values for selected human MMPs (M. Zanda, unpublished data).

MS560 as well as the MJ24 inhibitor are characterized by a similar affinity as the non-fluorinated MS560 analog (Becker et al., 2001). The tri- and di-fluormethyl groups do only faintly affect MMP binding, in agreement with our finding that these groups make only weak contacts with surrounding groups, since they extend to the bulk solvent. The similar affinity of the N-methyl substituted compound might mean that the additional methyl group can be accommodated aside the Leu187 side chain. Moreover, the decrease in binding upon ethyl or propyl group substitution could indicate some overcrowding of the active site. This could also result from a different arrangement of the opposite diastereomer, since a racemic mixture was applied. The much higher affinity of MS560 MMP-2 (Fig. 51 a; which might be overestimated) could reflect the much weaker hindering of the P1' residue by the much less bulky Thr424 side chain (Dhanaraj et al., 1999).

5.5   Comparison of the contribution by the flexible Arg424 side chain to the selectivity

The five inhibitors crystallized and investigated with respect to their MMP-9 binding are of different chemical type. Their binding geometry is dictated by some common restraints, namely the favourable interaction of the metal-liganding group with the catalytic zinc ion, the optimal utilization of hydrogen bond interactions with the "bulge-edge" and the "S1' wall" forming segment, and the optimal insertion into the S1' cavity. The simultaneous optimization of all three interactions requires compromises. The zinc interaction (Fig. 51), which might be energetically dominant, is further optimized by a slight shift of the catalytic zinc, allowed in particular by a slight rotation and shift of the His405 and His411 imidazoyl side chains, respectively. The backbone mimics positioning seems to be governed by formation of a favourable hydrogen bond with Leu188 N-H, achieved by an optimal positioning of the sulfon/carbonyl group, allowing some freedom with respect to both flanking enzyme segments. This positioning as well as the nature of the linkage determine the extension of the P1' group into the S1' cavity. As also shown by the good fit of the enzyme side chain in the different MMP-9 structures, the S1' cavity is well structured at the entrance as well as in its central region. This even holds, in spite of its exposure, for the S1' wall-forming segment. The cavity accessible for the P1' groups is a relatively narrow twisted tube of oval cross section. The inhibitor extending in its proximal part from back/left to front/right is rotated in its lower part. As shown by Fig. 51, the P1' group elements try to adapt to this cavity, under allowance of internal constraints. In addition, distal aromatic groups can make favourable interactions in particular with carbonyl groups (e.g., of Tyr420), but aromatic groups do not seem to be privileged over aliphatic groups.

Due to the close similarity of their structural elements, these conformational constraints are similar for all MMPs. Therefore, compounds with a short to medium-sized P1' group utilizing only the enzyme contacts mentioned above can exhibit quite different affinities to a given MMP, but will in general not strongly discriminate between different MMPs. Small differences with respect to hydrophobicity and flexibility, such as in the Leu187 side chain or in the Pro421 carbonyl group, might nevertheless allow some discrimination. As described by Matziari et al. (2004), relatively selective phosphinates can be obtained by substituting the P1' phenyl ring in ortho-position, in this way exploiting small differences at the entrance of the S1' cavity.

As determined for the inhibitors used in this study, discrimination between the different MMPs is better achievable by variation of the length of the P1' groups. That is very evident for MMP-1 (and MMP-7, not shown), where the S1' cavity is delimited by the (Arg and Tyr) side chain at position 397 to a size allowing accommodation of medium-sized amino acid side chains only. The binding of inhibitors with longer P1' groups to MMP-1, also illustrated by experimental structures (Lovejoy et al., 1999), confirms, that the Arg397 side chain, in spite of the stabilizing hydrogen bond to Arg397 O, can be pushed out of its pocket site, under the cost of free energy of binding. According to the binding affinity data reported here, binding of inhibitors with longer P1' groups to MMP-8, with an apparently restricted S1' cavity (Bode et al., 1994), is not severely hindered, indicating the almost unconstrained brushing aside of the Arg426 side chain (see Fig. 49). The same argument holds for MMP-3, where the His424 imidazoyl group, in particular in its protonated state (Johnson et al., 2000), forms across the pocket lumen a hydrogen bond with Ala417 thereby blocking accommodation of longer P1' groups (Dhanaraj et al., 1996). In all of our MMP-9 structures, the Arg424 side chain is disordered and fully mobile, and extends away from the S1' cavity. However, it will partially occupy the bottom of the S1' cavity (Rowsell et al., 2002), to some degree hindering the unconstrained penetration of longer P1' groups. In contrast, the S1' cavity of MMP-2, otherwise being very similar to that of MMP-9 (compare the sequences in Fig. 48), is fully open at its bottom, due to the Thr424 residue of MMP-2 (Dhanaraj et al., 1999). This suggests that the Arg424 side chain is causing the slight affinity reduction of most inhibitors with longer P1' groups towards MMP-9 compared with MMP-2. Probing of the bottom part of the S1' cavity remains a promising strategy to obtain more selective inhibitors.

In addition, the specificity loop, situated even further beneath and exhibiting the highest sequence and length variability between different MMPs, constitutes a hot spot to develop selective inhibitors. Its differential and mainly larger mobility, dramatically limits the accurate modelling of MMP-inhibitor complexes (Cuniasse et al., 2005). Another possibility to gain specificity is the usage of the non-prime side pockets, which seem to provide even better opportunities for designing inhibitors with higher specificity (BG Rao, Curr Pharm Des 11, 295-322, 2005). Based on the unique preference of MMP-9 for Arg side chains at both P2 as well as P1 (Kridel et al., 2001), usage of the S2
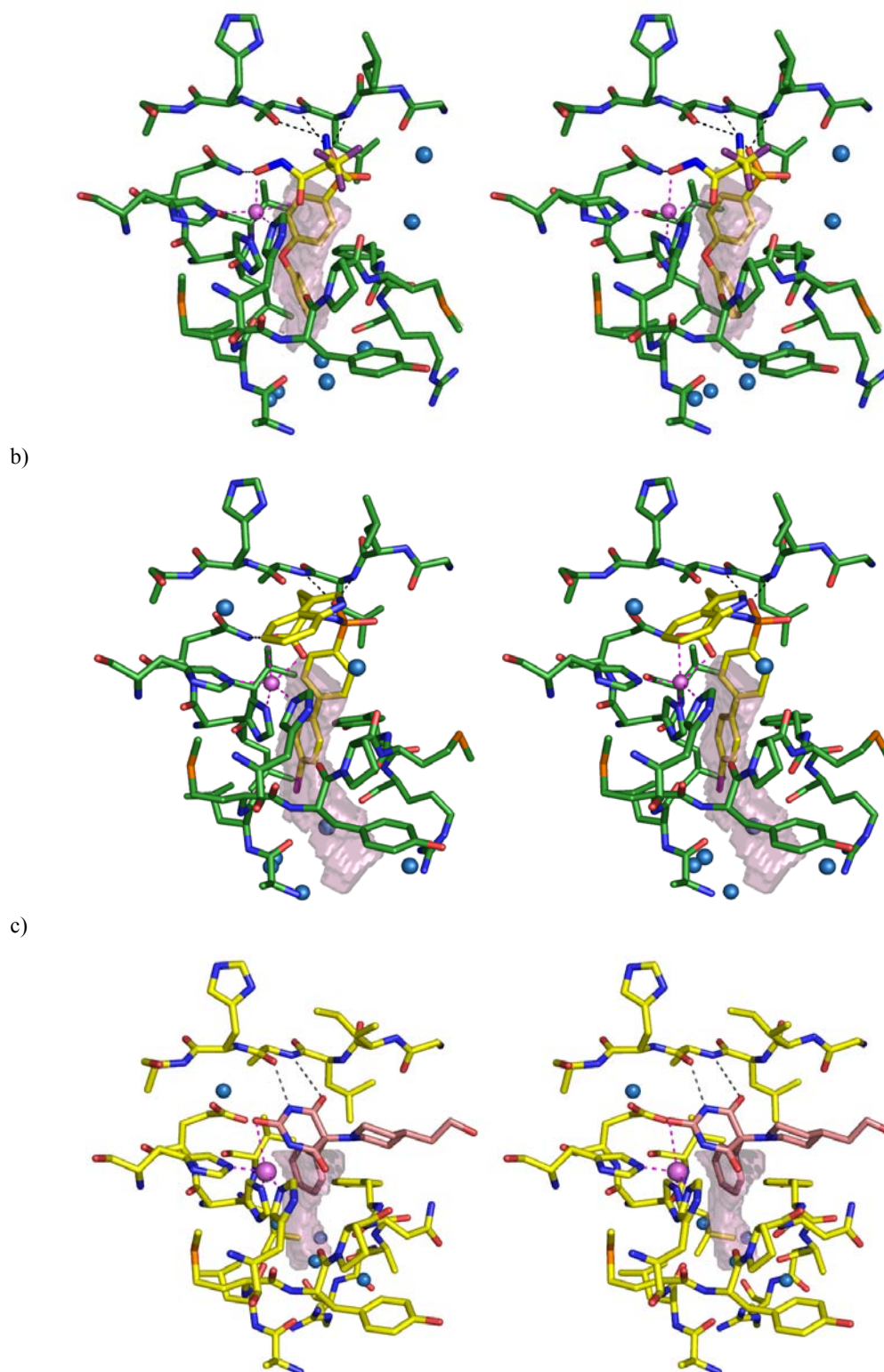
a)

b)

c)

Figure 51. Comparison of the S1´-cavities of MMP-9 with the MS560 (**a**) and An1 inhibitors (**b**) with MMP-8 in complex with (**c**). The cavities are depicted as transparent pink surfaces and were calculated with VOIDOO. The protein is presented in stick models.

118

subsite might be a particularly attractive strategy to obtain specific MMP-9 inhibitors (Chen et al., 2003).

5.6   MT1-MMP Hpex domain novel dimerization models

Dimerization emerges as an important mechanism to regulate the activation and activity of MMPs (Itoh et al., 2001; Overall et al., 2000). The membrane-type 1 matrix metalloproteinase (MT1-MMP, MMP14) was discovered as the first membrane – type MMP and identified as a specific activator of proMMP-2 at the cell surface. In normal conditions, the MT1-MMP activity is tightly regulated by TIMP-2, TIMP-3 and TIMP-4. It has been know for some time that MT1-MMP Hpex fixes through a bound TIMP-2, a proMMP-2 molecule presenting a scissile peptide bond toward a second non-inhibited MT1-MMP molecule (see Introduction, Fig. 19) (Strongin et al., 1995; Butler et al., 1997). The crystal structure of proMMP-2/TIMP-2 (Morgunova et al., 2002) shows in atomic resolution that both components interact via mixed hydrophobic/polar interfaces. This structural and additional experimental work (Fernandez-Catalan et al., 1998; Itoh et al., 2001), lead to attempts to model the hypothetical MT1-MMP-TIMP-2-proMMP-2 complex (Bode & Maskos, 2003; Itoh et al., 2001). It was suggested that MT1-MMP forms a homophilic complex through the hemopexin-like (Hpex) domain, and interestingly also the two (TM-14) transmembrane and the cytoplasmic (CYT) tail domains of MMP-14, bind each other arranging in a homodimer (Rozanov et al., 2001; Lehti et al., 2002) (Fig. 53). A similar homodimer was observed for the crystalline, non-covalent Hpex domain of MMP-9 (Cha et al., 2002).

All above described hypothesises convinced us to analyze the structure of the hepomexin-like domain of MT1-MMP. The protein crystallized as a monomer with two different, symmetrical and asymmetrical binding sites comprising larger interaction surfaces. The symmetrical MT1-MMP-Hpex dimer interface is characterized by a two fold rotation based on the crystallographic symmetry, and the interaction between blades II/III is mixed polar and hydrophobic. In this case, we modelled tentatively the symmetrical dimerization of full length MT1-MMP, based on the Hpex domain dimers (see Fig. 52), which appears to be possible for the binding through the transmembrane and cytoplasmic domain for both, A and B molecules. Furthermore, the complex

formation of Hpex MT1-MMP and TIMP-2 molecule via its C-terminal part seems to be possible in this configuration.
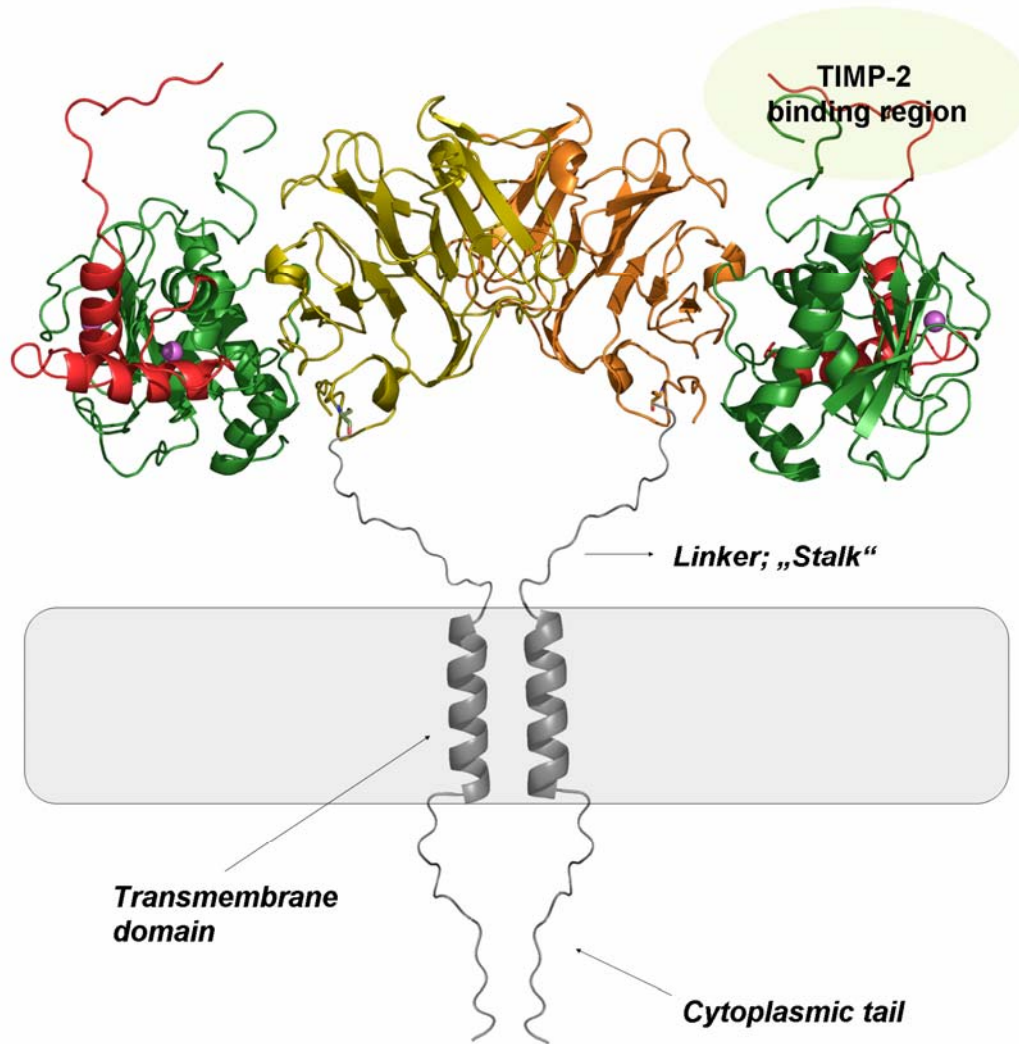

Figure 52. Proposed symmetrical dimerization model of the full length MT1-MMP of molecule A (indicated in olive) and molecule B (in orange) based on the symmetrical Hpex dimer found in the crystal structure. The catalytic domain is shown in green and prodomain in red, respectively. The catalytic and structural Zn^{2+} ions are indicated in magenta. Transmembrane domain and cytoplasmic tail stay together to the dimerization.

In the crystal structure a second, large non-symmetrical interaction surface was observed. Most likely, this dimerization interface between blades I/II/III/IV and I/II represents a typical crystal contact since it is much more polar and charged compared with the

symmetrical interaction surface (Fig. 53). Actually, the Hpex molecule B occupies the region at molecule A where the catalytic domain would be located in the full length MT1-MMP. One can conclude that the corresponding dimerization of the full length MT1-MMP it is not possible due to the large overlaps with the prodomain and the catalytic domain. Additionally, this conformation prevents binding of TIMP-2 and, consequently the formation of the activation complex MT1-MMP-TIMP-2-proMMP-2, as well as a proper membrane anchoring of both MT1-MMPs.
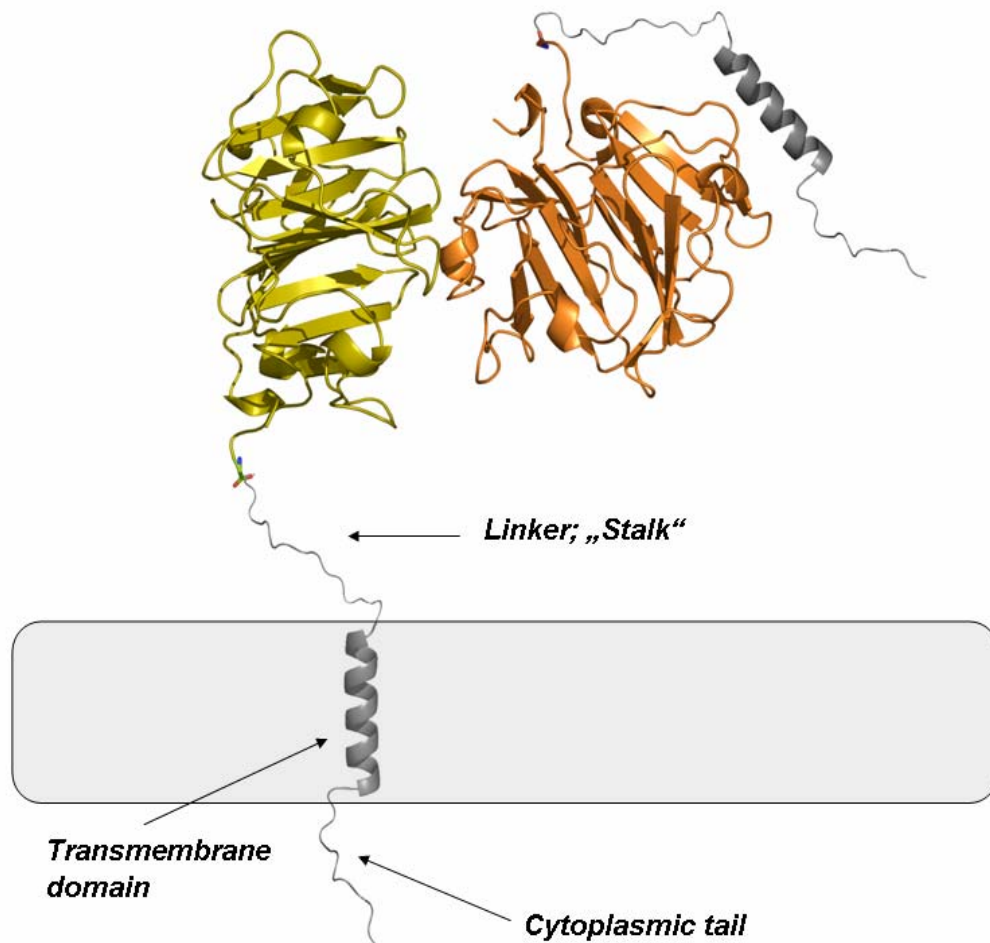
Figure 53. Non-symmetrical interaction of the MT1-MMP Hpex domains of molecule A (indicated in olive) and molecule B (in orange). The catalytic domain and the prodomain are not shown because of massive molecular overlaps.

There are conflicting data concerning the exact nature of the conserved metal ions bound within the propeller channel of the other Hpex structures. For example, in the case of the Hpex of MMP-2, the internal ions were interpreted from the bottom of the chanel (to its

top as Ca^{2+}, Cl^-, Na^{1+} (Libson et al., 1995) and Ca^{2+}, Cl^-, Ca^{2+} (Gohlke et al., 1996). Additionally, there is disagreement on the metal ion located at the bottom entrance. It was interpreted as calcium in the X-ray structure of MMP-1 Hpex domain (Li et al., 1995) and in both independently determined structures of MMP-2 (Libson et al., 1995, Gohlke et al., 1996) and MMP-13 (Gomis-Rüth et al., 1996) Hpex domains. By contrast, the metal ion at this position was interpreted as sodium ion, in both hemopexin structures (Faber et al., 1995; Paoli et al., 1999). In Hpex MMP-9, no calcium was found but one sodium ion which binds to the entrance of the channel of molecule A, but not to molecule B (Cha et al., 2002). In our, Hpex MT1-MMP we have found one chloride situated deeper in the channel and one sodium ion closer the exit side.

Chapter 6   Literature

Babine R.E., Bender S.L. (1997) Molecular Recognition of Proteinminus signLigand Complexes: Applications to Drug Design. *Chem Rev.* 97 (5); 1359-1472.

Backstrom J.R., Lim G.P., Cullen M.J., Tökés, Z.A. (1996) Matrix metalloproteinase-9 (MMP-9) is synthesized in neurons of the human hippocampus and is capable of degrading the amyloid-β peptide (1–40). *J. Neurosci.* 16; 7910–7919.

Bannikov G.A., Karelina T.V., Collier I. E., Marmer B. L., Goldberg G. I. (2002) Substrate binding of gelatinase B induces its enzymatic activity in the presence of intact propeptide. *J. Biol. Chem.* 277**;** 16022–16027.

Barrett, A.J. & Rawlings, N.D. (1991) Types and families of endopeptidases. *Biochem. Soc. Trans.* 19; 707-715.

Barrett A.J., Rawlings N.D. & Woessner J.F. (1998) Hendbook of Proteolytic Enzyme. *Academic Press, San Diego,* 1998.

Barrett, A.J., Rawlings, N.D. & Woessner J.F (1998b) Introduction: cysteine peptidases and their clans. London, *Academic Press*.

Becker J.W., Marcy A.I., Rokosz L.L., Axel M.G., Burbaum J.J., Fitzgerald P.M., Esser C.K., Hagmann W. K., Hermes J. D. (1995) Stromelysin-1; three-dimentional structure of the inhibited catalytic domain and of the C-truncated proenzyme. *Protein Sci,* 4(10); 1966-76.

Belaaouaj A. A., Li, A., Wun T. C., Welgus H. G., Shapiro S. D. (2000) Matrix metalloproteinases cleave tissue factor pathway inhibitor. Effects on coagulation. *J. Biol. Chem.* 275; 27123–27128.

Bergers G., Brekken R., McMahon G., Vu T.H., Itoh T., Tamaki K., Tanzawa K., Thorpe P., Itohara P., Werb Z., Hanahan D. (2000). Matrix metalloproteinase-9 triggers the angiogenic switch during carcinogenesis. *Nat. Cell Biol.* 2; 737-744.

Bernando M.M., Brown S., Li Z.H., Fridman R., Mobashery S. (2002) Design, Synthesis and Characterization of Potent, Slow-binding Inhibitors That Are Selective for Gelatinases. *J.Biol.Chem.,* 277; 11202-11207.

Black W.C., Bayly Ch.I., Davis D.E., Desmarasis S., Falgueyret P.J., Leger S., Sing Li CH., Masse F., McKay D.J., Palmer J.T., Persival M.D., Robichaud J., Tsou N., Zamboni R. (2005) XXX Trifluoroethylamines as Amide Isosters in Inhibitors of Cahepsin K.

Binkert Ch., Frigerio M., Jones A., Meyer S., Pesenti C., Prade L., Vianti F., Zanda M. (2005) Replacement of isobutyl by Trifluoromethyl in Pepstatin A Selectively Affects Inhibition of Aspartic Proteinases.

Birkedal-Hansen H., Moore W.G.I., Bodden M.K., Windsor L.J., Birkead-Hansen B., DeCarlo A., Engler J.A. (1993) Matrix Metalloproteianses: A Review. *Crit Rev Oral Biol and Med,* 4(2); 197-250.

Bohm G., Muhr R. and Jaenicke R. (1992) Quantitative-Analysis of Protein Far UV Circular-Dichroism Spectra by Neural Networks. *Protein Engineering*, 5; 191-195.

Bode W., Gomis-Rüth F.X, and Stöckler W. (1993) Astacins, serralysins, snake venom and matrix metalloproteinases exhibit identical zinc-binding environments (HEXXHXXGXXH and Met-turn) and topologies and should be grouped into a common family, the 'metzincins'. *FEBS Lett,* 331; 134-140.

Bode W., Reinemer P., Huber R., Kleine T., Schnierer S., Tschesche H. (1994) The X-ray crystal structure of the catalytic domain of human neutrophil collagenase   inhibitrd by a substrate analogue reveals the essentials for catalysis and specificity. *EMBO J*, 13; 1263-1269.

Bode W., Fernandez-Catalan C., Tschesche H., Grams F., Nagase H & Maskos K. (1999) Sstructural properties of matrix metalloproteinses. *Cell Mol. Life Sci.* 55; 639-652.

Bode W. & Huber R. (1992) Natural protein proteinase inhibitors and their interaction with proteinases. *Eur J Biochem,* 204(2); 433-51.

Bode W. & Maskos K., (2003) Structural basis of the matrix metalloproteinases and their physiological inhibitors, the tissue inhibitors of metalloproteinases. *Biol Chem.* 384(6); 863-72.

Bode W. & Maskos K., (2004) Matrix of Metalloproteinases; *Handbook of Metalloproteinases Vol. 3*; 130-147.

Backstrom J.R., Tökés, Z.A. (1995) The 84–kDa form of human matrix metalloproteinase-9 degrades substance P and gelatin. *J. Neurochem.* 64**;** 1312–1318.

Belkin A.M., Akimov S.S., Zaritskaya L.S., Ratnicov B.I., Deryugina E.I., Strongin A.Y.(2001) Matrix-dependent proteolysis of surface transglutaminase by membrane type metalloproteinase regulates cancer cell adhesion and locomotion. *J. Biol. Chem.* 276; 18415-18422.

Bergers G., Brekken R., McMahon G., Vu TH., Itoh T., Tamaki K., Tanzawa K., Thorpe P., Itohara S., Werb Z., Hanahan D. (2000) Matrix-metalloproteinase-9 triggers the angiogenic switch during carcinogenesis. *Nat Cell Biol.* 2; 737-744.

Birkedal-Hansen H., Moore W.G., Bodden M.K., Windsor L.J., Birkedal-Hansen B., DeCarlo A., Engler J.A. (1993) Matrix metalloproteinases: a review. *Crit. Rev. Oral Biol. Med.* 4; 197–250.

Brandstetter H., Grams F., Glitz D., Lang A., Hubert R., Bode W., Krell H. W., Engh R. A. (2001) The 1.8 Å Crystal Structure of a Matrix Metalloproteinase 8-Barbiturate Inhibitor Complex Reveals a Previously Unobserved Mechanism for Collagenase Substrate Recognition. *J Biol Chem.* 276(20); 17405-17412.

Brew K., Dinakarpandian D., Nagase H. (2000) Tissue inhibitors of metalloproteinases: evolution, structure and function. *Biochim Biophys Acta*. 1477(1-2); 267-83.

Brinckerhoff C.E., Matrisian L.M. (2002); Matrix metalloproteinases: a tail of a frog that became a prince. *Nat Rev Mol Cell Biol.* 3(3); 207-14.

Brooks P.C., Silletti S., von Schalscha T.L., Friedlander M., Cheresh D.A. (1998) Disruption of angiogenesis by PEX, a noncatalytic metalloproteinase fragment with integrin binding activity. *Cell* 92; 391-400.

Brown S., Margarida B., Korta L.P., Tanaka Y., Fridman R., and Mobashery, S. (2000) *J Am. Chem. Soc.* 122, 6799-6800.

Brunger A.T., Adams P. D., Clore G.M., DeLano W.L., Gros P., Grosse-Kunstleve R.W. (1998) Crystallography and NMR system: a new software suite for macromolecular structure determination. *Acta Crystallog.* Sect. D, 54; 905-921.

Bu Ch. H., Pourmotabbed T., (1995) Mechanism of activation of human neutrophil Gelatinase B. *J Biol Chem* 270 (31); 18563-18576.

Bu Ch. H., Pourmotabbed T. (1996) Mechanism of Ca^{2+}-dependent activity of Human Neutrophil Gelatinase B. *J Biol Chem* 271; 14308-14315.

Butler G.S, Butler M.J, Atkinson S.J, Will H, Tamura T, van W.S, Crabbe T, Clements J, d'Ortho M.P, Murphy G. (1998) The TIMP2 membrane type 1 metalloproteinase ''Receptor'' regulates the concentration and efficient activation of progelatinase A. A kinetic study. *J Biol Chem* 273; 871–880.

Butler G. S., Will H., Atkinson S.J., Murphy G. (1997) Membrane-type-2 matrix metalloproteinase can initiate the processing of progelatinase A and is regulated by the tissue inhibitors of metalloproteinases. *Eur J Biochem*. 244(2); 653-7.

Buttner F.H., Hughes C. E., Margerie D., Lichte A., Tschesche H., Ceterson B., Bartnik E., (1998) Membrane type 1 matrix metalloproteinase (MT1-MMP) cleaves the recombinant aggrecan substarte rAgg1mut at the aggrecanase and the MMP sites. Characterization of MT1-MMP catabolic sites on the interglobular domain of aggrecan. *Biochem. J.*, 333; 159-165.

Bigg H.F, Morrison C.J, Butler GS, Bogoyevitch M.A, Wang Z, Soloway P.D, Overall C.M. (2001) Tissue inhibitor of metalloproteinases-4 inhibits but does not support the activation of gelatinase A via efficient inhibition of membrane type 1-matrix metalloproteinase. *Cancer Res* 61; 3610–3618.

Cañete-Soler R., Litzky L., Lubensky I., and Muschel R.J. 1994. Localization of the 92 kDa gelatinase mRNA in squamous cell and adenocarcinomas of the lung using *in situ* hybridization. *Am. J. Pathol.* 144; 518–527.

Cao J., Kozarekar P., Pavlaki M., Chiarelli C., Bahou W.F., Zucker S. (2004) Distinct roles for the catalytic and hemopexin domains of membrane type 1-matrix metalloproteinase in substrate degradation and cell migration. *J Biol Chem* 279; 14129–14139.

Cuniasse P., Devel L., Makaritis A., beau F., Georgiadis D., Matziari M., Yiotakis A., Dive V. (2004) Future challenges facing the development of specific active-site directed synthetic inhibitors of MMPs. 87; 393-402.

Coussens L.M., Tinkle C.L., Hanahan D., Werb Z. (2000) MMP-9 supplied by bone marrow derived cells contributes to skin carcinogenesis. *Cell* 103(3); 481-90.

Coussens L.M. & Werb Z. (2002) Inflamation and cancer. *Nature* 420(6917); 860-7.

Cuniasse P., Devel L., Makaritis A., Beau F., Georgiadis D., Matziari M., Yiotakis A., Dive V. (2005) Future challenges facing the development of specific active site directed synthetic inhibitors of MMPs. *Biochimie.* 87(3-4); 393-402.

Cha H., Kopetzki E., Huber R., Lanzerdorfer M., Brandstetter H. (2002) Structural basis of the adaptive molecular recognition by MMP9. *J Mol Biol.* 320(5); 1065-79.

Chambers A.F., Matrisian L.M. (1997) Changing views of the role of matrix metalloproteinases in metastasis. *J Natl Cancer Inst.* 89; 1260-70.

Chen L., Noelken M.E., Nagase H. (1993) *Biochemistry* 32; 10289-10295.

Chen E.J., LiW., Godzik A., Howard E.W., Smith J.W. (2003) A residue in the S_2 Subsite controls substrate selectivity of matrix metalloproteinase-2 and matrix metalloproteinase-9. *J. Biol. Chem.* 278; 17158-17163.

Chun T.H., Sabeh F., Ota I., Murphy H., McDonagh K.T., Holmbeck K., Birkedal-Hansen H., Allen E.D., Weiss S.J. (2004) MT1-MMP dependent neovessel formation with within the confines of the three-dimensional extracellular matrix. *J. Cell. Biol.* 167; 757-767.

Cuniasse P., Devel L., Makaritis A., Beau F., Georgiadis D., Matziari M., Yiotakis A. Dive V. (2004) Future challanges facing the development of specific active-site-directed synthetic inhibitors of MMPs. Biochimie 87; 393-402.

Cornelius L.A., Nehring L.C., Harding E., Bolanowski M., Welgus H.G., Kobayashi D. K., Pierce R.A., Shapiro S.D. (1998) Matrix metalloproteinases generate angiostatin: effects on neovascularization. *J. Immunol.* 161**;** 6845–6852.

Cuzner M.L., Opdenakker G. (1999) Plasminogen activators and matrix metalloproteases, mediators of extracellular proteolysis in inflammatory demyelination of the central nervous system. *J. Neuroimmunol.* 94**;** 1–14.

Davies B., Waxman J., Wasan H., Abel P., Williams G., Krausz T., Neal D., Thomas D., Hanby A., and Balkwill F. (1993) Levels of matrix metalloproteases in bladder cancer correlate with tumor grade and invasion. *Cancer Res.* 53**;** 5365–5369.

Deryugina E.I., Ratnicov B.I., Postnova T.I., Rozanov D.V., Strongin A.Y. (2002a) Processing of of inegrin alpha v subunit by membrane type 1 matrix metalloproteinse stimulates migration of breast carcinoma cells on vitronectin and enhances tyrosine phosporylation of focal adhesion kinase. *J. Biol.Chem*. 277; 9749-9756.

Deryugina E.I., Soroceanu L., Strongin A.Y., (2000b) Up-regualation of vascular of endothelial growth factor by membrane-type matrix metalloproteinase stimulates human glioma xenograft growth and angiogenesis. *Cancer Res.* 62; 580-588.

Desrivières S., Lu H., Peyri N., Soria C., Legrand Y., Menashi S. (1993) Activation of the 92 kDa type IV collagenase by tissue kallikrein. *J. Cell Physiol.* 157**;** 587–593.

Desrochers P.E., Mookhtiar K., Van Wart H.E., Hasty K.A., Weiss S.J. (1992) Proteolytic inactivation of α1–proteinase inhibitor and α1–antichymotrypsin by oxidatively activated human neutrophil metalloproteinases. *J. Biol. Chem.* 267**;** 5005–5012.

Devel L.**,** Rogakos V., David A., Makaritis A., Beau F., Cuniasse P., Yiotakis Y., Dive V. (2006) Development of Selective Inhibitors and Substrate of Matrix Metalloproteinase-12. *J Biol Chem.* 281; 11152-11160.

Dive V., Georgiadis D., Matziari M., Makaritis A., Beau F., Cuniasse P., Yiotakis A. (2004) Phosphinic peptides as zinc metalloproteinase inhibitors. *Cell.Mol.Life.Sci.* 61; 2010-2019.

Dreborg, S.; Akerblom, E.B. (1990) *Critical Reviews in Therapeutic Drug Carrier Systems* 6; 315-365.

Drenth, J., Jansonius, J.N., Koekoek, R. & Wolthers, B.G. (1971) The structure of papain. *Adv. Protein Chem.* 25; 79-115.

Duncan M.E., Richardson J.P., Murray G.I., Melvin W.T., Fothergill J.E. (1998) Human matrix metalloproteinase-9: activation by limited trypsin treatment and generation of monoclonal antibodies specific for the activated form. *Eur. J. Biochem.* 258**;** 37–43.

Elkins P.A., Ho Y.S., Smith W.W., Janson C.A., D'Alessio K.J., McQueney M.S., Cummings M.D., Romanic A.M. (2002) Structure of the C-terminally truncated human ProMMP9, a gelatin-binding matrix metalloproteinase. *Acta Cryst.* D58; 1182-1192.

Ellerbroek S.M, Wu YI, Overall C.M, Stack M.S. (2001). Functional interplay between type I collagen and cell surface matrix metalloproteinase activity. *J Biol Chem* 276; 24833–24842.

Emonard H. and Hornebeck, W. (1997) Binding of 92 kDa and 72 kDa progelatinases to insoluble elastin modulates their proteolytic activation. *Biol. Chem.* 378**;** 265–271.

Endo K., Takino T., Miyamori H., Kinsen H., Yoshizaki T., Furukawa M., Sato H. (2003) Cleavage of syndecan-1 by membrane type matrix metalloptoteinas-1 stimulates cell migration. *J. Biol. Chem.* 278; 40764-40770.

Faber H.R., Groom C.R., Baker H.M., Morgan W. T., Smith A., Baker E.N. (1995) 1.8 Å crystal structure of the C-terminal domain of rabbit serum haemopexin. *Structure* 15;3(6);551-9.

Fang K.C., Raymond W. W., Lazarus S.C., Caughey G.H. (1996) Dog mastocytoma cells secrete a 92–kD gelatinase activated extracellularly by mast cell chymase. *J. Clin. Invest.* 97**;** 1589–1596.

Ferry G., Lonchampt M., Pennel L., de Nanteuil G., Canet E., Tucker G. C. (1997) Activation of MMP-9 by neutrophil elastase in an in vivo model of acute lung injury. *FEBS Lett.* 402**;** 111–115.

Fernandez-Catalan C., Bode W., Huber R., Turk D., Calvete J.J., A. Lichte., Tschesche H., Maskos K. (1998) Crystal structure of the complex formed by the membrane type 1-matrix metalloproteinase with the tissue inhibitor of metalloproteinases-2, the soluble progelatinase A receptor. *EMBO J.* 17; 5238–5248.

Fernandez-Patron C., Zouki C., Whittal R., Chan J.S., Davidge S.T., Filep J.G. (2001) Matrix metalloproteinases regulate neutrophil-endothelial cell adhesion through generation of endothelin-1[1–32]. *FASEB J.* 15; 2230–2240.

Finkelstein, A.V., Ptitsyn, O.B. and Kozitsyn, S.A. (1977) Theory of Protein Molecule Self Organization .2. Comparison of Calculated Thermodynamic Parameters of Local Secondary Structures with Experiments. *Biopolymers* 16; 497-524.

Fosang A.J., Neame P.J., Last K., Hardingham T.E., Murphy G., Hamilton, J.A. (1992) The interglobular domain of cartilage aggrecan is cleaved by PUMP, gelatinases, and cathepsin B. *J. Biol. Chem.* 267**;** 19470–19474.

Fosang A.J., Last K., FujiiY., Seiki M., Okada Y. (1998) Membrane type 1 MMP (MMP14) cleaves at three sites in the aggrecan integlobulr domain. *FEBS Lett.* 430; 186-190.

Friedberg M.H., Glantz M.J., Klempner M.S., Cole B.F., and Perides G. (1998) Specific matrix metalloproteinase profiles in the cerebrospinal fluid correlated with   the presence of malignant astrocytomas, brain metastases, and carcinomatous meningitis. *Cancer* 82**;** 923–930.

Fukui N., McAlinden A., Zhu Y., Crouch E., Broekelmann T.J., Mecham R.P., Sandell L.J. (2002) Processing of type II procollagen amino propeptide by matrix metalloproteinases. *J. Biol. Chem.* 277**;** 2193–201.

Gearing A.J., Beckett P., Christodoulou M., Churchill M., Clements J., Davidson A.H., Drummond A.H., Galloway W.A., Gilbert R., Gordon J.L., Leber T. M., Mangan M., Miller K., Nayee P., Owen K., Patel S., Thomas W., Wells G., Wood L.M., Woolley, K. (1994) Processing of tumour necrosis factor- precursor by metalloproteinases. *Nature* 370**;** 555–557.

Gohlke U., Gomis-Ruth F.X., Crabbe T., Murphy G., Docherty A.J., Bode W. (1996) The C-terminal (haemopexin-like) domain structure of human gelatinase A (MMP-2) – structural implications for its function. *FEBS Letters.* 378, 126-130.

Goldberg G.I., Strongin A., Collier I.E., Genrich L.T., Marmer B.L. (1992) Interaction of 92–kDa type IV collagenase with the tissue inhibitor of metalloproteinases prevents dimerization, complex formation with interstitial collagenase, and activation of the proenzyme with stromelysin. *J. Biol. Chem.* 267; 4583–4591.

Gomis-Rüth F.X. (2003) Hemopexin domains. *Handbook of Metalloproteins Vol.3.* 631-646.

Gomis-Rüth F.X. (2003) Structural Aspects of the Metzincin Clan of Metalloendopeptidases. *Mol Biotechnol* 24; 157-202.

Gomis-Rüth F. X., Maskos K, Betz M, Bergner A, Huber R, Suzuki K, Yoshida N, Nagase H, Brew K, Bourenkov GP, Bartunik H, Bode W. (1997) Mechanism of inhibition of the human matrix metalloproteinase stromelysin-1 by TIMP-1. *Nature.* 389; 77–81.

Gomis-Rüth F.X., Gohlke U., Betz M., Knauper V., Murphy G., Lopez-Otin C., Bode W. (1996) The helping hand of collagenase-3 (MMP-13); 2.7Å crystal structure of its C-terminal haemopexin-like domain. *J Mol Biol.* 6;264(3):556-66.

Grams F., Brandstetter H., D'Alo S., Geppert D., Krell H.W., Leiner H., Livi W., Menta E., Oliva A., Zimmermann G. (2001) Pyrimidine-2,4,6-Triones: A New Effective and Selective Class of Matrix Metalloproteinase Inhibitors. *Biol. Chem.* 382; 12771285.

Gress T. M., Müller-Pillasch F., Lerch M. M., Friess H., Büchler M., and Adler G. (1995) Expression and *in-situ* localization of genes coding for extracellular matrix proteins and extracellular matrix degrading proteases in pancreatic cancer. *Int. J. Cancer* 62; 407–413.

Groll M., Ditzel L., Löwe J., Stock D., Bochtler M., Bartunik H. D., & Huber R. (1997) Structure of 20S proteasome from yeast at 2.4Å resolution. *Nature* 386; 463-471.

Groneberg R.D., Burns C.J., Morrissette M.M., Ullrich J.W., Morris R.L., Darnbrough S., Djuric S.W., Condon S.M., McGeehan G.M., Labaudiniere R., Neuenschwander K., Scotese A.C., (1999) *Kline J.A.J. Med. Chem.* 42, 541–544.

Gross J. and Lapiere C.M. (1962) Co llagenolytic activity in amphibian tissues: a tissue culture assay. *Proc. Nat. Acad. Sci. USA* 48; 1014-1022.

Gururajan R., Grenet J., Lahti J.M., Kidd V.J., (1998) Isolation and characterizytion of Two Novel Metalloproteianse Genes Linked to the *Cdc2L* Locus on Human Chromosome 1p36.3. *Genomics* 52; 101-106.

Hamdy F.C., Fadlon E.J., Cottam D., Lawry J., Thurrell W., Silcocks P.B., Anderson J. B., Williams J. L., and Rees R. C. (1994) Matrix metalloproteinase 9 expression in primary human prostatic adenocarcinoma and benign prostatic hyperplasia *Br. J. Cancer* 69; 177–182.

Harayama T, Ohuchi E, Aoki T, Sato H, Seiki M, Okada Y. (1999) Shedding of membrane type 1 matrix metalloproteinase in a human breast carcinoma cell line. *Jpn J Cancer Res* 90; 942–950.

Hibbs M.S., Hoidal J.R., Kang A.H. (1987) Expression of a metalloproteinase that degrades native type V collagen and denatured collagens by cultured human alveolar macrophages. *J. Clin Invest.* (80); 1644–1650.

Himelsten B.P., Canete-Soler R., Bernhard E.J., Dilks D.W., and Muschel R.J. (1994) Metalloproteinases in tumor progression: the contribution of MMP-9. *Invasion Metastasis* 14; 246–258.

Hiraoka N., Allen E., Apel I.J., Gyetko M.R., Weiss S.J. (1998) Matrix metalloproteinases regulate neovasularization by acting as pericellular fibrinolysis. *Cell*, 95; 365-377.

Holmbeck K., Bianco P., Yamada S., Birkedal-Hansen H. (2004) MT1-MMP; A tethered collagenase. *J. Cell. Physiol.* 200; 11-19.

Hotary K., Allen E., Punturieri A., Yana I., Weiss S. J. (2000) Regulation of cell invasion and morphogenesis in a three-dimentional type I collagen matix by membrane-type matrix metalloproteianses 1, 2 and 3. *J. Cell Biol.* 149; 1309-1323.

Hotary K.B., Allen E.D., Brooks P.C., Datta N.S., Long M.W., Weiss S.J. (2003) Membrane type I matrix metalloproteinase usurps tumor growth control imposed by the three – dimensional extracellular matix. *Cell* 114; 33-45.

Hooper, N. M. Proteases in Biology and Medicine. *Portland Press, London,* 2002.

Imper V., Van Wart H. E. (1998) Substrate specificity and mechanisms of substrate recognition of the matrix metalloproteinases. In *Matrix Metalloproteases* (Parks, W. C. and Mecham, R. P., eds) pp. 219–242, Academic, St Louis, MS.

Itoh Y, Takamura A, Ito N, Maru Y, Sato H, Suenaga N, Aoki T, Seiki M. (2001) Homophilic complex formation of MT1-MMP facilitates proMMP-2 activation on the cell surface and promotes tumor cell invasion. *EMBO J* 20; 4782–4793.

Itoh Y., Nagase H., (2002) Matrix metalloproteinases in cancer. *Essays Biochemn.* 38; 21-36.

Itoh Y, Takamura A, Ito N, Maru Y, Sato H, Suenaga N, Aoki T, Seiki M. (2001) Homophilic complex formation of MT1-MMP facilitates proMMP-2 activation on the cell surface and promotes tumor cell invasion. *EMBO J* 20; 4782–4793.

Jozic D., Bourenkov G., Lim N.H., Visse R., Nagase H., Bode W., Maskos K. (2005) X-ray Structure of Human proMMP-1. *J Biol Chem* 10(11); 9578-9585.

Kajita M., Itoh Y., Chiba T., Mori H., Okada A., Kinoh H., Seiki M. (2001) Membrane type 1 matrix metalloproteinase cleaves CD44 and promotes cell migration. *J. Cell. Biol.* 153; 893-904.

Karelina T.V., Hruza G.J., Goldberg G.I., and Eisen A.Z. (1993) Localization of 92 kDa type IV collagenase in human skin tumors: comparison with normal human fetal and adult skin. *J.Invest. Dermatol.* 100; 159–165.

Knäuper V., Will H., Lopez-Otin C., Smith B., Atkinson S.J., Stanton H., Hembry R.M. Murphy G. (1996) Cellular mechanism for human procollagenase-3 (MMP-13) activation. Evidence that MT1-MMP (MMP14) and gelatinase A (MMP-2) are able to generate active enzyme. *J. Biol.Chem*. 271; 17124-17131.

Kinoshita T, SatoH, Okada A, Ohuchi E, Imai K, Okada Y, Seiki M. (1998) TIMP-2 promotes activation of progelatinase A by membrane-type 1 matrix metalloproteinase immobilized on agarose beads. *J Biol Chem* 273; 16098–16103.

Kleifeld O., Kotra L.P., Gervasi D.C., Brown S., Bernardo M.M., Fridman R., Mobashery S., Sagi I. (2001). X-ray Absorption Studies of Human Matrix Metalloproteinase-2 (MMP-2) Bound to a Highly Selective Mechanism-based Inhibitor. *J Biol Chem*. 276; 17125-17131.

Koshikawa N., Giannelli G., Cirulli V., Miyazaki K., Quaranta V. (2000) Role of cell surface metalloprotease MT1-MMP in epithelial cell migration over laminin-5. *J.Cell Biol*., 148; 615-624.

Laemmli U.K., (1970) Cleavage of structural proteins during the assembly of the head of bacteriofage T4. *Nature* 227; 680- 685.

Laskowski R.A., MacArthur M.W., Moss D.S. Thorton J.M. (1993) PROCHECK: a program to check the stereochemical quality of protein structures. *J.Appl. Crystallog.* 26; 283-291.

Legrand C., Gilles C., Zahm J. M., Polette M., Buisson A. C., Kaplan H., Birembaut P., Tournier J. M., (1999) Airway epithelial cell migration dynamics. MMP-9 role in cell-extracellular matrix remodelling. *J. Cell. Biol*. 146; 517-529.

Lehti K, Lohi J, Valtanen H, Keski-Oja J. (1998) Proteolytic processing of membrane-type-1 matrix metalloproteinase is associated with gelatinase A activation at the cell surface. *Biochem J* 334; 345–353.

Lehti K, Lohi J, Juntunen M.M, Pei D, Keski-Oja J. (2002) Oligomerization through hemopexin and cytoplasmic domains regulates the activity and turnover of membrane-type 1 matrix metalloproteinase. *J Biol Chem* 277; 8440–8448.

Li Y., Aoki T., Mori Y., Ahmad M., Miyamori H., Takino T., Sato H. (2004) Cleavege by limican by membrane-type matrix metalloproteinase-1 abrogates this proteoglycan-mediated suppresion of tumor cell colony formation in soft agar. *Cancer Res*. 64; 7058-7064.

Li J., Brick P., Ohare M.C., Skarzynski T., Lloyd L.F., Curry V.A., (1995) Structure of full-length porcine synovial collagenase reveals a C-terminal domain containing a calcium-linked, four-bladed beta-propeller. *Structure* 3,541-549.

Libson A.M., Gittis A.G., Collier I.E., Marmer B., (1995) Crystal structure of the haemopexin-like domain of gelatinase A. *Nature Struct. Biol.* 2, 938-942.

Liotta L.A., Stetler-Stevenson W.G. (1990) Metalloproteinases and cancer invasion. *Semin.Cancer Biol.* 1; 99-106.

Lu, Y. A.; Felix, A. M. *Peptide Research* 1993*,* 6; 140-146.

Luttun A., Lutgens E., Manderveld A., Maris K., Collen D., Carmeliet P., Moons L. (2004) Loss of matrix metalloproteinase-9 or matrix metalloproteinase-12 protects apolipoprotein E-deficient mice against atherosclerotic media destruction but differentially affects plaque growth. *Circulation* 109; 1408-1414.

Mackay A.R., Hartzler J.L., Pelina M.D., Thorgeirsson U.P. (1990) Studies on the ability of 65–kDa and 92–kDa tumor cell gelatinases to degrade type IV collagen. *J. Biol. Chem.* 265; 21929–21934.

Mammen M., S.-K. C.G. M.W. *Angewandte Chemie International Edition* 1998, 37; 2754-2794.

Maskos K., Bode W. (2003) Structural basis of matrix metalloproteinases and tissue inhibitors of metalloproteinases. *Mol Biotechnol*, 25(3); 241-66.

Masure S., Billiau A., Van Damme J., Opdenakker G. (1990) Human hepatoma cells produce an 85 kDa gelatinase regulated by phorbol 12–myristate 13–acetate. *Biochim. Biophys. Acta* 1054**;** 317–325.

Mathai Mammen, S.-K. C.G. M.W. Angewandte Chemie International Edition 1998, 37; 2754-2794.

Matziari M, Beau F, Cuniasse P, Dive V*,* Yiotakis A. (2004). Evaluation of P1' diversified phosphinic peptides leads to the development of highly selective inhibitors of MMP-11. J Med Chem. 47, 325-336.

Mazzone M., Baldassarre R., Beznoussenko G., Giacchetti G., Cao J., Zucker S., Luini A., Buccione R. (2004) Intracellular processing and activation of membrane type 1 matrix metalloproteinase depends on its partitioning into lipid domains. *J. Cel.l Sci.* 117; 6275-6287.

Mehul B., Bawumia S., Martin S.R., Hughes R.C. (1994) Structure of baby hamster kidney carbohydrate-binding protein CBP30, an S-type animal lectin. *J. Biol. Chem.* 269**;** 18250–18258.

McCawley, L.J., and Matrisian, L.M. (2000) *Mol. Med. Today* 6; 149-156.

McQuibban G.A., Butler G.S., Gong J.H., Bendall L., Power C., Clark-Lewis I., Overall C.M. (2001) Matrix metalloproteinase activity inactivates the CXC chemokine stromal cell-derived factor-1. *J. Biol. Chem.* 276**;** 43503–43508.

Mohan R., Chintala S.K., Jung J.C., Villar W.V., McCabe F., Russo L.A., Lee Y., McCarthy B.E., Wollenberg K.R., Jester J.V., Wang M., Welgus H.G., Shipley J.M., Senior R.M., Fini M.E., (2002) Matrix metalloproteinase gelatinase B (MMP-9) coordinates and effects epithelial regeneration. *J. Biol. Chem.* 277; 2065-2072.

Mordomi T., Ogata Y., Sasaguri Y., Morimatsu M., Nagase H. (1992) *Biochem J* 285; 603-611.

Morgunova E., Tuuttila A., Bergmann U., Isupov M., Lindqvist Y., Schneider G. & Tryggvason K. (1999) Structure of human pro-matrix metalloproteinase-2 ; activation mechanism revealed. *Science* 284, 1667-1670.

Mori H, Tomari T, Koshikawa N, Kajita M, Itoh Y, Sato H, Tojo H, Yana I, Seiki M. (2002). CD44 directs membrane-type 1 matrix metalloproteinase to lamellipodia by associating with its hemopexin-like domain. *EMBO J.* 21; 3949–3959.

Moore W.M., Spilburg C.A. (1986) Purification of human collagenases with a hydroxamic acid affinity column. *Biochemistry,* 25; 5186-5195.

Mott J.D. & Werb Z., (2004) Regulation of matrix biology by matrix metalloproteinases. *Curr Opin cell Biol.* 16(5); 558-64.

Murphy G., Houbrechts A., Cockett M.I., Williamson R.A., O'Shea M., Docherty A.J. (1991) The Nterminal domain of tissue inhibitor of metalloproteinases retains metalloproteinase inhibitory activity. *Biochemistry* 30**;** 8097–8102.

Murphy G. Docherty A.J.P. (1992) The matrix metalloproteinases and their inhibitors. *Am. J. Respir. Cell Mol. Biol.* 7**;** 120–125.

Murphy G., Willenbrock F. (1995) Tissue inhibitors of matrix metalloendopeptidases. *Methods Enzymol.* 248; 496–510.

Murphy G., Gavrilovic J., (1999) Proteolysis and cell migration: creating a path? *Curr Opin Cell Biol*, 11; 614-21.

Mutter M., Hagenmai H., Bayer E. *Angewandte Chemie-International Edition* 1971;10, 811.

Nagase H., Enghlid J. J., Suzuki K., Salvesen G. (1990) *Biochemistry* 29; 5783-5789.

Nagase H. (1997) Activation mechanisms of matrix metalloproteinases. *Biol. Chem*. 378, 151-160

Nagase H., Woessner J. F. Jr., (1999) Matrix Metalloproteinases. *J. Biol. Chem*., 274; 21491-94.

Nagase H., Visse R., Murphy G. (2006) Structure and function of matrix metalloproteinases and TIMPs. *Cardiovasc Res.* 69(3); 562-73.

Naot D, Sionov RV, Ish-Shalom D. (1997). CD44: Structure, function, and association with the malignant process. *Adv Cancer Res* 71; 241–319.

Nguyen Q., Murphy G., Hughes C.E., Mort J.S., Roughley P.J. (1993) Matrix metalloproteinases cleave at two distinct sites on human cartilage link protein. *Biochem. J.* 295**;** 595–598.

Nomura H., Fujimoto N., Seiki M., Mai M., and Okada Y. (1996) Enhanced production of matrix metalloproteinases and activation of matrix metalloproteinase 2 (gelatinase A) in human gastric carcinomas. *Int. J. Cancer* 69; 9–16.

O'Connell J.P., Willenbrock F., Docherty A.J.P., Eaton D., Murphy G. (1994) *J Biol. Chem.* 269; 14967-14973.

Ochieng J., Fridman R., Nangia-Makker P., Kleiner D. E., Liotta L. A., Stetler-Stevenson, W. G., Raz A. (1994) Galectin-3 is a novel substrate for human matrix metalloproteinases-2 and –9. *Biochemistry* 33**;** 14109–14114.

Ogata Y., Itoh Y., Nagase H. (19959 Steps involved in activation of the pro-matrix metalloproteinase 9 (progelatinase B)-tissue inhibitor of metalloproteinases-1 complex by 4–aminophenylmercuric acetate and proteinases. *J. Biol. Chem.* 270; 18506–18511.

Oh J, Takahashi R, Kondo S, Mizoguchi A, Adachi E, Sasahara R. M, Nishimura S, Imamura Y, Kitayama H, Alexander D. B, Ide C, Horan T. P, Arakawa T, Yoshida H, Nishikawa S, Itoh Y, Seiki M, Itohara S, Takahashi C, Noda M. (2001) The membrane-anchored MMP inhibitor RECK is a key regulator of extracellular matrix integrity and angiogenesis. *Cell* 107; 789–800.

Okada Y., Gonoji Y., Naka K., Tomita K., Nakanishi M., Nagase H. (1992) *J Biol Chem* 267; 21712-21719.

Olson M.W., Gervasi D.C., Mobashery S., Fridman R. (1997) Kinetic analysis of the binding of human matrix metalloproteinase-2 and –9 to tissue inhibitor of metalloproteinase (TIMP)-1 and TIMP-2. *J. Biol. Chem.* 272**;** 29975–29983.

Oltenfreiter R., Staelens L., Lejeune A., Dumont F., Frankenne F., Foidart J.M., Slegers G. (2004) New radioiodinated carboxylic and hydroxamic matrix metalloproteinase inhibitor tracers as potential tumor imaging agents. *Nucl. Med.Biol.* 31; 459-468.

Oltenfreiter R., Staelens L., Hillaert U., Heremans U., Noel A., Frankenne F., Slegers G. (2005) Synthesis, radiosynthesis, in vitro and preliminary in vivo evaluation of biphenyl carboxylic and hydroxamic matrix metalloproteianse (MMP) inhibitors as potential tumor imaging agents. *Appl. Rad. Isot.*, 62; 903-913.

Osenkowski P, Toth M, Fridman R. (2004) Processing, shedding, and endocytosis of membrane type 1-matrix metalloproteinase (MT1-MMP). *J Cell Physiol* 200; 2–10.

Otwinowski Z., Minor W. (1997) Processing of x-ray diffraction data collected in oscillation mode. *Methods Enzymol.* 276; 306-326.

Overall Ch.M., Tam E, McQuibban G.A., Morrison Ch., Wallon U.M., Bigg H.F., King A. E., Roberts C. R. (2000). Domain interactions in the Gelatinase A-TIMP-2-MT1-MMP activation complex. *J Biol Chem.* 275; 39497-39506.

Overall C.M. (2002) Molecular Determinants of Metalloproteinases Substate Specificity. *Mol Biotechnol* 22; 51-86.

Overall C.M., & Kleifeld O. (2006) Towards third generation matrix metalloproteinase inhibitors for cancer therapy. *Br J Cancer* 94(7); 941-6.

Pace C.N., (1995) Evaluating contribution of hydrogen bonding and hydrophobic bonding to protein folding. (1995) *Methods Enzymol* 259;538-54.

Patterson B.C., Sang Q.A. (1997) Angiostatin-converting enzyme activities of human matrilysin (MMP-7) and gelatinase B/type IV collagenase (MMP-9). *J. Biol. Chem.* 272**;** 28823–28825.

Pei D., Kang T., Qi H., (2000). Casteine Array Matrix Metalloproteianse (CA MMP)/MMP-23 IS a Type II Transmembrane Matrix Metalloproteinase Regulated by a Single Cleavage for Both Secretion and Activation. *J. Biol. Chem.,* 275; 33988-97.

Peppin G.J. and Weiss S.J. (1986) Activation of the endogenous metalloproteinase, gelatinase, by triggered human neutrophils. *Proc. Natl. Acad. Sci. U. S. A.* 83**;** 4322–4326.

Pourmotabbed T., Solomon T.L., Hasty K.A., Mainardi C.L. (1994) Characteristics of 92 kDa type IV collagenase/gelatinase produced by granulocytic leukemia cells: structure, expression of cDNA in *E. coli* and enzymic properties. *Bioch Biop Acta*, 1204; 97-107.

Proost P., Van Damme J., Opdenakker G. (1993a) Leukocyte gelatinase B cleavage releases encephalitogens from human myelin basic protein. *Biochem. Biophys. Res. Commun.* 192; 1175–1181.

Pyke C., Ralfkiær E., Huhtala P., Hurskainen T., Dano K., and Tryggvason K. (1992) Localization of messenger RNA for Mr 72,000 and 92,000 type IV collagenases in human skin cancers by *in situ* hybridization. *Cancer Res.* 52; 1336–1341.

Rao J.S., Steck P.A., Mohanam S., Stetler-Stevenson W.G., Liotta L.A., and Sawaya R. (1993) Elevated levels of Mr 92,000 type IV collagenase in human brain tumors. *Cancer Res*. 53; 2208–2211.

Rao J.S., Yamamoto M., Mohaman S., Gokaslan Z.L., Fuller G.N., Stetler-Stevenson W. G., Rao V. H., Liotta L. A., Nicolson G. L., and Sawaya R. E. (1996) Expression   and localization of 92 kDa type IV collagenas gelatinase B (MMP-9) in human gliomas.*Clin. Exp. Metastasis* 14; 12–18.

Reinemer P., Grams F., Huber R., Kleine T., Schnierer S., Piper M., Tschesche H., Bode W. (1994) Structural implications fort he role of the N terminus in the ,superactivation' of collagenases. A crystallographic study. *FEBS Lett.* 338(2); 227-33.

Rodriguez-Manzaneque J. C. et.al. (2001) Thrombospodin-1 suppresses spontaneous tumour growth and inhibits of activation of matrix metalloproteinase-9 and mobilization of vascular endothelial growth factor. *Proc. Natl. Acad. Sci. USA 98, 1285-1290.*

Rowsell S., Hawtin P., Minshull C.A., Jepson H., Brockbank S.M.V., Barratt D., Slater A.M., McPheat W., Waterson D., Henney A. M. & Pauptit R. A. (2002) Crystal Structure of Human MMP-9 with a Reverse Hadroxamate Inhibitor. *J.Mol.Biol.* 319; 173-181.

Rozanow D.V., Deryugina E.I., Ratnikov B.I., Monosov E.Z., Marchenko G.N., Quigley J.P., Strongin A.Y. (2001) Mutation analysis of membrane type-1 metalloproteinase (MT1-MMP). The role of the cytoplasmic tail Cys(574), the active site Glu(240)

Rozanow DV, Hahn-Dantona E., Strickland DK., Strongin AY. (2004) The low density lipoprotein receptor-related protein LRP is regulated by membrane type-1 matrix metalloproteinase (MT1-MMP) proteolysis in malignant cells. *J. Biol. Chem* 279; 4260-4268.

Sabeh F., Ota I., Holbeck K., Birkedal-Hansen H., Soloway P., Balbin M., Lopez-Otin C., Shapiro S., Inada M., Krane S., Allen E., Chung D, Weiss SJ. (2004) Tumor cell traffic through the extracellular matrix is controlled by the membrane-anchored collagenase MT1-MMP. *J Cell Biol* 167; 769-781.

Sakata K., Maeda, T., Nakagawa H. (1989) Activation by cathepsin G of latent gelatinase secreted from rat polymorphonuclear leukocytes. *Chem. Pharm. Bull. (Tokyo)* 37; 1321–1323.

Salo T., Makela M., Kylmaniemi M., Autio-Harmainen H., Larjava H. (1994) Expression of matrix metalloproteinase-2 and -9 during early human wound healing. *Lab. Invest.* 70; 176-182.

Salvino J.M., Mathew R., Kiesow T., Narensingh R., Mason H.J., Dodd A., Groneberg R., Burns C.J., McGeehan G., Kline J., Orton E., Tang S.-Y., Morrissette M., Labaudiniere R. (2000) *Bioorg. Med. Chem. Lett.* 10, 1637–1640.

Sambrook J., Fritsch E.F., & Maniatis T. (1989) Molecular cloning; A laboratorial mannual. New York, USA, Cold Spring Harbor Laboratory Press.

Sang Q. X., Birkedal-Hansen H., Van Wart H. E. (1995) Proteolytic and nonproteolytic activation of human neutrophil progelatinase B. *Biochim. Biophys. Acta* 1251**;** 99–108.

Sato H., Takino T., Okada Y., Cao J., Shinagawa A., Yamamoto E., Seiki M. (1994) A matrix metalloproteinase expressed on the surface of invasive tumour cells. *Nature,* 370; 61-65.

Sato H., Kinoshita T., Takino T., Nakayama K., seiki M. (1996) Activation of the recombinant membrane type 1-matrix metalloproteinase (MT1-MMP) by furin and its interaction with tissue inhibitor of metalloproteianses (TIMP)-2. *FEBS Lett.* 393; 101-104.

Sato T, del Carmen Ovejero M, Hou P, Heegaard A.M, Kumegawa M, Foged NT, Delaisse JM. (1997) Identification of the membrane-type matrix metalloproteinase MT1-MMP in osteoclasts. *J Cell Sci* 110; 589–596.

Schaschke N., Dominik A., Matschiner G., Sommerhoff C.P.. Moroder L. (2001) Bivalent inhibition of human beta-tryptase. *Chem Biol*. 8(4); 313-27.

Schägger H., & von Jagow G. (1987) Tricine-sodium dodecyl sulfate-polyacrylamide gel electrophoresis for teh separation of proteins in the range from 1 to 100 kDa. *Anal Biochem.* 166; 368-379.

Schechter, I., and Berger, A. (1967). On size of active site in proteases .I. Papain. *Biochemical and Biophysical Research Communications* 27; 157-&.

Schönbeck U., Mach F., Libby P. (1998) Generation of biologically active IL-1β by matrix metalloproteinases: a novel caspase-1–independent pathway of IL-1β processing. *J. Immunol.* 161**;** 3340–3346.

Seiki M. (1999) Membrane-type matrix metalloproteinases. *Apmis* 107; 137-143.

Seiki M., (2002) Membrane-type 1 matrix metalloproteinase: a key enzyme for tumour invasion. *Canc. Let.* 194; 1-11.

Seiki M. (2003) membrane-type matrix metalloproteinase; A key enzyme for tumor invasion. *Cancer Lett*. 194; 1-11.

Senior R.M., Griffin G.L., Fliszar C.J.,Shapiro S.D., Goldberg G.I., Welgus H.G. (1991) Human 92– and 72–kilodalton type IV collagenases are elastases. *J. Biol. Chem.* 266; 7870–7875.

Shapiro S.D., Fliszar C.J., Broekelmann T.J., Mecham R.P., Senior R.M., Welgus H.G. (1995) Activation of the 92–kDa gelatinase by stromelysin and 4 aminophenylmercuric acetate. Differential processing and stabilization of the carboxyl-terminal domain by tissue inhibitor of metalloproteinases (TIMP). *J. Biol. Chem.* 270**;** 6351–6356.

Sheu B.C., Hsu S.M., Ho H.N., Lien H.C., Huang S.C., Lin R.H. (2001) A novel role of metalloproteinase in cancer-mediated immunosuppression. *Cancer Res.* 61**;** 237–242.

Shipley J.M., Doyle A.R., Fliszar C.J., Ye Q.Z., Johnson L.L., Shapiro S.D., Welgus H.G., Senior R.M. (1996) The Structural Basis for the Elastolytic Activity of the 92-kDa and 72-kDa Gelatinases. *J.Biol.Chem.* 271; 4335-4341.

Silletti S., Kessler T., Goldberg J., Boger DL., Cheresh DA. (2001) Disruption of matrix metalloproteinse-2 binding to integrin αvβ3 by an organic molecule inhibitors angiogenesis and tumor growth in vivo. *Proc Natl Acad Sci.USA*. 98; 119-124.

Sires U. I., Murphy G., Baragi V. M., Fliszar C. J., Welgus H. G., Senior R. M. (1994) Matrilysin is much more efficient than other matrix metalloproteinases in the proteolytic inactivation of α1–antitrypsin. *Biochem. Biophys. Res. Commun.*204**;** 613–620.

Skiles J. W., Gonnella N. C., Jeng A. Y. (2001) The design, structure, and therapeutic application of matrix metalloproteinase inhibitors. *Curr Med Chem.* 8(4); 425-74.

Smith P.K., Krohn R.I., Hermanson G.T., Mallia A. K., Gartner F.H., Provenzano M.D., Fujimoto E.K., Goeke N.M., Olson B.J. & Klenk D.C. (1985) Measurement of protein using bicinchoninic acid. *Anla Biochem* 150; 76-85.

Sopata I, Malinski S. (1991) Actiavtion of the latent human neutrophil gelatinase by urea. *Acta Biochim Pol*. 38(1); 67-70.

Sounni NE., Devy L., Hajitou A., Frankenne F., Munaut C., Gilles C., Deoranne C., Thompson EW., Foidart JM., Noel A. (2002) MT1-MMP expression promotes tumor growth and angiogenesis through an up-regulation of vascular endothelial growth factor expression. *FASER J.* 16; 555-564.

Sounni NE., Roghi C., Chabottaux V., Jansen M., Munaut C., Maquoi E., Galvez BG., Gilles C., Frankennne F., Murphy G., Foidart JM., Noel A. (2004) Up-regulation of vascular endothelial growth factor –A by active membrane type-1 matrix metalloproteinase through activation of Src-tyrosine kinases. *J. Biol Chem*. 279; 13564-13574.

Springman E. B., Angleton E. L., Birkedal-Hansen H., Van Wart H. W., (1990) *Proc Natl Acad Sci USA* 87; 364-368.

Steinmetzer T., Renatus M., Kunzel S., Eichinger S., Bode W., Wikstrom P., Hauptmann J., Sturzebecher J. (1999) Design and evaluation of novel bivalent inhibitors based an amidinophenylalanines. *Eur J Biochem* 265(2); 598-605.

Stamenkovic I. (2000) Matrix metalloproteinases in tumor invasion and metastasis. *Semin Cancer Biol.* 10(6);415-33.

Stanton H, Gavrilovic J, Atkinson S. J, d'Ortho M. P, Yamada K. M, Zardi L, Murphy G. (1998) The activation of ProMMP-2 (gelatinase A) by HT1080 fibrosarcoma cells is promoted by culture on a fibronectin substrate and is concomitant with an increase in processing of MT1-MMP (MMP-14) to a 45 kDa form. *J Cell Sci* 111; 2789–2798.

Sternlicht M. D. & Werb. Z. (2001) How matrix metalloproteinases regulate cell behaviour. *Annu. Rev. Cell Dev. Biol.* 17; 463-515.

Stetler-Stevenson W. G., Krutzsch H. C., Wacher M. P., Margulies I. M. K., Liotta L. A. (1989) *J Biol Chem* 264; 1353-1356.

Stetler-Stevenson W.G. (1999) Matrix Metalloproteinases in angiogenesis: a moving target for therapeutic intervention. *J. Clin. Invest.* 103; 1237-1241.

Strongin AY, Collier I, Bannikov G, Marmer BL, Grant GA, Goldberg GI. (1995) Mechanism of cell surface activation of 72-kDa type IV collagenase. Isolation of the activated form of the membrane metalloprotease. *J Biol Chem* 270; 5331–5338.

Suenaga N, Mori H, Itoh Y, Seiki M. (2005). CD44 binding through the hemopexinlike domain is critical for its shedding by membrane-type 1 matrix metalloproteinase. *Oncogene* 24; 859–868.

Takahashi C, Sheng Z, Horan T. P, Kitayama H, Maki M, Hitomi K, Kitaura Y, Takai S, Sasahara R. M, Horimoto A, Ikawa Y, Ratzkin B. J, Arakawa T, Noda M. (1998) Regulation of matrix metalloproteinase-9 and inhibition of tumor invasion by the membrane-anchored glycoprotein RECK. *Proc Natl Acad Sci USA* 95; 13221–13226.

Takemura M., Azuma C., Kimura T., Tokugawa Y., Miki M., Ono M., Saji F., and Tanizawa O. (1992) Malignant cell-specific gelatinase activity in human endometrial carcinoma. *Cancer* 70; 147–151.

Takemura M., Azuma C., Kimura T., Kanai T., Saji F., and Tanizawa O. (1994) Type-IV collagenase and tissue inhibitor of metalloproteinase in ovarian cancer tissues. *Int. J. Gynecol. Obstet.* 46; 303–309.

Tamura Y., Watanabe F., Nakatani T., Yasui K., Komurasaki T., Tsuzuki H., Maekawa R., Yoshioka T., Kawada K., Sugita K., Ohtani M. (1998) Highly selective and Orally Active Inhibitors of Type IV Collagenase (MMP-9 and MMP-2): *N* Sulfonylamino Acid Derivatives. *J.Med.Chem*. 41; 640-649.

Thiennu H. Vu., Shipley J. M., Bergers G., Berger J. E., Helms J. A., Hanahan D., Shapiro S. D., Senior R. M., Werb Z. (1998) MMP-9/Gelatinase B Is a Key Regulator of Growth Plate Angiogenesis and Apoptosis of Hypertropic Chondrocytes. *Cell* 93; 411-422.

Toth M., Hernandez-Barrantes S., Osenkowski P., Bernardo M. M, Gervasi D. C., Shimura Y., Meroueh O., Kotra L. P., Galvez B. G., Arroyo A. G., Mobashery S., Fridman R. (2002) Complex pattern of membrane type 1 matrix metalloproteinase shedding. Regulation by autocatalytic cells surface inactivation of active enzyme. *J Biol Chem* 277; 26340–26350.

Toth M, Osenkowski P, Hesek D, Brown S, Meroueh S, Sakr W, Mobashery S, Fridman R. (2004) Cleavage at the stem region releases an active ectodomain of the membrane type 1-matrix metalloproteinase. *Biochem J* 387; 497–506.

Triebel S., Blaser J., Reinke H., Knauper V., Tschesche H. (1992) *FEBS Lett*. 298; 280-284.

Turk D., (1992) Weiterentwicklung eines Programms für moleculargraphik und Elektornendichte-Manipulation und seine Anwendung auf verschiedene Structuraufklärungen. PhD Thesis, technische Universität Munich, Germany

Vagin A., Teplyakov A (2000) An approach to multi-copy search in molecular replacement *Acta Crystallog. Sect. D*, 56; 1622-1624.

Van Coillie E., Van A., I, Wuyts A., Vercauteren R., Devos R., Wolf-Peeters C., Van Damme J., Opdenakker G. (2001) Tumor angiogenesis induced by granulocyte chemotactic protein-2 as a countercurrent principle. *Am. J. Pathol.* 159; 1405–1414.

Van den Steen P. E., Dubois B., Nellssen I., Rudd P. M., Dwek R. A. and Opdenakker Ch. (2002). *Crit. Rev. Biochem. Mol. Biol.* 37; 375-536.

Van Wart H.E., Brikedale H. (1990) The cysteine switch: a principle of regulation of metalloproteinase activity with potential applicability to the entire matrix metalloproteinase gene family. *Proc. Natl. Acad. Sci. U. S. A.* 87**;** 5578–5582.

van den Oord J. J., Paemen L., Opdenakker G., De Wolf-Peeters C. (1997) Expression of gelatinase B and the extracellular matrix metalloproteinase inducer EMMPRIN in benign and malignant pigment cell lesions of the skin. *Am. J. Pathol.* 151**;** 665–670.

Vassiliou S.,Mucha A., Cuniasse P., Georgiadis D., Lucet-Levannier K., Beau F., Kannan R., Murphy G., Knauper V., Rio M. C., Basset P., Yiotakis A., Dive V. (1999) Phosphinic pseudo-tripeptides as potent inhibitors of matrix metalloproteinases; a structure activity study. *J Med Chem*. 42(14); 2610-20.

Visse R., Nagase H. (2003) Matrix metalloproteinases and tissue inhibitors of metalloproteianses. Structure, function and biochemistry. *Circ res* 92; 827-839.

Walker B., Lynas J.F. (2001) Strategies for the inhibition of serine proteases. *Cell. Mol. Life Sci.* 58; 596-624.

Wang Z, Juttermann R, Soloway P. D. (2000) TIMP-2 is required for efficient activation of proMMP-2 in vivo. *J Biol Chem* 275; 26411–26415.

Wang P, Nie J, Pei D. (2004). The hemopexin domain of membrane-type matrixmetalloproteinase-1 (MT1-MMP) Is not required for its activation of proMMP2on cell surface but is essential for MT1-MMP-mediated invasion in three dimensional type I collagen. *J Biol Chem* 279; 51148–51155.

Whittaker M., Floyd Ch. D., Brown P., Gearing A.J.H. (1999) Design and Therapeutic Application of Matrix Metalloproteinase Inhibitors.Chem. *Rev.* 99; 2735-2776.

Wilhelm S. M., Collier I. E., Marmer B. L., Eisen A. Z., Grant G. A., Goldberg G. I., (1989) *J Biol Chem* 264; 17213-17221.

Will H, Atkinson S. J, Butler G. S, Smith B, Murphy G. (1996) The soluble catalyticdomain of membrane type 1 matrix metalloproteinase cleaves the propeptide of progelatinase A and initiates autoproteolytic activation. Regulation by TIMP-2 and TIMP-3. *J Biol Chem* 271; 17119–17123.

Woessner J. F., in Clark I. M. (ed.), Methods in Molecular Biology. (2000) *Matrix Metalloproteinase Protocols,* Humana Pres, Totowa, NJ, 151; 1-23.

Wojtowicz-Praga S. M., Dickson R. B., Hawkins M. J. (1997) Matrix metalloproteinase inhibitors. *Invest New Drugs*, 15; 61-75.

Wolf K, Mazo I, Leung H, Engelke K, von Andrian UH, Deryugina EI, Strongin AY, Brocker EB, Friedl P. 2003. Compensation mechanism in tumor cell migration: Mesenchymal-amoeboid transition after blocking of pericellular proteolysis. *J Cell Biol* 160; 267–277.

Yamaoka, T.; Tabata, Y.; Ikada, Y. *Journal of Pharmaceutical Sciences* (1994) 83; 601-606.

Yana I., Weiss SJ. (2000) Regulation of membrane type-1 matrix metalloproteinase activation by proprotein convertases. *Mol. Biol. Cell.* 11; 2387-2401.

Yu Q., Stamenkovic I. (1999) Localization of matrix metalloproteinase to the cell surface provides a mechanism for CD44-mediated tumor invasion. *Genes Dev.* 13; 35-48.

Yu Q., Stamenkovic I. (2000) Cell surface-localized matrix metalloproteinase-9 proteolytically activates TGF-β and promotes tumor invasion and angiogenesis. *Genes Dev.* 14**;** 163–176.

Zucker S., Lysik R. M., Zarrabi M. H., and Moll U. (1993) Mr 92,000 type IV collagenase is increased in plasma of patients with colon cancer and breast cancer. *Cancer Res.* 53**;** 140–146.

Zalipsky S. *Bioconjugate Chemistry* (1995) 6; 150-165.

Zucker S., Pei D., Cao J., Lopez-Otin C. (2003) Membrane type-matrix metalloproteinases (MT1-MMP). *Curr Top Dev Biol*. 54; 1-74.

Chapter 7　　　Appendix

7.1　　　Abbreviations

Å	Ångstrøm, 1 Å = 10^{-10} m
BLAST	Basical local alignment search tool
CD	Circular dichroism
^{o}C	Celsius degree
ddH$_2$O	*aqua bidestilata*
DEAE	Diethyl aminoethyl
DESY	Deutsches Elektronen Synchrotron
DNA	Deoxyribonucleic acid
DTT	Dithiothreitol
E. coli	*Escherichia coli*
g	9.81 m/s²
HCl	Hydrochloric acid
K	Kelvin degree
K$_{av}$	Partition coefficient
Kb	Kilo base
K$_d$	Dissociation constant
KDa	Kilo Dalton, 1 Da = 1 g mol^{-1}
M	Molarity (mol/l)
MAD	Multi-wavelength anomalous dispersion
M$_r$	Relative molecular mass
MDa	Mega Dalton
min	minutes

MR	Molecular replacement
mRNA	messenger RNA
NaCl	Sodium chloride
NaOH	Sodium hydroxide
NCS	Non-crystallographic symmetry
nm	nanometer
NMR	Nuclear magnetic resonance
PAGE	Polyacrylamide gel electrophoresis
PEG	Polyethylene glycol
PMSF	Phenylmethanesulfonylfluoride
r.m.s.d.	root-mean-square deviation
RNA	Ribonucleic acid
rRNA	ribosomal RNA
SDS	Sodium dodecylsulfate
TCA	Trichloroacetic acid
Tris-HCl	N-Tris-(hydroxymethyl)-aminomethane
tRNA	transfer RNA
v/v	volume per volume
w/v	weight per volume

7.2 Index of Figures

7.2　　　**Index of Tables**